EXTENDED LOADING

OF

CRYOGENIC TANKS

By

C. F. Tiffany , P. M. Lorenz and R. C. Shah

Prepared For

NATIONAL AERONAUTICS AND SPACE ADMINISTRATION
NASA LEWIS RESEARCH CENTER
LIQUID ROCKET TECHNOLOGY BRANCH
CLEVELAND, OHIO

Contract NAS 3-6290

GPO PRICE $ _____

CFSTI PRICE(S) $ _____

Hard copy (HC) _____

Microfiche (MF) _____

FINAL REPORT

EXTENDED LOADING OF CRYOGENIC TANKS

By

C. F. Tiffany, P. M. Lorenz and R. C. Shah

Prepared for

National Aeronautics and Space Administration

Contract NAS 3-6290

Technical Management
NASA Lewis Research Center
Cleveland, Ohio

Liquid Rocket Technology Branch
Gordon T. Smith

Aerospace Group
THE BOEING COMPANY
Seattle, Washington

EXTENDED LOADING OF CRYOGNIC TANKS
BY

C. F. Tiffany, P. M. Lorenz and R. C. Shah

ABSTRACT

Plane-strain flaw growth characteristics under sustained loading and combined cyclic-sustained loading conditions as well as static fracture toughness values were obtained for 2219-T87 aluminum and 5Al-2.5 Sn (ELI) annealed titanium. Investigations were conducted at room temperature, -320°F and -423°F in ambient air, liquid nitrogen and liquid hydrogen environments, respectively. The experimental approach was based on linear-elastic fracture mechanics. Results from surface-flawed uniaxial specimens and cylindrical tanks were compared. It was concluded that the effects of cyclic and sustained loading may be combined and used in the design of cryogenic pressure vessels.

PREFACE

This report describes an investigation by The Boeing Company from
June 1965 to December 1966 on plane-strain sustained flaw growth
in thick-walled cryogenic tanks under Contract NAS 3-6290. The
work was administered by Mr. Gordon T. Smith of the NASA Lewis
Research Center.

Boeing personnel who participated in the investigation include
C. F. Tiffany, project supervisor; P. M. Lorenz, principal investi-
gator; and R. C. Shah, research engineer. Structural testing of
specimens and cryogenic tanks was conducted by A. A. Ottlyk and
J. R. Hughes. Manufacturing support was provided by O. Faerber.
Technical illustrations and art work were prepared by D. Good.

SUMMARY

The experimental work performed on this program was directed toward establishing design criteria, obtaining sustained and combined cyclic sustained stress flaw growth data, and developing design utilization methods for cryogenic pressure vessels. Experimental data together with the overall assessment of the problem of cryogenic pressure vessel design lead to confirmation of the design criteria based on the evaluation of fracture toughness of the material, its flaw growth characteristics, and assurance of adequate flaw growth potential. Key factors are the "No Failure" threshold stress intensity levels, selection of adequate proof test level, and interaction between cyclic and sustained loading.

The experimental approach was based upon Griffith-Irwin fracture criteria and utilized uniaxially surface-flawed fracture toughness specimens as well as pressure vessels made from 2219-T87 aluminum and 5Al-2.5Sn(ELI) titanium. Tests were conducted at -423°F, -320°F, and at room temperature, under static, sustained, and combined cyclic-sustained loading conditions. The obtained data was integrated with cyclic data from NAS 3-4194 program and presented in the form useful in design of cryogenic pressure vessels.

It has been shown that subcritical flaw growth and subsequent failure can occur under conditions of sustained stress. The cause of this growth is, at present, unknown, but may be related to high stress creep fracture of the plastically yielded material at the flaw tip, which exists even though the gross stress field is elastic. The intent of the effort described in this report was not to determine the reasons for such growth, but to determine the conditions under which it can occur and how it affects pressure vessel service performance.

A series of surface flawed fracture specimens with different initial flaw sizes and/or applied stress levels (i.e. different initial stress intensity values) have been tested to generate curves of K_{Ii} or K_{Ii}/K_{Ic} versus time to failure. Characteristically, it has been found that for a given material-environment combination there is a stress intensity level below which failure will not occur. This has been called the threshold stress intensity level. It was further observed that below this level time at maximum stress has little or no effect on subcritical cyclic flaw growth rates, but above the threshold failure cyclic life of specimens was significantly reduced.

All room-temperature specimens were tested in ambient atmosphere. The -320°F and -423°F tests were conducted in liquid nitrogen and liquid hydrogen environments, respectively. The sustained load testing was done by subjecting surface-flawed specimens to a target stress level, then leaving the specimens under the load for a specified period of time or until failure. Test specimens that did not fail under sustained loading after times ranging from a few minutes to several days were "marked" by subjecting them to low stress fatigue. Purpose of the "marking" was to introduce a differently textured fatigue area around the periphery of the flaw and thus, upon subsequent fracture, be able to determine the extent, if any, of sustained flaw growth.

A series of titanium and aluminum specimens were instrumented for detection and measurement of flaw opening displacements during the test run by using single wire strain gages mounted on the platelets attached to the lips of the surface flaw. The combined cyclic-sustained testing was done by modifying the 0-100-0 trapezoidal loading profile used on NAS 3-4194 program. The modification consisted of an increased hold time at maximum load from 15 seconds to 2.5 and 30 minutes, respectively.

v

Fractographic technique used for flaw size measurement has been developed during the experimental effort sponsored by the NASA Lewis NAS 3-4194 program and essentially consists of illuminating fracture surface with the polarized light.

Sustained testing of cylindrical tanks was done by pressurizing a given test tank to a desired hoop stress and holding at that pressure for a predetermined period of time or until failure. Flaw marking in the tanks, whenever the tank did not fail during the test, was accomplished by subjecting each tank to a repeated pressurization at relatively low pressure levels. Marking of some flaws was done by removing a portion of the shell containing surface flaw, straightening adjacent regions or by welding straight extensions when necessary. The flaw-containing portion of the shell was then marked as if it were an ordinary uniaxial surface-flawed specimen.

The sustained stress flaw growth data obtained on this program can be used in estimating the life of cryogenic pressure vessels subjected to extended periods of time at pressure, such as will be encountered in long term space missions. Also, the results of this program can be used in conjunction with the cyclic flaw growth data obtained on NASA Contract NAS 3-4194 (reported in CR 54837) to estimate the life of pressure vessels subjected to combined cyclic and sustained pressures. Assurance of safe life for extended pressure storage can be obtained by insuring that during the required life the maximum applied stress intensity in the vessel does not exceed the sustained stress threshold stress intensity value for the specific material and environment. A successful proof pressure test can be used to determine the maximum possible initial applied stress intensity in the vessel. The maximum initial to critical stress intensity ratio is equal to one divided by the ratio of the proof pressure to the maximum operating pressure. From the results of this program it is concluded

that below the "No Failure" threshold stress intensity level (i.e. that stress intensity above which delayed time failures can occur), time at pressure has little or no effect on cyclic flaw growth rates. Hence, the data reported in CR 54837 can be safely used to determine the number of pressure cycles required to increase the initial stress intensity to the threshold level. Above the threshold level, time at pressure can have a large effect on cyclic flaw growth rates and as a result cyclic life can be severely limited.

TABLE OF CONTENTS

LIST OF SYMBOLS

K_I — Opening mode stress intensity factor

K_{Ii} — Opening mode stress intensity factor at initial conditions

K_{Ic} — Critical stress intensity or fracture toughness of material

a — Semi-minor axis of the ellipse $\frac{x^2}{c^2} + \frac{y^2}{a^2} = 1$ or crack depth of the semi-elliptical surface flaw

$2c$ — Crack length of the semi-elliptical surface flaw

ϕ — Defined as $x = c \cos \phi$ and $y = a \sin \phi$

α — Polar angle measured from minor axis as shown in Figure 3

Φ — Complete elliptical integral of the second kind having modulus k defined as $k = \left(\frac{c^2 - a^2}{c^2} \right)^{1/2}$

σ — Uniform stress applied at infinity and perpendicular to the plane of crack

σ_{ys} — Uniaxial tensile yield strength

Q — $\Phi^2 - 0.212 \, (\sigma / \sigma_{ys})^2$

ν — Poisson's ratio of the material

E — Young's modulus

t — Thickness of plate

η — Crack opening displacement at the center of the elliptical crack

η_o — Flaw opening displacement at a point where the minor axis of flaw intersects the specimen surface

R — Internal radius of cylindrical shell

p — Applied pressure to the cylindrical shell

LIST OF ILLUSTRATIONS

LIST OF ILLUSTRATIONS (Continued)

LIST OF TABLES

1.0 INTRODUCTION

Cryogenic pressure vessels used in extended space missions will be
subjected to both multiple pressure cycles and prolonged periods of
time at a relatively constant pressure. The success of the mission
is dependent upon the prevention of premature vessel failure, i.e.,
either vessel leakage or catastrophic fracture. In order to prevent
failure it is necessary to predict with a reasonable degree of accuracy
the minimum possible service life. If this predicted life falls short of
that required, the design, i.e., materials, stress levels, etc., may
have to be modified.

Excluding the problem of possible service damage such as that due to
meteoroid impact, the minimum life of a pressure vessel depends upon
the largest flaw or defect sizes initially present in the vessel, the
critical flaw sizes required to cause fracture at normal operating stress
levels and the subxdritical flaw growth characteristics of the vessel
materials. With knowledge of the fracture toughness values of the
tankage materials, the applied stress levels, and the appropriate stress
intensity equations, the critical flaw sizes can be predicted. Deter-
mination of the initial flaw sizes depends on nondestructive inspection
procedures, which are of limited value in accurately defining flaw and
size. However, as pointed out in references 1 and 2, a properly
designed proof test will indicate the maximum possible initial flaw
sizes in the vessel. The two types of subcritical flaw growth of concern
are cyclic and sustained stress growth, which may or may not be
aggravated by the service environment.

This report describes an investigation by The Boeing Company from
June 1965 to December 1966 on plane-strain sustained flaw growth
in thick-walled cryogenic tanks under Contract NAS 3-6290. The

Specific aims of the program were to:

1)   Generate fracture toughness and sustained stress flaw growth
     data by testing unaxially loaded surface-flawed specimens;

2)   Establish how and under what conditions uniaxial data can be
     applied to cryogenic pressure vessel design;

3)   Verify the applicability of the uniaxial data to cryogenic tank
     design by pressure testing surface-flawed cylindrical tanks.

The materials selected for testing were 2219-T87 aluminum plate
1.25-inch thick and 5A1-2.5Sn(ELI) titanium plate 0.188-inch thick.
The aluminum was tested at room temperature, -320°F and -423°F,
and the titanium at -320°F and at -423°F. The room temperature
tests were conducted in ambient air; the -320°F and -423°F tests
were conducted in an environment of liquid nitrogen and liquid hydro-
gen, respect'vely. Flaw growth characteristics of both materials
were estal ished under sustained and combined cyclic-sustained
loading conditions.

The report is divided into sections describing experimental approach,
generated test data, and discussion of results. A brief discussion of
the stress intensity equations used in this investigation and the use
of the stress intensity concept in the evaluation of subcritical flaw
growth is presented in Section 2.0. Among elastic solutions discussed
are Irwin's solution for semi-elliptical surface flaw, Kobayashi's
solution for deep surface flaws and Smith's solution for semi-circular
surface flaw as well as his estimates for semi-elliptical deep surface
flaws. Detailed information on materials, fabrication, and testing
procedures is listed in Sections 3.0, 4.0 and 5.0, respectively.
The experimental results are presented in Section 6.0. Test
results for 2219-T87 aluminum and 6A1-4V titanium are grouped
according to test temperatures. Specific information on specimen

2

dimensions, test conditions and detailed test results are tabulated at the end of the report. Following the description of each group of data there is a graphic summary illustrating major trends. The overall discussion of test results, their significance and applicability to cryogenic pressure vessel design are discussed in Section 7.0, followed by Section 8.0 containing conclusions.

The information contained in this report is also released as a Boeing Document D2-114034-1.

2.0   TECHNICAL BACKGROUND

Following is a brief discussion of the stress intensity equations used
in this investigation and the use of the stress intensity concept in the
evaluation of cyclic, sustained stress and combined cyclic and
sustained stress subcritical flaw growth.

2.1   STRESS INTENSITY EQUATIONS

Relationships between stress intensity, flaw size, and nominal stress
field have been derived for a number of crack geometries and loading
conditions. In order to predict pressure vessel performance, solutions
for the semi-elliptical surface flaws are uppermost in importance. To
date several approximate solutions are available.

Irwin [3] first obtained a solution for a semi-elliptical surface flaw in a
plate and estimated that the solution may be valid for flaws with depth
up to about one-half the material thickness. As part of the Boeing
research and development program (IR&D), Kobayashi[4] arrived at
an approximate stress intensity solution for deep flaws having small
depth-to-length ratios, i.e., a/2c values. Smith derived a solution
for the semi-circular flaw in a semi-infinite body[5]. This solution
provided further refinement of the free surface correction Irwin used
in his equation. As part of the Boeing IR&D program, Smith estimated
what the free surface corrections should be for the semi-elliptical
surface flaws in a semi-infinite space [6].   He also obtained an
approximation of the stress intensity for the semi-circular surface
flaws which become very deep with respect to the thickness [6].
Using the single-edge-notch solution, i.e., a/2c = 0 of Gross, et.al., [7]
and his solution for the deep semi-circular flaw, Smith roughly
estimated stress intensity factors for deep surface flaws of intermediate
shape, i.e., a/2c ratios between 0 and .5 [6].

The experimental evidence obtained to date suggests that:

1) Irwin's estimated flaw depth limitation of 0.5t for his solution is approximately correct;

2) The stress intensity for deep semi-circular flaws can be reasonably approximated using Smith's solution;

3) The Kobayashi solution for deep flaws provides a reasonable approximation of the stress intensities for flaws with a/2c ratios < .30, but may tend slightly to underestimate the values for very small a/2c ratios;

4) The Smith estimates for deep semi-elliptical flaws will overestimate the stress intensities for flaws with small a/2c ratios, i.e., a/2c < .20.

Recognizing the inadequacy of the available stress intensity solutions for deep surface flaws (particularly for small a/2c ratios), Boeing initiated an IR&D program late in 1966 to obtain an analytical (numerical) solution to provide a better stress intensity value for flaw shapes ranging in a/2c from 0 to 0.5 and for flaw depths approaching the material thickness. This work is currently being performed and is scheduled to be completed by fall of 1967.

The stress intensity relationships for the surface flaw obtained by Irwin, Kobayashi, and Smith are summarized below.

2.1.1   Irwin Analysis

The Irwin relationship[3] for the semi-elliptical surface flaw in a finite thickness plate is as follows:

$$K_1^* = 1.1 \sqrt{\pi} \ \sigma \ (a/Q)^{1/2} \left[\frac{1}{c^2} (a^2 \cos^2 \phi + c^2 \sin^2 \phi) \right]^{1/4} \quad (1)$$

---

* See List of Symbols for definition of terms.

The maximum value of K_I occurs at the end of the semi-minor axis of the ellipse and has the value:

$$K_I = 1.1 \sqrt{\pi} \ \sigma \ (a/Q)^{1/2} \tag{2}$$

A plot of Q versus a/2c is shown in Figure 1.

The 1.1 coefficient was an estimate to account for the free surface effect. The equations were believed to be valid for flaw depths up to about one-half the plate thickness.

2.1.2   Kobayashi Analysis

For surface flaws that have a small depth to length ratio, i.e., a/2c, but are deep with respect to the plate thickness, Kobayashi assumed the following form for the stress intensity:

$$K_I = 1.1 \ M_K \ \frac{\sigma \sqrt{\pi a}}{\Phi} \tag{3}$$

where: $M_K = M_{kf} \times M_{kp}$

Following Irwin [3], the multiplying constant, 1.1, is taken to account for the effect of free surface on the stress intensity factor.

M_{kf} is the elastic stress magnitication due to deep flaw in an infinite strip under the conditions of plane strain.

M_{kp} is the stress magnification due to plastic yielding in an infinite plate under the conditions of plane strain.

A plot of M_K, i.e. $M_{kf} \times M_{kp}$, versus a/t is given in Figure 2 for $(\sigma / \sigma_{ys}) = 0.4$ and 0.8 for $\nu = 1/3$.

6

2.1.3 Smith Analysis

Smith's [5] linear elastic analysis of a semi-circular surface flaw in a semi-infinite body resulted in the following stress intensity relationship:

$$K_I = M_1 \; \frac{2 \sigma \sqrt{a}}{\sqrt{\pi}}$$

This result corresponds to that shown in equations (1) and (2) except that the 1.1 free surface correction assumed by Irwin is replaced by the M_1 coefficient, which is dependent upon location on the flaw periphery (Figure 3) and plasticity correction is not incorporated. From the figure it can be seen that M_1 varies from about 1.03 at the point of maximum flaw depth to 1.21 at the free surface. Unlike the Irwin equation the point of maximum stress intensity is predicted at the surface rather than at maximum flaw depth. However, for most materials the resistance to fracture is higher at the surface (i.e., higher than the plane strain fracture toughness value), so it is probable that fracture will initiate at a point below the surface where the applied stress intensity becomes tangent to the fracture toughness value. This is illustrated schematically in Figure 4.

For semi-elliptical flaws in semi-infinite bodies Smith [5] estimated the free surface coefficient, M_1'. This result is shown in Figure 5. The stress intensity relation thus becomes:

$$K_I = M_1' \; \sqrt{\pi} \; \sigma \; (a/Q)^{1/2} \tag{5}$$

where:

$$M_1' = M_1 \left[(\tfrac{a}{c})^2 \; \cos^2 \phi + \sin^2 \phi \right]^{1/4} \left[\frac{1.1}{M_1} - \left(\frac{1.1}{M_1} - 1 \right) \frac{a}{c} \right]$$

As seen in Figure 5 the point of maximum stress intensity occurs at the point of maximum flaw depth for all flaws with a/2c ratios less

7

than about .35 to .40. This is consistent with Irwin's analysis; however, the magnitude of the free surface corrections are slightly less than the 1.1 he estimated. Smith [6] obtained the stress intensity factors for semi-circular flaws in a finite thickness plate and estimated the stress intensity factors for semi-elliptical surface flaws in a plate as a function of a/2c and a/t ratios. The resulting relationship is:

$$K_I = M_1' \ M_k' \ \sqrt{\pi} \ \sigma \ (a/Q)^{1/2} \qquad\qquad (6)$$

M_k' is the finite thickness (or deep flaw stress intensity magnification) correction. The M_k', versus a/t curve for the semi-circular flaw and the estimated curves for semi-elliptical flaws with a/2c ratios of .20, .25 and .30 are shown in Figure 6.

In the analysis of the uniaxial and biaxial fracture specimen data obtained in this investigation equation (6) was used to determine stress intensity values. In the previous cyclic flaw growth investigation of 2219-T87 aluminum and 5Al-2.5Sn(ELI) annealed titanium, equation (2) was used to determine stress intensity values. For the majority of flaw sizes and shapes, i.e., a/2c ratios between .25 and .35 and a/t values < .5, used in these two investigations, equations (2) and (6) result in stress intensity values nearly the same.

2.2 SUBCRITICAL FLAW GROWTH

The use of stress intensity factors in the evaluation of subcritical cyclic flaw growth was presented in the final report on NASA Contract NAS 3-4194, "The Investigation of Plane Strain Cyclic Flaw Growth in Thick Walled Pressure Vessels" [8]. Briefly, it was shown that the total cyclic life of a pressure vessel is primarily a function of the magnitude of the maximum initial stress intensity as compared to

the critical value, i.e., the K_{Ii}/K_{Ic} ratio. This initial stress intensity is dependent upon the maximum cyclic stress level, σ , and the initial flaw size (a/Q). For a given material, temperature, and load profile a single K_{Ii}/K_{Ic} versus cycles curve can be obtained and used in conjunction with the knowledge of the initial flaw sizes (or maximum possible size as determined by a proof test) and the applied stresses to estimate cyclic life.

Because of the difficulty in making direct growth measurements during plane strain cyclic flaw growth tests, an "end point" approach was used. In this approach a series of specimens are cycled to failure, the initial and critical flaw sizes measured off the fracture face, the initial and critical stress intensities plotted against the total cycles to failure.

Figure 7 shows such a plot for 5Al-2.5Sn(ELI) titanium tested in liquid nitrogen. Several other illustrative and useful ways to plot such data are possible. One is shown in Figure 8. The applicability of this uniaxial fracture specimen data to biaxial stress fields (i.e. pressure vessels) has been demonstrated and the use of the data in predicting pressure vessel cyclic life, determining nondestructive inspection flaw acceptance limits, and selecting design factors presented [1] [2] [8] [9].

In addition to fatigue it has been shown that subcritical flaw growth and subsequent failure can occur under conditions of sustained stress [2] [10]. This growth is often environmentally dependent and has generally been attributed to either stress corrosion or hydrogen cracking. However, at high stress intensity levels this growth can occur in materials and environments not normally considered susceptible to these mechanisms. The cause of this growth is, at present, unknown, but may be related to high stressed creep fracture of the plastically yielded material at the flaw tip, which exists even though the gross stress field is

elastic.

The intent of the effort described in this report was not to determine the reasons for such growth, but to determine the conditions under which it can occur and how it affects pressure vessel service performance.

A series of surface flawed fracture specimens with different initial flaw sizes and/or applied stress levels (i.e. different initial stress intensity values) have been tested to generate curves of K_{Ii} or K_{Ii}/K_{Ic} versus time to failure. Characteristically, it has been found [2] [10] that for a specific material and environment there is a stress intensity level below which flaw growth and subsequent failure will not occur. This has been called the threshold stress intensity level [2]. Further, it has been hypothesized that below this level time at maximum stress should have little or no effect on subcritical cyclic flaw growth rates [2], but above the threshold failure could occur in as little as one cycle if the time at stress was sufficiently long. The key to predicting pressure vessel service performance is thus the accurate determination of the threshold level. Early experimental efforts utilized a "No Failure" threshold critieria whereby a number of specimens were loaded to various initial stress intensity levels and held until failure or for some predetermined maximum time. The threshold level was then selected as the K_{Ii} value just above that level where no failures were observed. This raised the question of whether or not failure would have occurred had those specimens, loaded just below the threshold level, been held for a longer time. In an attempt to eliminate nonconservative estimate of the threshold level, a "No Growth - No Failure" threshold criteria was needed. If the flaws remained stationary with time at load there would be no reason to believe they would grow with much longer times at load, and the selected threshold level would be safe for use in design and service life prediction. To prove the flaws did not grow, the speci- mens that did not fail during sustained loading were subjected to low stress fatigue and then pulled to fracture. The fracture face was then

10

examined to determine any presence of sustained stress growth. This general approach was used on a number of specimens tested in this program and is illustrated schematically in Figure 9.

An alternate procedure for ascertaining any flaw growth is the use of crack-growth-detection instrumentation during the course of the test run. Analytical solution of Green and Sneddon [11] for the elliptical crack embedded in an elastic solid, subjected to the uniform load normal to the crack surface and at infinity, gives an expression for the crack-opening displacement; it occurs at the diametrical center of the elliptical crack and is given by the equation

$$\eta = 4 \frac{(1 - \nu^2)}{E} \frac{\sigma a}{\Phi} \tag{7}$$

By following Irwin's [3] procedure to account for the effect of plastic yielding in equation (1), the flaw opening displacement for a surface flaw can be represented as

$$\eta_o = C_1 \frac{\sigma a}{\sqrt{Q}} \tag{8}$$

If η_o is measured and C_1 can be determined, then values of $a/\sqrt{Q}$ can be computed. In order to achieve this, a strain gage can be placed over the center of the crack at the face of a surface flawed specimen. To avoid large local strains, the gage must be left unbonded over some length. The strain recorded by such a gag ᵢ be proportional to the flaw opening displacement. Additional des ᵢion of the procedure for detection of flaw growth in establishing threshold stress intensity levels is given in Section 4.1.

Prior to investigation the authors believed the "No Failure" and the "No Growth - No Failure" threshold levels could be the same. That is, if flaw growth occurred it eventually would attain critical size and cause

fracture. Consequently, any evidence of flaw growth was considered unsafe. As pointed out in subsequent sections, this no longer appears to be true. The experimental evidence presented herein suggests that for some materials "No Failure - No Growth" criteria can be overly restrictive and the existence of a small amount of flaw growth may not necessarily lead to an eventual failure.

3.0 MATERIALS AND FABRICATION PROCEDURES

3.1 MATERIALS

The 5Al-2.5Sn(ELI) titanium plate, 0.188 by 24 by 72 inches, was purchased in the annealed condition per AMS 4910. The interstitial element content was not to exceed the following limits: C = 0.08 max.; N_2 = 0.05 max.; O_2 = 0.12 max.; H_2 = 0.0175 max.; and Fe = 0.25 max. The minimum yield strength of the annealed material was set at 100 ksi. The 5Al-2.5Sn(ELI) titanium plates were of the same melting heat and the same rolling batch. Chemical composition of the material, as reported by the supplier, was C = 0.025, Fe = 0.15, N_2 = 0.009, Al = 5.0, H_2 = 0.006 - 0.007, Sn = 2.2, Mn = 0.003, O_2 = 0.08. Vendor test results indicated typical mechanical properties of the material at room temperature to be F_{tu} = 122.5 ksi; F_{ty} = 115.0 ksi; Elong. = 17.0 percent. This material heat was designated by the vendor as G-28. All 5Al-2.5Sn (ELI) titanium specimens were fabricated and tested in the annealed condition. Chemical composition of the titanium plate is shown in Table 1.

Weld filler wire for welding titanium tanks was purchased per AMS 4953 except that maximum limits for the interstitial elements were set lower than those of the plate material: C = 0.01 max.; N_2 = 0.007 max.; O_2 = 0.063 max.; H_2 = 0.005 max.; Fe = 0.09 max. Chemical composition of the 5Al-2.5Sn(ELI) titanium wire is also listed in Table 1.

The 2219-T87 aluminum plate 1.25 x 72 x 120 inches was purchased per BMS 7-105C (equivalent to MIL-A-8920A ASG) in the T37 solution heat treated condition. Chemical composition of the material in percent by weight was reported by the vendor to fall within the following limits: V = 0.05 to 0.15; Zr = 0.10 to 0.25; Cu = 5.8 to 6.8; Mn =

0.20 to 0.40; Mg = 0.02 max.; Zn = 0.10 max.; Ti = 0.02 to 0.10; Si = 0.20 max.; Fe = 0.05 max.; others = 0.05 to 0.15. Mechanical properties of the material at room temperature in the T87 condition were 71.4 ksi ultimate strength, 58.7 ksi yield strength, and 9.5 percent elongation. This batch of material (8 plates) was designated by the vendor as Lot No. JE 52388-0. The material was used to fabricate all tank shells and all test specimens designated by AA, CA, and DA prefixes. Chemical composition of the aluminum plate is shown in Table 1.

Weld filler wire used to weld aluminum tanks was 0.063 inch in diameter and was purchased per BMS 7-75B Type II (equivalent to ASTM B-285-21T, "Tentative Specification for Aluminum and Aluminum-Alloy Welding Rods and Bare Electrodes". Chemical composition of the 2319 aluminum wire is also given in Table 1.

Several aluminum specimens were fabricated using remnants of the material used on the NAS 3-4194 program. These specimens were identified with a "C" prefix. Mechanical properties of the lot, as reported by the vendor, were 24.6 ksi ultimate, 12.3 ksi yield strength, and 17.6 percent elongation in the annealed condition and 58.7 ksi ultimate, 39.0 ksi yield strength, and 11.0 percent elongation in the T62 condition. Chemical composition of the material was within the same limits as Lot No. JE 52388-0, shown in Table 1. Mechanical properties of the material at room temperature in the T87 condition were F_{tu} = 69.5 ksi, F_{ty} = 56.5 ksi, and 15 percent elongation.

Toward the end of the program three specimens, designated by "AC" prefixes, were fabricated from the 2219-T87 plate used on the program in support of the evaluation of Saturn S-IC tankage materials (Ref. 12). Chemical composition and properties of that material batch were also within the BMS 7-105C specification. Mechanical properties of the

material in the T87 condition were F_{tu} = 69.2 ksi, F_{ty} = 57.3 ksi.

3.2   FABRICATION PROCEDURES

3.2.1   Uniaxial Test Specimens

Smooth tensile specimens used for determining mechanical properties of the annealed 5Al-2.5Sn(ELI) titanium are shown in Figure 10. Surface-flawed specimens used to determine sustained and cyclic flaw growth characteristics of the titanium at -320°F and -423°F are shown in Figure 11.

Smooth test specimens used for the determination of mechanical properties of the 2219-T87 aluminum are shown in Figure 12. Surface-flawed specimens 0.6-inch thick are shown in Figure 13. The 0.6-inch-thick specimens were fabricated from the 1.25-inch-thick plate to provide uniaxial test specimens of the same thickness as the shell walls of the test tanks. The material used for fabrication of specimens was cut into specimen blanks, then heat treated from T37 to T87 condition.

All initial flaws in titanium and aluminum surface-flawed specimens were prepared by using an electric discharge machine (EDM) to introduce initial flaws with a terminating radius of less than 0.003 inch. The EDM flaws were then extended under low stress tension fatigue. The maximum cyclic stress level used on 5Al-2.5Sn(ELI) titanium specimens was 40 ksi, and for the surface-flawed 2219-T87 aluminum, from 15 to 20 ksi. The number of cycles required to extend the initial flaws varied from specimen to specimen, depending upon the initial flaw size, but was usually between 3 and 90 thousand cycles for titanium and between 4 and 25 thousand cycles for aluminum. The specimens were cycled at 700 to 1200 cycles per minute.

Low stress fatigue extension is considered part of specimen preparation for testing and is assumed to have no effect upon measured fracture toughness of flaw growth characteristics of either material (Reference 1).

3.2.2   Biaxial Test Specimens (Cylindrical Tanks)

Sustained flaw growth characteristics of 5Al-2.5Sn(ELI) titanium under biaxial loading conditions were determined at -423°F using 15-inch-diameter cylindrical pressure vessels shown in Figure 14. Extension of the EDM flaws was initially scheduled to use low-stress cyclic pressurization of a complete tank at room temperature. However, due to premature titanium weld-metal failures encountered during the course of the NAS 3-4194 program, the EDM flaws were extended by low-stress flexing of shell sections. Basic weld settings using a gas tungsten arc (GTA) welding process are shown in Table 2. All weldments in titanium tanks were left in the as-welded condition. Shell thickness of the completed tanks was reduced from .200 to about .170 inch by chem-milling.

Sustained flaw growth characteristics of 2219-T87 aluminum under biaxial loading conditions were determined using 19-inch-diameter 2219-T87 aluminum tanks shown in Figure 15. Aluminum plate used for fabrication of the 19-inch-diameter test tanks was break-formed to make shell sections with 9.38 internal radius and 30-inches long. The shell sections were trimmed to size, then welded using GTA welding process. The basic weld settings are shown in Table 2. The weld edge preparations are shown in detailed views in Figure 15. The completed shell was then aged to T87 condition.

Initial EDM flaws in the 2219-T87 test tanks were extended by

pressurizing the entire tank with tap water at a cyclic frequency of about 20-25 cycles per minute. As the first of the aluminum tanks was tested immediately after the EDM extension, it was discovered that the material had delaminated during final phases of the EDM extension. The EDM extension was done at 18.3 ksi hoop stress. In the second tank, the EDM was extended by cyclic pressurization at a lower (15.9 ksi) hoop stress. Fractographic examination of the second tank also revealed a sizable delamination formed during the EDM extension.

The problem of delamination was successfully resolved on the third and fourth aluminum tanks by local submergence of EDM flaws in liquid nitrogen during low-stress cyclic extension of the EDM flaws. Thermal stresses locally induced by temperature differential in the shell of the tank were about 4-5 ksi hoop stress, permitting reduction of hoop stresses. EDM flaws in both tanks were extended by such pressure-cycles; both had good fatigue extension with no delaminations.

4.0   EXPERIMENTAL PROCEDURE

4.1   UNIAXIAL SPECIMENS

All room-temperature specimens were tested in ambient atmosphere
in an enclosed building with temperatures ranging between 65 and 85°F.
A strain rate of 0.005 in./in./minute was used on all smooth tensile
specimens until the material yield strength was reached. A strain rate
of 0.02 in./in./minute was then used for the remaining portion of the
loading sequence until failure. Static fracture toughness specimens
were pulled at a rate needed to precipitate a complete fracture within 1
to 3 minutes after initial application of the load. The same loading rates
were also used for liquid nitrogen (-320°F) and liquid hydrogen (-423°F)
testing.

The -320°F and -423°F tests were conducted in liquid nitrogen and liquid
hydrogen environments, respectively. The liquid nitrogen was introduced
into a wrap-around cryostat to keep the gage area of each specimen com-
pletely submerged during the entire test sequence. The -423°F tests
were conducted in a similar manner, except that the entire specimen
including grips was submerged in liquid hydrogen.

The sustained load testing was done by subjecting surface-flawed
specimens to a target stress level, then leaving the specimens under
the load for a specified period of time or until failure. Each fractured
specimen was dried with hot air, then protectively wrapped to preserve
it for fractographic analysis and flaw size measurements. Some speci-
mens that did not fail under sustained loading after times ranging from
a few minutes to several days were "marked" by subjecting them to low
stress fatigue similar to initial EDM extension except at slightly higher
stress levels. Purpose of the "marking" was to introduce a differently
textured fatigue area around the periphery of the flaw and thus, upon

subsequent fracture, be able to determine the extent, if any, of sustained flaw growth. Marking of the specimens was done usually at the same temperature and in the same environment used for sustained load testing. Exceptions were specimens tested at -423°F in a liquid hydrogen environment and several specimens tested at room temperature and at -320°F. Several specimens were tested under sustained loading at room temperature but were marked at -320°F. This was done to see possible differences in flat growth indications as a result of different marking techniques. Subsequent to marking, the specimens were either pulled to failure, then examined, or subjected to still another test run under sustained load. In some instances this was repeated two or three times resulting in several test runs on the same specimen. In other specimens multiple test runs in the same specimen were conducted without intermittent marking but rather by raising the load level after a period of time.

A series of titanium and aluminum specimens were instrumented for detection and measurement of flaw opening displacements during the test run. Essential elements of such instrumentation excluding recording equipment are shown in Figure 16. The single strand wire gage was bonded with Duco or Mithra 200 cement on each end. The gage sensitivity was determined from the gage resistance, R, gage factor K, resistance change, ΔR, and strain using conventional relationship of $\varepsilon = \Delta R / RK$. Flaw opening measurements were made using standard readout systems such as BLH SR4 indicators as well as X-Y plotter systems that were ΔR calibrated. Since no evaluation of the gage systems with partially unbounded lengths were made for sustained load applications in cryogenic environments, it was decided to limit presentation of the data to qualitative indications of the increase of resistance as a function of load without calculating actual opening in terms of micro-inches. Test sequences on all instrumented specimens followed the same general pattern used for the non-instrumented specimens.

19

The combined cyclic-sustained testing was done by modifying the 0-100-0 trapezoidal loading profile used on NAS 3-4194 program. The modification consisted of an increased hold time at maximum load from 15 seconds to 2.5 and 30 minutes, respectively. The trapezoidal loading profile was generated by dividing each cyclic period into four equal parts. The first part was spent in going from zero load to maximum load; the second in holding the specimen at maximum load; the third in unloading; and the fourth part at zero load.

In addition to the specimens tested under modified trapezoidal loading, selected specimens were tested at cyclic frequencies of 34, 5, and 2 cycles per minute. The load profiles in 5 and 2 cycles per minute were essentially trapezoidal, but the 34 cycles per minute profile was generated by the sinusoidal load programmer. All cyclically loaded specimens were tested until failure. Fractured specimens were protectively wrapped and subjected to fractographic analysis and flaw size measurements.

Fractographic technique used for flaw size measurement has been developed during the experimental effort sponsored by the NASA Lewis NAS 3-4194 program (Reference 8) and essentially consists of a beam of white light passing through the first polaroid filter, which is positioned so that its plane of polarization is parallel to the upper edge of an optical glass reflector. Light transmitted through the first filter is plane-polarized and reflected from the glass plate vertically downward on fracture specimens without rotating the polarization plane. Upon striking the specimen surface, some of the plane-polarized light rays are reflected under a shallow angle with respect to the horizontal plane and are scattered outside the optical axis of a camera. Others are reflected upward, pass through glass plate without rotation, and then are cross-polarized by the second polarizing screen. Still other rays strike the somewhat obliquely oriented flat surfaces and are reflected upward with resultant

rotation of the polarizing plane. These rays pass more readily through the second polarizing plate and are recorded on the film. The degree of shading or contrast attained is apparently a measure of relative density and distribution of reasonably flat and obliquely oriented surfaces.

Initial and critical surface flaw dimensions were determined directly from fractographs showing outlines of initial and critical flaw regions. Depth of the flaws (a-dimensions) were measured directly from the fractograph. Flaw lengths, due to flaw shape irregularities, were calculated first by planimetering flaw area, then calculating the surface flaw length (2c-dimension), assuming the shape to be truly elliptical. Static fracture toughness (K_{Ic}) and applied stress intensity levels for all specimens were calculated using equation (6).

4.2   BIAXIAL SPECIMENS (CYLINDRICAL TANKS)

Sustained testing of cylindrical tanks was done by pressurizing a given test tank to a desired hoop stress and holding at that pressure for a predetermined period of time or until failure. A schematic diagram of a pressure and control system used for room temperature testing of aluminum tanks is shown in Figure 17. Testing of the aluminum tanks at -423°F was done using two different pressure systems. One system utilized a cryogenic pump of 20 gallons per minute pumping capacity at 6000 psi outlet pressure; the other, high pressure helium bottles. Schematic representation of the two systems is shown in Figures 18 and 19, respectively.

Care was exercised to protect fracture surfaces from staining or other damage that would obscure evidence of flaw growth. Each aluminum tank had two identical flaws. Titanium tanks were fabricated earlier and contained only one flaw each, but each flaw was the same shape and size. Flaw marking in the tanks, whenever the tank did not fail during

the test, was accomplished by subjecting each tank to a repeated pressurization at relatively low pressure levels. Marking of some flaws was done by removing a portion of the shell containing surface flaw, straightening adjacent regions or by welding straight extensions when necessary. The flaw-containing portion of the shell was then marked as if it were an ordinary uniaxial surface-flawed specimen. Subsequent to marking the portion of the shell was pulled to failure to expose fracture faces for fractographic examination.

One aluminum tank, after burst at lower than expected pressure level, was sectioned to determine fracture toughness of the shell material and to compare it with the uniaxial data. A portion of the material was cut from the shell, straightened (except for about one inch in the middle), and a surface-flawed specimen machined from it. To eliminate the curvature and yet not introduce residual stresses, thickness of the entire specimen was machined down from 0.60 to 0.4 inch. The specimen was then EDM flawed, fatigued, and pulled to failure at -320°F in the usual manner.

Creep characteristics of the 2219-T87 aluminum and 5Al-2.5Sn(ELI) titanium were spot-checked by testing standard creep specimens at room temperature in ambient air and at -320°F in a liquid nitrogen environment. The creep data was generated only to the extent necessary for comparison of the behavior of the two materials under sustained load in the absence of an artificial flaw.

5.0   TEST RESULTS

5.1   2219-T87 ALUMINUM TEST DATA

5.1.1 Mechanical Properties and Static Fracture Toughness

Mechanica! roperties of the 2219-T87 aluminum plate were determined
at room temperature, -320°F and -423°F in ambient air, liquid nitrogen,
and liquid hydrogen environments, respectively. Two smooth tensile
specimens were tested at -423°F and one each at -320°F and at room
temperature. All specimens were pulled in the long transverse grain
direction, i.e., the plate rolling direction was transverse with respect
to the longitudinal axis of the specimens. Table 3 lists ultimate strength,
0.2 percent offset as well as 0.02 percent offset yield strength, elongation
in 2.0 inch gage length and percent reduction of area. The results are
plotted in Figure 20 as a function of test temperature and compared with
similar data generated during the course of NAS 3-4194 program.
(Reference 8). Solid lines in Figure 20 are directly abstracted from
the NAS 3-4194 final report NASA CR-54837.

Static fracture toughness of 2219-T87 aluminum was determined at room
temperature, -320°F and at -423°F. Three surface-flawed specimens
were pulled at each temperature. All specimens were pulled in the long
transverse grain direction. Specimen dimensions, flaw sizes, and
calculated fracture toughness values are listed in Table 4 for all three
test temperature. The results are plotted in Figure 21 and compared
with similar data generated during the course of NAS 3-4194 program.
The solid line in Figure 21 represents static fracture toughness values
reported in the NAS 3-4194 final report.

5.1.2   2219-T87 Aluminum (Sustained Flaw Growth at Room
         Temperature)

Sustained flaw growth characteristics of 2219-T87 aluminum at room
temperature were investigated by testing five groups of specimens.
The Group I test series was designed to provide information on sustained
stress threshold level; Group II, to verify that information by testing
specimens for prolonged periods.   Test specimens in Group III were
used to generate data with shorter hold time at sustained stress.
Group IV specimens were used to check the effect of flaw marking
techniques.   These specimens were marked at -320°F rather than at
room temperature. Finally, Group V test specimens were instrumented
for detection and measurement of the flaw opening displacements.

5.1.2.1   Group 1 (Room Temperature)

A total of ten specimens were tested. Specimen dimensions, test con-
ditions, and flaw size measurements are listed in Table 5, Group I
section. The make-up of the table is typical for all aluminum fracture
toughness specimens and consists of 14 major headings. The first four
list specimen identification number, specimen size, conditions of cyclic
extension of the EDM flaws, and flaw size before the test run. The
fifth shows conditions of the sustained test run in terms of temperature,
maximum stress level, time in hours at maximum stress and applied
stress intensity level K, as calculated at the point of maximum flaw
growth. The distinction was necessitated by the fact that in some
specimens the extent of flaw growth was largest in the direction other
than the maximum depth; i.e., $\alpha \neq 0$.

Flaw size after the test run, angular direction of maximum flaw growth,
α , actual flaw growth increment as measured perpendicularly to the

24

flaw curvature at the point of maximum flaw growth and the calculated K level at that point are shown under the sixth heading. Conditions of flaw marking, flaw size after marking and fracture stress at failure are shown under the next three headings.

The next four columns list K_{Ic} values calculated at the point of maximum flaw depth along minor axis, i.e., $\alpha = 0$, K_{Ic} values at $\alpha \neq 0$, K_{Ii}/K_{Ic} ratio of initial to critical stress intensity calculated at the beginning of the test run, and K_{If}/K_{Ic} ratio of stress intensity calculated at the point of largest flaw growth increment at the end of the test run, i.e., using final dimensions of the flaw. The last column shows symbols used to represent corresponding points in the graphic presentation of the results.

5.1.2.2   Group II (Room Temperature)

This group consists of two specimens subjected to sustained loading for a prolonged period. Pertinent specimen and flaw dimension as well as test conditions are listed in Table 5, Group II section. One specimen was held at the load for 123.7 hours, the other for 115.6 hours.

5.1.2.3   Group III (Room Temperature)

These specimens were tested to provide greater variation of time at sustained loading. Detailed information pertaining to specimen dimensions and test conditions is shown in Table 6, Group III section. Make-up of the table is identical to Table 5. The material used to fabricate all specimens except specimen No. CA-44 came from a portion of a plate used in NAS 3-4194 program. Hold time at maximum stress covered a range from 0.02 to 30.0 hours.

5.1.2.4   Group IV (Room Temperature)

This group was added to the program after it was discovered that
marking at -320°F eliminated some flaw growth indications produced
by marking at room temperature for stress intensity levels below
22.0 ksi $\sqrt{in}$.   Test results for this group of specimens are listed
in Table 6, Group IV section.   These specimens were flaw marked
at -320°F.

5.1.2.5   Group V (Room Temperature)

These specimens were tested to generate flaw opening displacement
data that in turn could be related to the flaw growth.   The results are
summarized in Table 7, Group V section.   Table make-up is the same
as those preceding.   Specimen CA-34 was loaded to progressively
higher stresses until flaw opening continued to increase without
corresponding increase of stress level.   The loading was then stopped
until flaw growth (increase in flaw opening) ceased.   Four such runs
were made initially covering stresses of 27.9, 32.5, 32.2, and 41.8
ksi.   The fourth run continued for 18.7 hours; the specimen was then
unloaded and marked at room temperature.   During the four runs of
0.4, 1.1, 1.3, and 18.7 hours, the flaw increased by 0.012 inch.
Summary of the flaw opening displacement indications for the 18.7 hour
run is shown in Figure 22.   In the column of "Flaw Size After the Test
Run" under "Flaw Depth", a flag note $\triangleright$ indicates that incremental
flaw growth for individual test runs could not be readily established.
After marking, the specimen once again was subjected to sustained
load testing under progressively higher stress levels.   After the final
test run at 43.1 ksi for 0.2 hour, the specimen broke at 43.7 ksi in
an effort to reach 44.4 ksi stress level.

A second specimen (DA-33) was similarly tested in two sequences. A complete set of graph charts for flaw opening versus time to failure records for the first test sequence is shown in Figures 23 and 24. The sequence was started by applying load at ten percent increments of the full scale deflection and allowing a minute or two waiting period to mark position of the pen on the chart. The purpose of incremental loading was to check linearity of crack opening as a function of load level. As a load corresponding to the load index value of 70 percent was reached, the flaw opening continued to increase while the load remained at a steady level of 70 percent. Suspecting possibility of a gage creep, the load was dumped to zero; in about ten minutes the specimen was reloaded to 70 percent. The gage stretched plastically during the first loading sequence to 70 percent and did not react to increasing loading until 60 percent level was reached. At 60 percent level, the strain-load relationship did not appear to have been impaired by prior plastic stretching of the gage as judged by the same span between 70 and 60 percent level indications during the second load sequence. The recording pen was reset to the original zero and the load was raised to a new target value of 75 percent (full deflection of 100 percent corresponds in this case to 260,000 lbs. load). The specimen was then left at that load for 16.6 hours, after which it was unloaded and marked by subjection to 2,000 cycles at 32.1 ksi stress level.

Strain gage output versus time for the second test sequence (after the cyclic marking) is shown in Figure 25. As seen from the load index numbers on the trace, the gage did not respond until 60 percent load index number was reached. Upon reaching the 70 percent level the strain gage output between 60 and 70 percent was smaller than a corresponding increase from 60 to 70 percent during the initial load sequence (see Figure 23). The increase in load to 78.2, then to 80.3 percent load index value resulted in continued increase of flaw opening. The specimen was left at that load until fracture.

5.1.2.6   Data Analysis for 2219-T87 Aluminum at Room Temperature

The combined test data generated for the 2219-T87 aluminum at room temperature is plotted in Figure 26 in terms of K_{Ii}/K_{Ic} ratio versus time to fracture or at sustained load. All specimen test runs are divided into four categories: those that did not fail and showed no evidence of flaw growth; those that did not fail but had small amounts of flaw growth followed by apparent arrest; those that did not fail during the test run but exhibited appreciable amounts of flaw growth in the manner precluding certain arrest; and those that failed under the sustained loading. The No-Failure threshold stress intensity level was established by visually fitting a curve to separate data points representing sustained load failures and flaw growth with no apparent arrest from the specimens exhibiting small amounts of flaw growth with subsequent arrest as well as specimens with no indications of flaw growth. The No-Growth threshold level line was drawn to separate the latter two categories of specimens, i.e., those showing no flaw growth and those showing some flaw growth with subsequent arrest.

The distinction between arresting and unstable flaw growth in 2219-T87 aluminum at room temperature is illustrated in Figure 27 by plotting the data in terms of K_I/K_{Ic} ratio versus time to failure or at sustained load. The main difference in this manner of presentation as opposed to that in Figure 26 is that the K_I/K_{Ic} ratio reflects changes in applied stress intensity level as a result of flaw growth during the test run. At the beginning of the test run the K_I/K_{Ic} ratios are calculated using K_{Ii}; at the end of the run the K_I/K_{Ic} ratios are calculated by using K_{If} to reflect increase in stress intensity due to the flaw growth. The progressive increase in stress intensity is tracked by grouping specimens with nearly identical initial stress intensity levels and following along the best-fit line through their respective terminating K_{If}/K_{Ic} points. In several instances direct flaw opening measurements were

28

available to assist in shaping the lines. The No-Failure and the No-Failure - No Flaw growth threshold stress intensity level lines were then drawn to separate corresponding groups of specimens and provide substantiation of the similar grouping shown in Figure 26. See Section 6.2.1 for detailed discussion of results shown in Figures 26 and 27.

5.1.3   2219-T87 Aluminum (Sustained Flaw Growth at -320°F)

Sustained flaw growth characteristics of 2219-T87 aluminum at -320°F were investigated by testing four groups of specimens: Group I specimens were used to establish threshold stress intensity level; Group II to verify threshold stress intensity level by subjecting specimens to sustained loading for prolonged periods. Effect of initial flaw extension technique upon sustained flaw growth was checked with specimens of Group III; Group IV specimens were instrumented for detection and measurement of flaw opening displacements.

5.1.3.1   Group I (-320°F)

A total of nine specimens were tested. Specimen dimensions, test conditions and flaw size measurements are listed in Table 8, Group I section. Initial stress intensity values (K_{Ii}) were calculated for all specimens at the point of maximum flaw growth. K_{If} values were calculated including the extent of flaw growth during the test run. K_{Ic} values were calculated only for the specimens deliberately pulled to failure. In other cases average K_{Ic} value for the material was used.

5.1.3.2   Group II (-320°F)

Two specimens were tested in this group: CA-40 and CA-48. Test results

are listed in Table 8, Group II section. Specimen CA-40 was held at maximum load of 43.3 ksi for 120.0 hours. The flaw was then marked and the load increased to 48.7 ksi. The specimen failed after 0.2 hour at that load. Specimen CA-48 was held at a maximum load of 37.9 ksi for 125.1 hours, then marked and pulled to failure. Marking of both specimens was done at -320°F.

5.1.3.3   Group III (-320°F)

Test results are listed in Table 9, Group III section. Specimen AC-7 had prior load history at room temperature. (See Table 6, Group IV data). At the end of room temperature test run this specimen was marked at -320°F, then subjected to sustained load at -320°F. The initial flaw for the -320°F test run was initiated at -320°F. It is assumed that prior exposure to sustained load at room temperature affected only the region that was subsequently traversed by the -320°F marking. Specimen AC-7 was subjected to stress intensity at 26.9 ksi $\sqrt{in}$ for one hour, then marked and pulled to failure at -320°F. No indication of any flaw growth was present. Specimen AC-9 was subjected to two test runs of one hour each. The first run was at K_{Ii} of 22.7 ksi $\sqrt{in}$ and the second at K_{Ii} of 31.1 ksi $\sqrt{in}$. After the second test run, the specimen failed during cyclic marking at -320°F with the flaw almost completely growing through the thickness.

5.1.3.4   Group IV (-320°F)

Both specimens in this group (AA-59 and DA-36, Table 9, Group IV section) were instrumented for detection and measurement of flaw opening displacements during sustained load test runs. Single wire strain gages in both specimens were applied to provide a slack in the

unbounded portion of the gage. In this manner the extent of plastic straining of the gage during testing was reduced. Flaw opening curves for both specimens are shown in Figure 28.

Specimen AA-59 had the largest flaw and was subjected to lower stress levels. The loading was done in three increments of 5 percent total scale deflection. Upon reaching load index of 59.1 percent the specimen was left for 0.37 hour. As the flaw remained stable, the load was raised to 60.9 percent of 38.6 ksi level. The specimen was left at that load for 16.0 hours, then the load was raised to 39.6 ksi as it appeared that flaw remained stationary (no increase in flaw opening). After 0.4 hour at that load the flaw still appeared stable and the load was raised once more, now to 40.6 ksi, or a load index of 64.0. The flaw opening began to increase rapidly and the specimen failed within 30 seconds.

Specimen DA-36 had a considerably smaller initial flaw than specimen AA-59. In order to generate the same initial stress intensity of about 38 ksi $\sqrt{in}$ the specimen was stressed to a high stress level of 56.3 ksi. The specimen was loaded in two stages, first to 80 percent index level in increments of 10 percent. Due to deliberately introduced slack in the single gage wire, the gage did not respond until a load value of 60 percent was reached. Upon reaching the 80 percent level the load was dropped first to 70, then to 60 percent level, then raised in several increments until 88.7 percent level was reached. Immediately upon reaching that load, the flaw opening displacement increased at a gradually faster rate until the specimen failed under sustained loading at the end of 0.3 hour.

5.1.3.5   Data Analysis for 2219-T87 Aluminum at -320°F

The combined test data generated for the 2219-T87 aluminum at -320°F

31

is plotted in Figure 29 in terms of K_{Ii}/K_{Ic} ratio versus time to failure or at sustained load. The -320°F test data are divided into four categories with respect to the extent of flaw growth, just as were the room temperature data points. The No-Failure threshold stress intensity line is drawn below data points depicting failures and flaw growth with no apparent arrest. The No-Growth threshold stress intensity line is drawn between data points for small amount of flaw growth with subsequent arrest and data points with no flaw growth indications. Included in the figure is a sustained load test data point obtained using a 35-inch diameter pressure vessel in the course of the material evaluation for Saturn S-IC tankage on NAS 8-5608 program.

The arresting and unstable flaw growth in 2219-T87 aluminum at -320°F is illustrated in Figure 30. The plot is similar to the one used to represent room temperature data in Figure 27. The K_I/K_{Ic} ratios are calculated at the beginning and end of each test run. The No-Failure threshold level is established by separating test runs with unstable flaw growth from the ones that were stabilized. Test results generated during the course of the Saturn S-IC program are also included.

5.1.4   2219-T87 Aluminum (Sustained Flaw Growth at -423°F)

Sustained flaw growth characteristic of 2219-T87 aluminum at -423°F were investigated by testing two groups of specimens. Specimen dimensions, test conditions and flaw sizes for both groups are listed in Table 10. The Group I specimens were tested to determine the threshold stress intensity level. Initial flaw depths for different specimens varied from one third to one half the specimen thickness. Duration of test run for each specimen in this group was between 10 to 12 hours. All specimens were marked and pulled to failure at room temperature. With the exception of specimen CA-45, static fracture toughness, as

measured in the specimen after exposure to sustained loading at -423°F, was very close to the average room temperature value. Examination of specimen CA-45 revealed a sizable delamination at the tip of a flaw apparently formed during flaw marking. Fracture face of this specimen was photographed using ordinary illumination and is shown in Figure 31 together with a cross section view of the specimen. The high value of 39. 7 ksi$\sqrt{\text{in}}$ apparently was caused by delamination at the tip of the flaw.

Specimen DA-18 was the only specimen tested in Group II. The initial flaw was deeper than expected, thus generating a stress intensity of 37.8 ksi$\sqrt{\text{in}}$ or 86 percent of the K_{Ic}. The specimen was unloaded at the end of 44 hours, marked, then pulled to failure. There was a flaw extension of 0.010 inch.

5.1.4.1   Data Analysis for 2219-T87 Aluminum at -423°F

The available test data for the 2219-T87 aluminum tested at -423°F are plotted in Figure 32 in terms of K_{Ii}/K_{Ic} ratio versus time at maximum load. The same data are plotted in terms of K_I/K_{Ic} ratio using K_I values at the beginning and K_{If} at the end of each test run in Figure 33. The No-Failure and the No-Growth - No Failure threshold stress intensity levels were estimated to fall at 87 and 75 percent, respectively. The two points at about 88 and 89 percent of the K_{Ic} value were considered to represent unstable flaw growth although increase of the flaw size in these specimens was not rapid enough to preclude arrest if the test sequence was continued for a longer period.

5.1.5   2219-T87 Aluminum (Combined Cyclic-Sustained Flaw Growth at -320°F)

This work was done with the intention of combining cyclic flaw growth data

33

obtained in previously concluded NAS 3-4194 program (Reference 8) with the sustained flaw growth data generated on this program. Specimens were tested under cyclic loading but with different hold time at maximum stress level. The purpose of the test was to show that if hold time at maximum load is varied and the specimens in question are subjected to stress intensity below the threshold level, there will be little if any effect upon cyclic life. If, on the other hand, similar specimens are subjected to stress intensity above the threshold stress intensity level, there will be a significant effect upon cyclic life. Two groups of specimens were tested for this purpose. The first group was subjected to stress intensity levels below the threshold level; the other, above.

5.1.5.1   Group I (Cyclic-Sustained at -320°F)

This group consisted of six specimens. Specimen dimensions, test conditions, and flaw size measurements are listed in Table 11, Group I section. Specimens AA-56, -55, and -6 contained deep initial flaws (about 50 percent of thickness) and were cycled at relatively low stress levels. Specimens DA-29, -26, and -30 had shallow initial flaws (about 25 percent thickness) and were cycled at somewhat higher stress levels. Since all specimens in this group were targeted at stress intensity levels below the threshold value, cyclic life was expected to be comparable to the values generated in the NAS 3-4194 program.

5.1.5.2   Group II (Cyclic-Sustained at -320°F)

A total of nine specimens were tested. Specimen dimensions, test conditions, and flaw size measurements are listed in Table 11, Group II section. Five specimens coded with an AA prefix contained deep flaws and were subjected to relatively low but considerably higher stress

levels than those applied to comparable specimens in Group I. The resultant stress intensity levels were to be higher and the specimens, while under cyclic loading with prolonged period of time at maximum stress levels, were expected to fail sooner. Specimens coded with the DA prefix contained small flaws and were subjected to higher stress lev. l.. Likewise, they were expected to fail sooner than comparable specimens in Group I. Specimen AA-57 was a rerun of specimen AA-53. Due to malfunction of equipment, specimen ʌA-53 received several overloads during cyclic testing and was deliberately pulled to failure at the end of 48 cycles. All remaining specimens failed under cyclic loading at -320°F.

5.1.5.3   Analysis ̶ Combined Cyclic-Sustained Test Results for
2219-T87 Aluminum at -320°F

The combined cyclic-sustained flaw growth data for the 2219-T87 aluminum at -320°F are plotted in Figure 34 in terms of K_{Ii}/K_{Ic} ratio versus cycles to failure. The K_{Ic} value used in calculations is the average fracture toughness of 41.8 ksi$\sqrt{in}$ as determined earlier by testing three static test specimens at -320°F. The K_{Ii} values were computed using equation (6), except that in place of depth correction factor M_k' an average value 1/2 $(M_{kc}' + M_{ki}')$ was used. In this manner, cyclic life of specimens with deep flaws was compensated for the effect of flaw depth and could be compared with cyclic life established for specimens with shallow flaws. The M_I' factors also should have been replaced with the average value 1/2 $(M_{Ic}' + M_{Ii}')$. However, as is evident in Table 11, the a/2c values were changing very little as the flaw increased in depth until critical value was reached; and since M_I' is a function of the a/2c ratio only for α = constant (in this case α = 0), the M_I' calculated for initial flaw size was considered sufficiently accurate for use on deep flaws.

The solid line passing through the point on the ordinate corresponding to K_{Ii}/K_{Ic} ratio equal to one in Figure 34 and extending to the right into 5000 cycles region has been directly abstracted from NASA CR-54837. This line represents cyclic flaw growth data generated on NAS 3-4194 using shallow-flawed 2219-T87 aluminum specimens tested at -320°F. The data points shown in Figure 34 represent information obtained on the present program. The time at maximum load is depicted by the symbols noted in the legend. The threshold stress intensity line is drawn just below the points departing from the solid line as a result of longer hold time at maximum load. One exception is specimen DA-28 with considerably shorter life than could be expected, since time at maximum load was only 0.007 minute. Fractographic examination of specimen DA-28 and a thorough review of loading record failed to reveal any discrepancies that would explain shorter life span.

The same combined cyclic-sustained flaw growth data is represented in a somewhat different way in Figure 35. This data is plotted in terms of applied stress intensity K_{Ii} as listed in Table 11 versus actual-to-calculated cyclic life ratio. Actual cyclic life in number of cycles to failure was taken directly from Table 11. The calculated cyclic life was derived by using cyclic flaw growth rates, as established and reported previously in the NAS 3-4194 program, and initial and critical flaw dimensions as measured on specimens tested on this program. Cyclic life was calculated as follows:

Each region of cyclic flaw growth from initial to critical value was divided into equal parts; in this case, five increments were used. For each increment an average K_{Ii} value was calculated using equation (6). If applied stress level was close to the 45 ksi, as in specimens

DA-29, -26, and -30, the average flaw growth rate $[d(a/Q)/dN$ in - inch per cycle] for that increment of flaw growth was taken directly from Figure 62 in NAS 3-4194 final report NASA CR-54837. Knowing the $\Delta(a/Q)$ for the increment, a total number of cycles (ΔN) required to traverse that distance for a given K_{Ii} stress intensity level was calculated. The process was repeated for the remaining increments and total calculated cyclic life for the specimen was arrived at by adding all ΔN quantities.

In cases when applied stress levels varied widely from the one used in establishing Figure 62 (NAS 3-4194 report), cyclic flaw growth data as reported in CR-54837 for 2219-T87 aluminum at -320°F under 0-100-0 cyclic loading profile was recalculated to get flaw growth rates (d/dN of a/Q in micro-inches per cycle) for a corresponding stress level. The reasons for doing so are discussed in Section 6.1.3 of the NASA CR-54837 report (Reference 8). Resorting to this technique, it was possible not only to account for the effects of deep flaws but also to compare actual flaw growth rates with those obtained from the end-point-analysis of NAS 3-4194 data. The threshold stress intensity line is drawn just below the points exhibiting significant departure from the calculated cyclic life. At this point it may be of interest to compare the threshold stress intensity levels shown in Figures 29, 30, 34, and 35.

5.1.6   2219-T87 Aluminum Tank Tests

Two 2219-T87 aluminum test tanks were tested at room temperature. Pertinent tank dimensions, condition of EDM extension, flaw sizes before and after testing, duration of test runs, test conditions, and

final burst together with flaw marking data are listed in Table 12.
The first tank (Serial No. 0001) was pressurized to a hoop stress of
33.2 ksi and held for 178 hours. The hoop stress was calculated by
PR/t formula using nominal internal radius of 9.7 inches, internal
pressure of 2050 psi and actual shell thickness in the vicinity of the
flaw (in this case 0.600 inch). The tank flaw was marked in two
stages. There were 500 pressure cycles at an equivalent hoop stress
of 18.3 ksi and additional 2500 cycles at a hoop stress of 19.4 ksi.
Upon conclusion of the marking the tank was burst at a hoop stress of
42.7 ksi with a resultant K_{Ic} value of 32.1 ksi$\sqrt{in}$ at the point of
maximum flaw growth.

Fractographic examination of fracture⁻ㅕ ·ctions revealed that (1)
the first flaw in the tank showed a severe delamination at the tip of the
EDM extension and (2) flaw growth to the extent of 0.012 of an inch was
along 78 degree line from the minor axis of the ellipse (a-direction).
Data points for the first tank are plotted in Figures 26 and 27 along
with the uniaxial data for room temperature testing. The overall
appearance of tank Serial No. 0001 after the burst test with a close-
up view of the fracture origin is shown in Figure 36.

Since the sustained test run of the first tank at K_{Ii} of 23.9 ksi$\sqrt{in}$
resulted in flaw extension, the second tank was subjected to lower K_{Ii}
value of 21.2 ksi$\sqrt{in}$. The tank was held at the load for 132 hours,
then marked and burst at room temperature. The resultant K_{Ic} value
at the point of maximum flaw growth (α = 71 degrees) was 32.1 ksi$\sqrt{in}$.
The flaw was still delaminated at the tip and, as in the first tank, there
was a flaw growth (0.010 inch along 71 degree line from minor

axis of the ellipse.) Data points for the second tank are also plotted
in Figures 26 and 27. Second flaw in tank Serial No. 0002, as well
as the one in the first tank, were sectioned and photographed to show
the extent of delamination. Figure 37 shows cross sectional view of
the two flaws. The initial as well as end point values (K_{Ic}'s) for the
two tanks were augmented by 7 percent as suggested in Section 6.4.1
in order to compensate for the curvature effect of cylindrical shell.

5.1.6.2   -423°F Tank Test Data

Two 2219-T87 aluminum test tanks were tested at -423°F in a liquid
hydrogen environment. Pertinent information on tank dimensions, flaw
extension, test conditions, marking and burst data are summarized in
Table 13. Test data are calculated for both flaws in each tank.

Tank No. 0003 was scheduled for sustained test run at K_{Ii} of about 90
percent of the K_{Ic} value of 43.8 ksi $\sqrt{in}$. Malfunction of the cryogenic
pump precluded use of the pressurization system shown in Figure 19.
Instead, a system utilizing high pressure helium bottles (Figure 18)
was used. First, the tank was completely filled and submerged in liquid
hydrogen, then pressurized with helium to 1960 psi; the pressure could
not be sustained and the test run terminated. After modifying the
system with addition of high pressure helium bottles, the tank was
again pressurized for a few minutes to 3190 psi; apparent leaks in the
system forced test termination. Final attempt was made after re-
working the seals and augmenting high pressure helium supply. The
tank burst at 3135 psi pressure level with ensuing explosion and fire
at the test site.

Fractographic examination of the first flaw indicated that the tank was
subjected to a stress intensity level of 42.2 ksi $\sqrt{in}$ or 96 percent of the

average K_{Ic} value for the material at -423°F. Upon sectioning, the K_{Ii} level in the second flaw was determined at 41.2 ksi $\sqrt{in}$. Both flaws were clear of delaminations. The extent of growth in the first flaw could not be positively established. Examination of the second flaw (after cyclic marking of the shell section) revealed flaw extension of 0.006 inch. The tank is shown in Figure 38.

Tank No. 0004 was to be subjected to sustained pressure of 2050 psi with the intent of generating stress intensity below the threshold level. The cryogenic pump was used in view of the violent burst experienced with the high pressure helium pressurization system. The cryogenic pump system was set-up essentially as diagrammed in Figure 19 except that pressure feed back was to be read off the dial and compensated by manual adjustments. During the first attempt the pump pressure output suddenly increased causing overpressure to 2360 psi. The pressure was dumped, but on the next attempt the same run-away tendency prevailed. By dropping the pressure to 250 psi the pump v 3 stabilized and a final attempt to pressurize was made. A new target pressure of 2390 was reached, but upon closing all valves pressure gradually dropped to 2090 psi in less than a minute. The pump was started to repressurize the tank, but the pressure overshot the target and the tank burst at 2620 psi. Chart record of the pressure versus time plot is shown in Figure 39. Numbers next to the pressure peaks are pressure readings in psig.

Fractographic examination of fracture faces revealed that tank No. 0004 was subected to 34.4 ksi $\sqrt{in}$ stress intensity level in the first flaw and 34.8 ksi $\sqrt{in}$ in the second. Fracture originated in the first flaw and ran longitudinally through both heads and through the second flaw. There were no delaminations at the tip of either flaw. Calculated values of stress intensity were augmented by 7 percent to account for shell curvature. Careful review of load calibration data and pressure gage •

readings failed to reveal any discrepancies other than relatively rapid tank loading sequence.

Possible variation of material properties in tank No. 0004 was checked by removing a portion of the shell and machining a static fracture toughness specimen from it. The specimen was pulled to fracture at -320°F with resultant fracture toughness value of 45.6 ksi$\sqrt{in}$. The effect of loading rate was checked at -320°F by programming a surface flawed specimen AC-5 (not shown in the Tables) through a loading sequence similar to the one experienced by tank No. 0004. Calculated fracture toughness value for that specimen was also comparable to the average fracture toughness K_{Ic} data for the material. Both tests suggest that there were no unusual discrepancies in the material properties.

5.2   5A1-2.5Sn(ELI) TITANIUM TEST DATA

5.2.1   Mechanical Properties and Static Fracture Toughness

Mechanical properties of the 5A1-2.5Sn(ELI) titanium plate were determined at room temperature, -320°F, and -423°F in ambient air, liquid nitrogen and liquid hydrogen environments, respectively. Two smooth tensile specimens were tested at -423°F and one each at -320°F and at room temperature. All tensile specimens were pulled in the longitudinal grain direction. Table 14 lists ultimate strength, 0.2 and 0.02 offset yield strength, and percent elongation in 1.0 and 2.0 inches gage length. Seizure of the extensometer rods during testing of specimen TT-3 limited test data for that specimen to ultimate strength and percent elongation. The test results are plotted in Figure 40 as a function of test temperature and compared with similar data generated during the course of NAS 3-4194 (Reference 8) program.

Solid lines in Figure 40 are abstracted directly from NAS 3-4194 final report, NASA CR-54837.

Static fracture toughness of 5Al-2.5Sn(ELI) titanium plate was determined at -320°F and at -423°F. Specimen dimensions, flaw sizes, and test conditions are listed in Table 15. All static fracture toughness specimens were pulled in the longitudinal grain direction. Average values for the material at -320°F were established by plotting static fracture toughness (K_{Ic}) together with K_{Ic} values obtained during sustained and combined cyclic-sustained testing. The data are summarized in Figure 41 in terms of K_{Ic} versus fracture stress level.

Average value for the material at -423°F was established by summarizing all statically tested specimens together with specimens that failed upon loading during the sustained load testing. The plot of these data is shown in Figure 42.

5.2.2   Sustained Flaw Growth at -320°F

Sustained flaw growth characteristics of 5Al-2.5Sn(ELI) titanium were investigated by testing three groups of specimens: Group I to provide information on sustained threshold stress intensity level; Group II to verify the results of the first group by testing specimens for a prolonged period and Group III to generate flaw opening displacement data using automatic recording devices.

5.2.2.1   Group I

Eleven specimens were tested. Specimen dimensions, flaw sizes, and test conditions are listed in Table 16. Table make-up is similar

to that for aluminum data. An average K_{Ic} for the material of 68.4 ksi$\sqrt{in}$ was used to calculate the K_{Ii}/K_{Ic} ratios. There was no cyclic marking of these specimens. Likewise, none of the specimens were instrumented for detection of surface-flaw opening displacement. Some differently textured regions near the flaw front were noted in some specimens, but these could not be conclusively identified as flaw extensions during the sustained load test sequences.

5.2.2.2   Group II

Results of the two specimens tested in this group are listed in Table 17. Specimen 5T-12 was subjected to several test runs at a constant stress level of 138.9 ksi. The first test ran 76.9 hours, then the test sequence was interrupted for 16.7 hours when the specimen was left unloaded. The specimen was unloaded, warmed to room temperature, and subjected to 7,000 cycles at 40.4 ksi stress level to mark the flaw outline and at the same time increase its size so that the next test run, even though at the same stress level, would be conducted at a higher stress intensity (K_{Ii}) value.

Upon conclusion of the marking, the specimen 5T-12 was once again subjected to sustained loading for 92.3 hours, then marked again at 40.0 ksi but using 10,000 cycles. The sustained test run was repeated for 24.1 hours. The specimen was then marked at room temperature and pulled to failure at -320°F. Examination of the fractured specimen using polarized light and an electron microscope suggests that there was no flaw growth during any of the sustained test runs.

Specimen 8T-3 was tested in a similar manner. There were four sustained load test runs of 119.7, 39.4, 64.5, and 26.7 hours, respectively. Intermittent marking was done after each run. The

stress level for each run was kept constant at 117.3 ksi. During the last run the flow of nitrogen into the cryostat was accidentally interrupted, the specimen warmed up and failed. Examination of the fractured surfaces revealed no evidence of sustained flaw growth during the test runs.

5.2.2.3   Group III

Several specimens were tested in this group. Specimen dimensions, flaw sizes and test conditions are summarized in Tables 18 and 19. Two specimens (5T-15 and 5T-18) failed under uninterrupted sustained load test run. The remaining specimens were subjected to multiple runs. Each specimen was instrumented with strain gages to measure flaw opening displacement during the test.

Specimen 4T-15 was subjected to sustained load of 158.3 ksi for 21.1 hours. After approximately three hours the load threaded rod section of the grips broke and had to be replaced. The specimen was allowed to warm to room temperature until a new rod was made and installed. The test was then resumed and continued until the specimen failed at 21.1 hours. The flaw opening measurements were taken manually using Wheatstone Bridge circuit. Flaw opening displacements for the entire test run are summarized in Figure 43.

Specimen 5T-18 was subjected to a sustained load of 165.0 ksi for 34.0 hours until failure. The flaw opening displacements were measured and recorded using automatic tracing device. Composite records of the flaw opening displacements for the entire run are shown in Figures 44, 45 and 46.

Specimen 5T-48 was subjected to several test sequences with two prolonged interruptions between the test runs. The malfunction of strain

gage instrumentation equipment precluded generation of complete flaw opening data for this specimen. Fractographic examination of the specimen revealed stained region at the tip of the initial flaw. Neither the exact extent nor the time of occurrence could be positively identified. The specimen failed at the end of the last run.

Specimen 6T-21 was subjected to sustained loading of 156.8 ksi stress level for 22.7 hours. The stress was raised to 164.6 ksi and the specimen failed after 0.4 hour at that stress level. There was a total flaw growth of 0.017 inch. Composite records of flaw opening displacement are shown in Figures 47, 48, and 49.

Specimen 9T-29 was subjected to several test runs at progressively higher stress levels. The flaw opening displacements remained stable during the sustained test runs until the specimen abruptly failed upon loading. It was presumed that the specimen did not have any flaw growth.

Specimen 9T-83 was also subjected to several test runs ranging in sustained stress levels from 117.3 ksi for the first test run to 133.6 ksi for the last. During the last run the specimen fractured after 0.01 hour at the load. The composite flaw opening displacement charts are shown in Figures 50 through 53. Some flaw growth took place during the last test run as indicated by the flaw opening displacements.

5.2.2.4   Analysis of Sustained Load Flaw Growth Data for 5A1-2.5Sn(ELI) Titanium at -320°F

The data obtained is divided into two groups: (1) data generated using high stress level (150 to 175 ksi), and (2) data generated using stress levels below 150 ksi. The first group is plotted in Figure 54 in terms of K_{Ii}/K_{Ic} ratios versus time to failure or at the maximum load. The

data points within the group are identified by symbols representing test runs culminating in a sustained load failure, test runs resulting in no sustained load failure but an indication of flaw growth, and test runs that resulted in no failure and no detectable flaw growth. There were also specimens in which possible extent of flaw growth could not positively be established. The No-Failure threshold level line is drawn below points representing failures and those with observed flaw growth.

The low-to-medium stress level specimens are summarized in Figure 55 in terms of K_{Ii}/K_{Ic} ratio versus time to failure or at maximum load. The No-Failure threshold stress intensity level line is drawn above the points showing no evidence of flaw growth.

5.2.3   5A1-2.5Sn(ELI) Titanium (Sustained Flaw Growth at -423°F)

Sustained flaw growth characteristics were investigated by testing one group of 13 specimens. Specimen dimensions, flaw sizes, and test conditions are summarized in Table 20. The initial flaw depths varied from 0.043 inch to 0.089 inch, and the stresses ranged from 83.6 to 162.8 ksi.

Upon conclusion of the sustained load test runs specimens were marked at room temperatures, then broke open at -320°F to expose fracture surfaces for flaw size measurements. Test specimens that failed upon loading at -423°F were used to calculate static fracture toughness values for the material at -423°F.

5.2.3.1   Analysis of Sustained Load Data for 5A1-2.5Sn(ELI) Titanium at -423°F

Data plotted in Figure 56 in terms of K_{Ii}/K_{Ic} ratio versus time to

46

failure or at maximum load is divided into three categories: (1) specimens that failed under loading, (2) specimens that exhibited flaw growth, and (3) specimens that had no indication of flaw growth. The No-Failure threshold level is drawn below the point representing failure under sustained load. Several points above the line could have had flaw growth, but conclusive identification was not possible. Some data points with no flaw growth are above the line, suggesting data overlap.

5.2.4   5Al-2.5Sn(ELI) Titanium (Combined Cyclic Sustained Flaw Growth at -320°F)

This portion of the experimental work provided correlation between test data generated under NAS 3-4194 program (Reference 8) and the sustained flaw growth data obtained during the course of the present program. Two groups of specimens were tested. The first group was subjected to stress intensity levels below the threshold; the other, above. Each group was subdivided into high and low stress level specimens.

5.2.4.1   Group I (Cyclic-Sustained Tests of 5Al-2.5Sn(ELI) Titanium at -320°F)

Twelve specimens were tested. Specimen dimensions, flaw sizes and test conditions are listed in Table 21. Four specimens were cycled to failure at a high stress level of 162.2 ksi or 90 percent of the uniaxial yield strength of the material. The remaining six specimens were cycled to failure at 138.9 ksi or 77 percent of the uniaxial yield strength. All initial flaws were confined within one third the material thickness. Critical flaw depths (flaw depth at fracture) in the four high stress (162.2 ksi) specimens were confined within one half the material thickness. Test specimens cycled to failure at a lower stress of 138.9 ksi

were brought to failure with the critical flaws exceeding one half the material thickness.

Specimens 3T-7 and 3T-10 were cycled to failure at a frequency of 35 and 5 cycles per minute, respectively. The loading profile in specimen 3T-7 was sinusoidal; the loading profile for specimen 3T-10 was generated by truncating sinusoidal wave and thus was similar to the trapezoidal loading used for specimens cycled at low frequency. Specimen 3T-8 was cycled at a frequency of one cycle per minute under trapezoidal loading profile. Specimen 3T-50 was cycled to failure while being subjected to prolonged hold-time (2.5 minutes) at maximum load.

The low stress specimens were cycled to failure in a similar manner except one additional specimen was tested at cyclic frequency of 2 cycles per minute and one with hold time of 30 minutes at maximum stress.

5.2.4.2   Group II (Cyclic-Sustained Tests of 5Al-2.5Sn(ELI) Titanium at -320°F)

These specimens were tested to determine the effect of hold time at maximum stress while the specimen is subjected to stress intensity level above the threshold value. As in Group I, high and low stress levels were used. Specimen dimensions, flaw sizes, and test conditions are summarized in Table 22. Test specimens coded with 3T prefix contained small initial flaws and were cycled at high stress levels (95 percent of the uniaxial yield strength of the material); test specimens coded with prefix 8T contained larger initial flaws and were cycled at lower stress level of about 74 percent. Several specimens broke upon loading or immediately upon reaching the load.

48

5.2.4.3   Analysis of Cyclic-Sustained Test Results for 5Al-2.5Sn
(ELI) Titanium at -320°F

The combined low-stress cyclic-sustained flaw growth data are plotted
in Figure 57 in terms of the K_{Ii}/K_{Ic} ratio versus cycles to failure.
Various hold times at maximum cyclic stress are identified by the
corresponding symbols. For comparison with previous data, a cyclic
life curve is reproduced from the NAS 3-4194 final report.

High stress test data are plotted in Figure 58 in a similar manner.
For comparison with previously obtained data, a cyclic life curve is
also reproduced from the NAS 3-4194 final report. In addition, a pre-
dicted cyclic life curve shows the correlation between sustained and
cyclic flaw growth data. The predicted cyclic life curve was con-
structed by using 82 percent No-Failure threshold stress intensity level
as determined by using sustained flaw growth data and calculating
cyclic life (number of cycles to failure) for lower stress intensities
but for long hold time at the maximum stress. For example, cyclic
life of a specimen cycled with a frequency of 1 cpm at a stress intensity
level of 82 percent of K_{Ic} would be 260 cycles. It may be hypothesized
that the same specimen, if held for a prolonged period of time at a
stress intensity slightly higher than 82 percent of the K_{Ic} value, would
fail under sustained load or during its first cycle. Subjecting a specimen
to cyclic loading with prolonged hold time at maximum stress at a K_I
level of 75 percent of the K_{Ic} value, the specimen would sustain 480
cycles if there were no sustained load interaction, i.e., if the threshold
level were at 100 percent of the K_{Ic} value. However, cyclic life of that
specimen will be reduced because in actual case there will be sustained
load interaction once the threshold value reaches 82 percent level.
The interaction will shorten cyclic life of the specimen by 260 cycles,
or the value of cyclic life in number of cycles to failure at stress in-
tensity level of 82 percent. Thus, cyclic life of a specimen at 75 per-
cent K_{Ic} level with long hold time at maximum stress would be 480 minus

260 cycles or 220 cycles. The point corresponding to K_{Ii}/K_{Ic} of 75 percent and 220 cycles becomes one point on the predicted curve that can be completed the same way by taking lower K_{Ii}/K_{Ic} values. For K_{Ii}/K_{Ic} of 70 percent, combined cyclic sustained life is 740 minus 260 or 480 cycles, etc.

If the predicted combined cyclic-sustained curve represents cyclic life with the long hold time at maximum stress, then all specimens tested at a shorter hold time at maximum stress should fall above the predicted line. Examination of available data verifies this.

5.2.5 Titanium Tank Tests

Two 5Al-2.5Sn(ELI) titanium tanks were tested on this program. Both tanks were tested at -423°F. Pertinent tank dimensions, conditions of flaw preparation and testing are listed in Table 23.

The first tank was targeted to be pressurized to 2975 psi. During the first test attempt, just as the tank was completely submerged in liquid hydrogen and the pump started, the vent stack from the large dewar caught fire and the test was aborted; the fire was confined with no damage to the test site or equipment. Another test was made after valve replacement at the vent stack. The tank was pressurized to a target pressure level to 2960 psi. The system was sealed, but pressure began to decay; the pump was periodically used to repressurize the system. During the run of about 1-1/2 hours the pressure fluctuated between 3100 and 2800 psi. The test was terminated as the pump began to cavitate.

At completion of the run the tank was pressure-cycled using hydraulic oil at room temperature to mark outline of the flaw and thus determine possible extent of slow growth during the sustained load test run. After

subjecting the tank to 5000 cycles at hoop stress of 50 ksi, it was burst at -423°F in liquid hydrogen. The tank reached a pressure of 4000 psi (line limit) but did not burst. The tank was cycled manually until failure. Upon third cycle the tank burst at 3775 psi. The burst was violent, scattering tank pieces over the entire test area. Unfortunately, the fracture faces containing surface flaw were obliterated. However, since both tanks contained identical flaws an estimate of the resultant initial and critical stress intensities could be made by using flaw dimensions from the second tank.

The second tank test was conducted after replacing damaged system components. The tank was pressurized to 3500 psi and held for 2-3/4 hours. The pump ran smoothly with no pressure peaks and no pump cavitations, but the system could not be sealed. The pump was put on automatic control and left running. As a precaution against possible burst and obliteration of fracture face, the tank was wrapped with two loose coils of annealed 6061 aluminum sheet 0.10 inch thick to absorb burst impact in case of fracture. Upon conclusion of the test run, the tank was removed from the cryostat and sectioned to examine and measure the flaw size. There was no flaw growth during sustained load test run. Calculated K_{Ii} was 48.9 ksi $\sqrt{in}$ or 90 percent of the K_{Ic} value for the material at -423°F. Using the same initial flaw size for the first tank resulted in calculated K_{Ic} value for that tank equal to 53.6 ksi $\sqrt{in}$. The average value for the material at -423°F is 54.5 ksi $\sqrt{in}$. Data points from both tanks are plotted together with the uniaxial data in Figure 56.

6.0 DISCUSSION OF TEST RESULTS

Several aspects of the present program warrant additional consideration.
Introduction of flaw opening displacement measurement data along with
the cyclic marking of the flaw peripheries after sustained load testing
provided a better understanding of the flaw growth phenomenon and its
significance. The analytical approach has been broadened to include
lateral flaw growth, limited consideration of the flaws that are deep with
respect to specimen thickness, and interaction between cyclic and
sustained loading conditions. The primary data analysis goal was
realistic assessment of the safe load carrying capabilities of the two
materials under sustained and cyclic loading conditions in the presence
of cryogenic environments.

6.1 THRESHOLD STRESS INTENSITY CONCEPT

As pointed out in Section 2.2, earlier experimental work involving
sustained load testing centered around the idea that by testing a series of
specimens at progressively higher stress intensity levels a curve
would be generated that separates "Failure" points from "No-Failure"
points. In application to actual hardware, the usable stress range or
the permissible flaw sizes in the material would be adjusted to insure
that none of the possible pre-existing flaws would generate stress intensity
level (K_I) above the threshold level. The approach is safe if the duration
of the laboratory test exceeds the expected time of service by an appreciable
margin. However, in situations where test time is limited or expected
design stress intensity levels are uncomfortably close to the threshold
value, the "Failure - No-Failure" criteria appear to be deficient.
An understanding of the flaw behavior at the stress intensity levels just
below the threshold levels becomes essential. More sophisticated data
analysis techniques coupled with metallurgical laboratory support

indicated that for a certain range of stress intensity levels below the "Failure - No-Failure" curve, flaws actually grew. Indications of partial growth were presumed to be synonymous with initiation of flaw growth that would eventually lead to fracture.

The necessity of describing, then predicting the behavior of crack-like flaws in a structure is reflected in the objectives set forth in this program. Work statement called for flaw growth measurements that, in selected cases, were to utilize at least two independent techniques. The two techniques (in addition to generating the Failure - No-Failure data used on this program) were partial exposure of specimens to sustained load with subsequent marking after the test run and strain gage measurements of flaw opening displacements during the test. This information, coupled with the laboratory analysis utilizing polarized light and, in some cases, electron microscope fractography, revealed more specific details on flaw behavior that were not available previously. It became apparent that in the 2219-T87 aluminum, flaws grew at relatively low stress intensity levels. But flaw opening displacement data and tracing of the flaw progression (growth) in several specimens subjected to similar stress intensity levels lead to the realization that the flaw growth inception was not always followed by continually increasing flaw growth and eventual failure. In fact, very definite indications of a complete flaw growth arrest were noted in some instrumented specimens. It is necessary, therefore, not only to distinguish the difference between "Failure - No Failure" and "No Growth - No Failure" criteria, but also between stable (self-arresting) and unstable (continually increasing) flaw growth. In the latter case it is presumed that if a laboratory test or a service is extended the possibility of a failure could not be excluded. In cases of No-Growth, of course, the possibility of failure may be completely ruled out.

6.2   2219-T87 ALUMINUM DATA

6.2.1   Sustained Flaw Growth at Room Temperature

Directing attention to Figure 26 which summarizes the sustained stress
life data for 2219-T87 aluminum at room temperature, and to Figure 27,
where the same data is plotted showing progressive increase of applied
stress intensity level as a result of flaw growth, it may be noted that
while the No Failure threshold stress intensity level is 90 percent of the
K_{Ic} for the material, the No Growth threshold is about 63 percent.
Flaw growth records and loading history of several specimens will be
used to illustrate the behavior of flaws at different stress intensity
levels.

Starting at the bottom of Figure 27 and proceeding upward it will be
noted that two specimens (C4-1 depicted by a symbol ⬧ , and AC-8
Q) were subjected to a stress intensity level of 43 and 47 percent
of K_{Ic} (see Table 6). Neither of the two specimens showed any signs
of flaw growth. The cluster of three specimens (C-6, C-7, C-9,
Table 6, symbols ⬦ , ρ , ◻ , respectively) were tested at a stress
intensity level of about 52 percent, and each showed a flaw increase
of 0.004 to 0.006 inch. The flag note ▷ next to the line represent-
ing the three points denotes that the flaw growth indication in these speci-
mens was a result of flaw marking technique rather than a true indication
of flaw growth.

Justification is readily verified by examining the test data at higher stress
intensities, i.e., data points for specimens C6-1 ◼,and second test run
in AC-8 ◙ , Table 6. The former was subjected to a stress intensity
of 59 percent and the latter to 62 percent of the K_{Ic} value for the material.
Neither specimen showed signs of flaw growth. The main difference between

the two groups of specimens is that specimens C-6, C-7 and C-9 were cyclically marked at room temperature while specimens C6-1 and AC-8 were marked at -320°F. Specimens C-7 and C6-1 are shown in Figure 59 illustrating the effect of marking technique.

There were 22 test runs, including two pressure vessels, for stress intensity levels between the No-Growth and No-Failure thresholds. Two specimens as well as both pressure vessels were held under sustained loading for more than 100 hours each. The extent of flaw growth in pressure vessels Serial No. 0001 and 0002 is illustrated in Figures 60 and 61, respectively. Both tanks had a severe delamination at the tip of the flaw and the flaw grew sideways in both tanks. Effectivenss of polarized light illumination for fractographic examination of specimens is evident when comparing pictures taken using white light illumination with those using polarized light. For comparison with the tanks, fractographs of two specimens (CA-41 ▼ and CA-43 ▼ Table 5, Group II section) are shown in Figures 62 and 63, respectively.

Returning to Figure 27, the self-arresting tendency of the flaws subjected to stress intensity level below the No-Failure threshold may be illustrated by considering three groups of specimens. The first group consists of specimens CA-43 ▼ and C8-1 ◕ (Tables 5 and 6, respectively). Both specimens were subjected to identical stress intensity of 81 percent of K_{Ic}. Assuming identical flaw behavior, the trace is drawn through initial and final points of both specimens. Examination of the trace indicates that flaw growth after the first hour under the load stops. The same phenomenon may be observed in the second and third groups comprised of specimens C-1 ⊠ and CA-39 X in the second group, and CA-37 ☐, second test run in AC-7 ▲ and C-4 ◈ in the third group (see tables 5 and 6 for detailed data). Fractographs of specimens C-1 and C-4 are shown in Figure 64. Both specimens, while void of delamination, showed that the flaw growth increment was larger in the sideways than in the depth (along

a-axis) direction. Final flaw sizes in specimens held for longer periods at comparable stress intensity levels suggest that the flaw growth was stabilizing.

Another group is comprised of specimens C-8 ▽ and CA-42 ⊖ . In both cases the flaw extended sideways. The flaw growth in specimen C-8 took place during the first minute at sustained load while specimen CA-42 was under the same stress intensity level for 4.6 hours. A trace through these two points in Figure 27 clearly indicates the self-arresting tendency even at this high stress intensity level.

At points above the No-Failure threshold level some actual failures under sustained load occurred. Furthermore, the two specimens instrumented for measurements of flaw opening displacement (specimens CA-34 ⊖ and DA-33 ⊟ in Table 7) clearly suggest that with time the flaw growth was continually increasing. Specimen DA-33 failed under sustained loading, as did specimens CA-12 ▲ and AA-50 ● (Table 5). Fractographs of specimens CA-34 and DA-33 are shown in Figure 65.

Thus, for specimens subjected to stress intensity levels above 90 percent of K_{Ic} failure under sustained load is likely to occur.

6.2.2   Sustained Flaw Growth at -320°F

Determination of the threshold stress intensity levels for the 2219-T87 aluminum tested at -320°F was based on more exact information; in addition to the sustained flaw growth data generated in the usual manner, data from specimens tested under combined cyclic-sustained loading on this program and from specimens tested under cyclic loading conditions on NAS 3-4194 program were available. These data offer an opportunity not only to supply additional information on the material

behavior but also to provide a direct check upon the threshold criteria. As pointed out in Section 2.0, the threshold stress intensity concept may be incorporated in cyclic testing of specimens by introducing a different hold time at maximum stress level. It was postulated earlier that for such cyclically loaded specimens there will be no significant effect upon cyclic life until the stress intensity reaches the threshold level. The available sustained and cyclic-sustained data for aluminum is used to illustrate the analysis as well as to arrive at a realistic conclusion for use of 2219-T87 aluminum in cryogenic applications.

Analysis of the sustained load test data for 2219-T87 aluminum at -320°F is similar to room temperature data. The -320°F sustained stress flaw growth data is summarized in Figures 29 and 30. The No-Growth threshold stress intensity level is at about 73 percent of the K_{Ic} value for the material and the No-Failure threshold level is at 82 percent of the K_{Ic}, just above the group of specimens exhibiting flaw growth arrest tendency (specimens AA-49 ▮ and CA-40 ▨). First and second test runs in specimen CA-38 identified by symbols ⊙ and ▣ , respectively, and the first run in specimen DA-31 identified by symbol ▮ are considered to fall into the category of flaw growth that would lead to eventual fracture. Above that level were several failures under sustained load. Flaw growth patterns for specimen DA-36 X were traced to failure and helped define curve shapes for similar specimens and a tank included in Figure 30. Tank test results were abstracted from the test program conducted in support of the material evaluation for Saturn S-IC tankage. Figure 66 shows fractographs of specimens CA-40 ▨ and DA-31 ▮ representing points below and above the No-Failure threshold stress intensity level, respectively. Note considerably larger flaw extension in specimen DA-31 as compared with specimen CA-40 even though the latter was held under load for 120 hours as compared to 18.9 hours for the former.

57

6.2.3   Combined Cyclic-Sustained Test Data at -320°F

Verification of the threshold stress level for the 2219-T87 aluminum
tested at -320°F is provided by the combined cyclic-sustained flaw
growth data obtained on this program and cyclic flaw growth data
generated earlier on NAS 3-4194 program. Both sets of data are
summarized in Figure 24. Interaction between sustained and cyclic
loading conditions does not commence until the applied stress intensity
level exceeds about 80 percent of the K_{Ic} value. The interaction manifests
itself by departure from the cyclic life curve established on NAS 3-4194
program. This coincides with the threshold value established for the
sustained data (Figures 29 and 30).

6.3   5 Al-2.5 Sn (ELI) TITANIUM DATA

Analysis of the titanium data generated on this program as well as the
test results obtained on NAS 3-4194 program indicates that behavior
of the two batches of material is comparable and the test results are
mutually complementary once a common plane of reference has been
established.

6.3.1   Sustained Flaw Growth

The sustained flaw growth data for 5Al-2.5 Sn(ELI) titanium at -320°F
are divided into two categories: (1) test specimens subjected to high
stress (above 150 ksi) and (2) test specimens subjected to stresses
below 150 ksi. Distinction by stress level in addition to stress
intensity K may cause some concern because of the apparent descriptive
insufficiency of the K parameter. The parameter K encompasses the
stress level as well as the flaw size. The stress level enters into the

58

picture via correction for plastic zone and assurance that
condition of gross elastic stress fields in the specimen are main-
tained throughout the test. Examination of the 5Al-2.5Sn(ELI)
titanium data indicates that the effect of stress level became prominent
only after the stress reached a value of the proportional strength limit
of the material. Thus, data obtained at a high stress level would not
be in compliance with the requirements for valid fracture testing.
Furthermore, the data obtained at such high stress levels, Figure 54,
i.e., above 150 ksi, will have limited application.

Taking 90 percent of the ultimate strength of 192.6 ksi or yield strength
of 180.2 ksi, dividing the former by 1.4 and the latter by 1.1, and
taking the lesser of the two results in a design allowable of about 124
ksi. (This value is for illustrative purposes only and does not incorpor-
ate the statistical confidence limits.) It would appear that for a simple,
well designed and built pressure vessel, the information on flaw behav-
ior under high sustained stress loads only provides a more complete
characterization of the material. Actually, however, many design devi-
ations together with unavoidable geometrical discontinuities and manu-
facturing imperfections, are likely to create local stress risers that
may exceed the design value and thus be susceptible to sustained flaw
growth as characterized by the high stress level test data. This would
fall into a rather specialized field of design and analysis not generally
part of daily industrial activity.

Consider now the low stress sustained flaw growth data in Figure 52
and compare these results with sustained data obtained at high stress
levels shown in Figure 55. The No-Failure threshold stress intensity
level for low stress specimens in Figure 55 is near 98 percent of the
K_{Ic} value and is practically the same as the critical stress intensity.
Unlike the aluminum specimens at room and at -320°F test temperatures,
no evidence of partial flaw growth could be detected at lower stress
intensity levels. Several instrumented specimens, while subjected to

59

low sustained stress levels (consult flaw opening displacement curves listed in conjunction with the presentation of the experimental results for titanium) failed to reveal increase in flaw opening during the test sequence and normally culminated in an abrupt fracture.

High stress specimens (Figure 54) present an entirely different situation. There were several failures under sustained load; several specimens had partial growth; one test run resulted in No-Failure - No-Flaw growth. Combined assessment of high stress data points indicates that for high stress level the No-Failure threshold stress intensity is about 82 percent of the K_{Ic} value for the material.

6.3.2   Combined Cyclic-Sustained Flaw Growth

Stress level influence in sustained flaw growth behavior of 5Al-2.5Sn (ELI) titanium at -320°F was confirmed by the combined cyclic-sustained testing of the same material. The combined cyclic-sustained data is also divided into groups of high (above 150 ksi) and low (below 150 ksi) stress levels. The low stress data is summarized in Figure 57 together with the curve representing test data generated on NAS 3-4194 program and reported in CR-54837. The No-Failure threshold is equal to fracture stress intensity (Figure 55). Therefore, under cyclic testing with different hold time at maximum stress, there should be no sustained stress interaction. All points should fall on the NAS 3-4194 K_{Ii}/K_{Ic} versus cycles-to-failure curve. Examination of Figure 57 verifies this. All points fell close to the curve representing NAS 3-4194 data, regardless of the length of time at a maximum load.

The high stress threshold stress intensity level established in Figure 54 is likewise substantiated by combined cyclic-sustained data. Correspondence with NAS 3-4194 data is not as pronounced as it was with low stress

data because the curve in the NAS 3-4194 report represents low stress data. Consequently, even at relatively fast cyclic speed the cyclic life of high stress specimens is shortened.

6.4   PRESSURE VESSEL TEST DATA

As was pointed out in Section 5.0, the tank testing performed on this program was plagued with difficulties including plate delamination, failures of the pressurization system, hydrogen fires with ensuing destruction of the test site and obliteration of one of the fracture faces. However, in spite of these difficulties and the uncertainties associated with some of the test data, the results indicate that the sustained stress flaw growth characteristics of the materials investigated are not significantly influenced by the biaxial stress field. Consequently, it is considered that within limits, the uniaxial specimen data can be used to predict the extended loading performance of pressure vessels.

Delaminations at the flaw tips in the 2219-T87 tanks tested at room temperature (see Figures 60 and 61) prevented sustained stress growth in the thickness direction (i.e., at the point of the theoretical maximum stress intensity), and as a result the flaws grew in a lateral direction with maximum growth occurring at angles, $\alpha \neq 0$. While the stress intensity can be calculated at any point on the periphery of a semi-elliptical surface flaw, it is not known to what extent the existence of a physical separation at the flaw tip affects the result. This uncertainty is compounded by the fact that the aluminum vessels used in this program were much smaller in diameter than those used in previous investigations (References 8 and 13), and the actual stress intensity at the root of a surface flaw is believed to be magnified above that obtained using equation (6), due to curvature.

61

However, curvature and delamination effects do not present a major
difficulty in the evaluation of the sustained stress flaw growth in
pressure vessels. Subcritical flaw growth is primarily a function of
the ratio of the initial to critical stress intensity and not the finite
stress intensity values. If the calculated critical value is in error by
some percentage, the initial value is likewise in error by about the
same percentage and the K_{Ii}/K_{Ic} ratio is not changed. Comparing the
uniaxial and biaxial sustained stress flaw growth data for 2219-T87
aluminum at room temperature (Figure 27) on the basis of K_{Ii}/K_{Ic} no
difference in behavior is seen. Likewise the flaw growth observed in
the second flaw in aluminum tank #003 tested at -423°F is consistent
with the uniaxial specimen results.

Comparison of calculated stress intensities using equation (6) with
data previously obtained by testing larger tanks, indicates the stress
intensity magnification due to curvature may be approximately 10
percent. This approximate 10 percent curvature effect can also be
seen by comparing the calculated K_{Ic} values for the preflawed aluminum
tanks with the values obtained from flat plate uniaxial fracture specimen
tests. From table 12 it is seen that for the two aluminum tanks tested
at room temperature the calculated K_{Ic} values were both 30.0 ksi$\sqrt{in}$.
This compares to an average value of 34 ksi$\sqrt{in}$ obtained from uniaxial
flat plate tests where similar lateral flaw growth was observed
(i.e., K_{Ic} values at $\alpha > 50°$). From table 13 it is seen that the
calculated K_{Ic} for the aluminum tank #003 tested at -423°F was
39.5 ksi$\sqrt{in}$. This compares with an average value of 43.9 ksi$\sqrt{in}$
obtained from the uniaxial flat plate fracture specimen tests.

At present there is no analytical solution for the effect of curvature
on the stress intensity at the tip of surface flaws in pressurized
cylinders. However, based upon the solution by Folias [14] for
through-the-thickness cracks in pressurized cylinders it is expected
that the magnification in stress intensity is a function of both the

flaw size and the R/t value. If the flaw sizes are small and/or if the R/t value is relatively large (perhaps greater than 35 based upon previous tank test results [13]) the curvature effect is small enough to be neglected. On the other hand, if the flaws are large and/or if the R/t value is small it does not appear unreasonable to expect that equation (6) could underestimate the stress intensity by the 10 percent experimentally observed in this investigation. It is apparent that in order to accurately apply the uniaxial fracture specimen data to the prediction of critical flaw sizes in small diameter thick walled vessels an analytical solution to this curvature problem is needed.

Aluminum tank #004 tested at -423°F yielded no flaw growth data and a very questionable K_{Ic} value. As noted in section 5.0 this tank failed after several very rapid unintentional pressure oscillations due to a pump malfunction. Although there were several attempts to determine the reason for the abnormally low K_{Ic} value (see Section 5.0), it still remains unexplained.

The two titanium tanks were tested under sustained pressure at -423°F and revealed no flaw growth at applied stress intensities of about 90 percent of the K_{Ic} value. This is consistent with the results obtained with uniaxial specimens. Also, a close correspondence between uniaxial and biaxial critical stress intensities was indicated. Because of the much larger diameter to the thickness ratio in the titanium tank, curvature effects are considered to be negligible.

7.0 CONCLUSIONS

The sustained stress flaw growth data obtained on this program can
be used in estimating the life of cryogenic pressure vessels subjected
to extended periods of time at pressure, such as will be encountered
in long term space missions. Also, the results of this program can
be used in conjunction with the cyclic flaw growth data obtained on
NASA Contract NAS 3-4194 (reported in CR 54837) to estimate the life
of pressure vessels subjected to combined cyclic and sustained pressures.
Assurance of safe life for extended pressure storage can be obtained
by insuring that during the required life the maximum applied stress
intensity in the vessel does not exceed the sustained stress threshold
stress intensity value for the specific material and environment. A
successful proof pressure test can be used to determine the maximum
possible initial applied stress intensity in the vessel. The maximum
initial to critical stress intensity ratio is equal to one divided by
the ratio of the proof pressure to the maximum operating pressure.
From the results of this program it is concluded that below the
"No Failure" threshold stress intensity level (i.e., that stress
intensity above which delayed time failures can occur) time at pressure
has little or no effect on cyclic flaw growth rates. Hence, the data
reported in CR 54837 can be safely used to determine the number of
pressure cycles required to increase the initial stress intensity to
the threshold level. Above the threshold level, time at pressure can
have a large effect on cyclic flaw growth rates and as a result cyclic
life can be severely limited. In fact, it appears possible that only
one prolonged pressure cycle could cause failure.

Some specific observations and conclusions regarding the two materials
investigated in this program are as follows:

1.   For the 2219-T87 aluminum it has been shown that small amounts
      of sustained stress flaw growth can occur below the "No Failure"

threshold stress intensity level; however, the growth apparently stops after a short time at load. A lower threshold exists below which there is no evidence of growth. This has been termed the "No Growth - No Failure" threshold level.

2. For storage involving days or even weeks of extended pressure loading it is considered possible to safely operate 2219 aluminum vessels at stress intensities between the upper and lower threshold levels. While it may be possible that these vessels could be safely pressurized for longer periods of time in this region, the present lack of substantiating test data makes it appear wise to limit the maximum stress intensity at the lower threshold level.

3. The accuracy of the estimated upper and lower threshold levels for the 2219-T87 aluminum at -423°F could be improved with additional test data.

4. For the 5Al-2.5Sn(ELI) titanium at stress levels above the proportional limit there is an increased susceptibility to delayed time failure under sustained stress as evidenced by a substantially decreased threshold level. As applied to titanium pressure vessels this is of particular significance in those areas of discontinuity where the actual stresses can be substantially above the nominal calculated values and quite possibly above the proportional limit of the material.

5. Because of the decrease in plane strain fracture toughness, K_{Ic}, with decrease in temperature, pressure vessels fabricated from 5Al-2.5Sn(ELI) titanium should be proof tested to a stress level above the maximum operating stress at a temperature equal to or below that expected in service.

6.   Because of the slight increase in fracture toughness with
      decrease in temperature, it appears that pressure vessels
      fabricated from 2219-T87 aluminum should be proof
      tested to a stress level above the maximum operating
      stress at or above the expected service temperature.

7.   The 2219-T87 aluminum and 5Al-2.5Sn(ELI) titanium
      uniaxial data obtained on this program   is considered to
      be applicable to biaxial loau. .g conditions, which exist
      in pressure vessels, even though the biaxial data obtained
      is not nearly as complete as originally planned.

REFERENCES

1. "Fracture Testing of High-Strength Sheet Materials", ASTM Special Committee of Fracture Testing of High Strength Metallic Materials, ASTM Bulletin, May 1961.

2. ASTM STP 381, "Fracture Toughness Testing and Its Applications", June 1964.

3. Irwin, G. R., "Crack Extension Force for a Part-Through Crack in a Plate", Journal of Applied Mechanics, Vol. 29, Trans. ASME, Vol. 84, Series E, December 1962.

4. Kobayashi, A. S., "On the Magnification Factors of Deep Surface Flaws", Structural Development Research Memorandum No. 16, The Boeing Company, December 1965.

5. Smith, F. W., "Stresses Near a Semi-Circular Edge Crack", PhD. Dissertation, University of Washington, 1966.

6. Smith, F. W., "Stress Intensity Factor for a Semi-Elliptical Flaw", Structural Development Research Memorandum No. 17, The Boeing Company, August, 1966.

7. Gross, B., Srawley, J. E., and Brown, W. F., "Stress Intensity Factors for a Single Edge Notch Tension Specimen by Boundary Collocation of a Stress Function", NASA TN D-2395, 1964.

8. Tiffany, C. F., Lorenz, P. M., and Hall, L. R., "Investigation of Plane Strain Flaw Growth in Thick-Walled Tanks", NASA CR-54837, February, 1966.

9. Tiffany, C. F., Masters, J. N., and Pall, F. A., "Some Fracture Considerations in the Design and Analysis of Spacecraft Pressure Vessels", presented at the ASM National Metals Congress, Chicago, October 1966.

10. Tiffany, C. F., and Masters, J. N., "Investigation of the Flaw Growth Characteristics of 6Al-4V Titanium Used in Apollo Spacecraft Pressure Vessels", NASA CR-65586, March 1967.

11. Green, A. E., and Sneddon, I. N., "The Distribution of Stress in the Neighborhood of a Flat Elliptical Crack in an Elastic Solid", Proc. Cambridge Phil. Soc., Vol. 46, 1950.

12. Tiffany, C. F., and Lorenz, P. M., "Fracture Toughness and Subcritical Flaw Growth Characteristics of Saturn 3-IC Tankage Materials", Boeing Document D2-22802, October 1963.

13. Tiffany, C. F., and Hall, L. R., "Investigation of Preflawed 2219 Aluminum Tanks", Boeing Document D5-13663, August 1966.

14. Folias, E. S., "An Axial Crack in a Pressurized Cylindrical Shell", International Journal of Fracture Mechanics, Vol. 1, No. 2, June 1965.
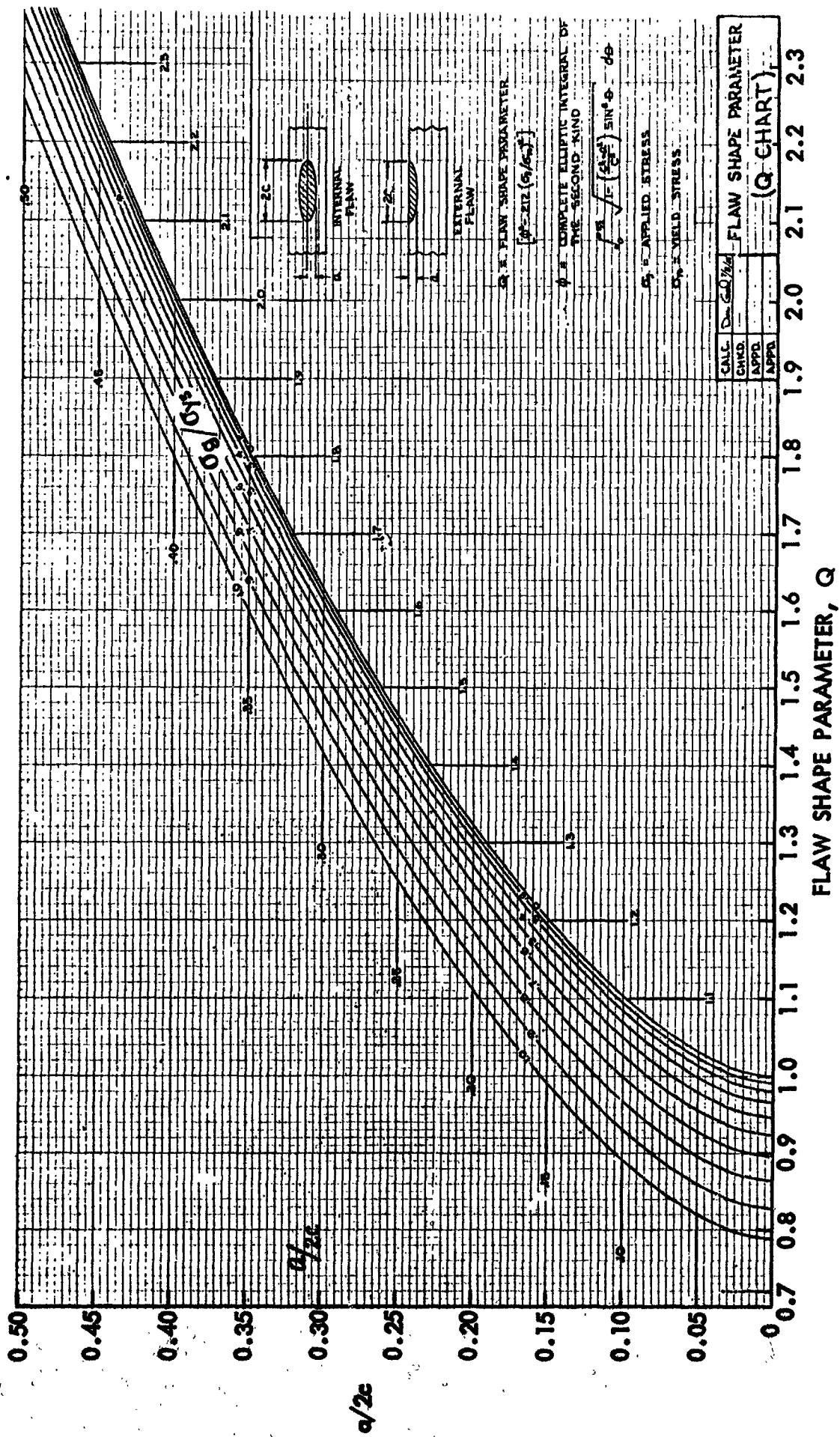
Figure 1 : SHAPE PARAMETER CURVES FOR SURFACE AND INTERNAL FLAWS
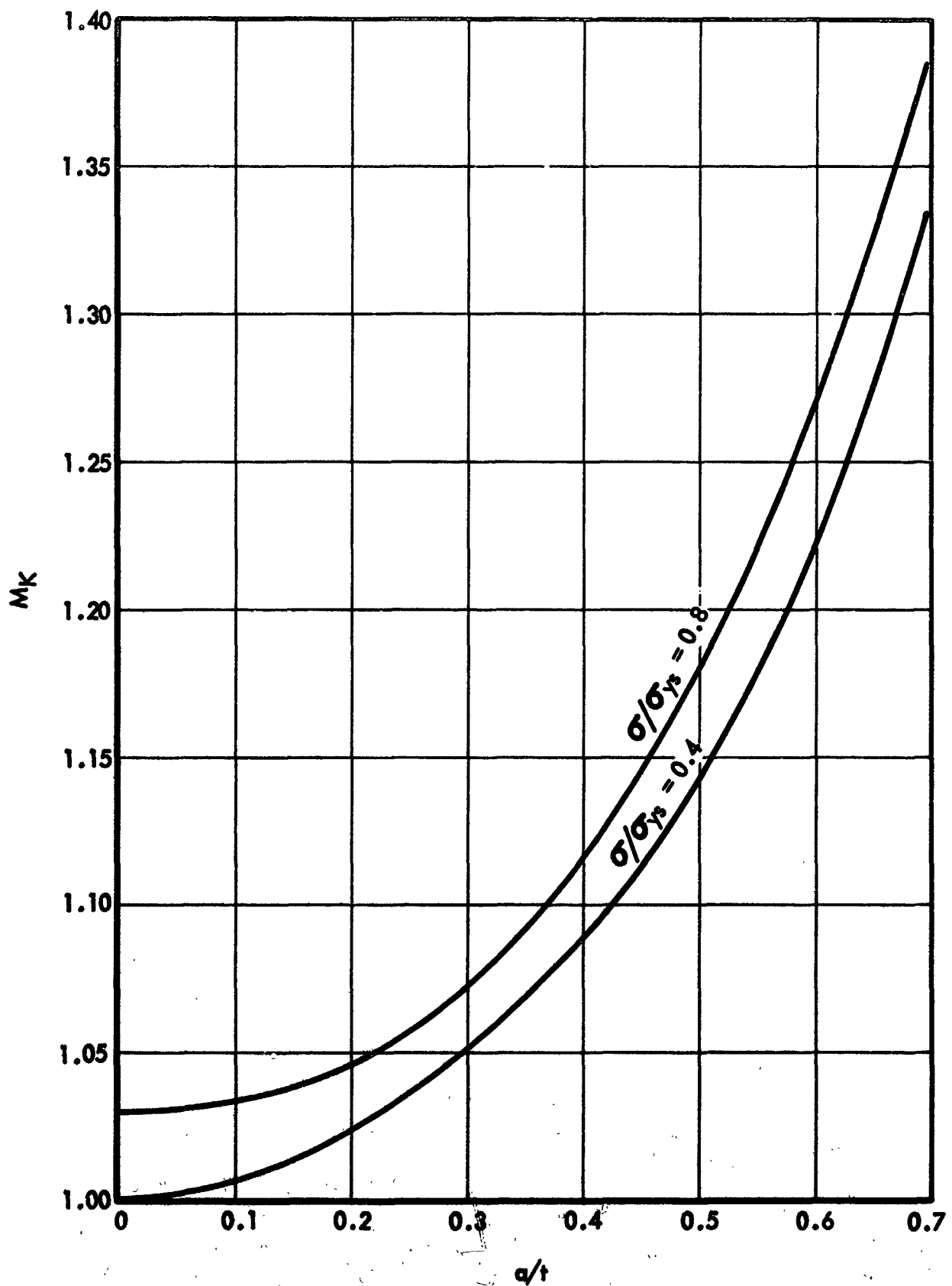
Figure 2 : RESULTANT STRESS MAGNIFICATION DUE TO DEEP
FLAW AND PLASTIC YIELDING FOR PLANE STRAIN.
$\nu = 1/3$, $a/2c < 0.3$
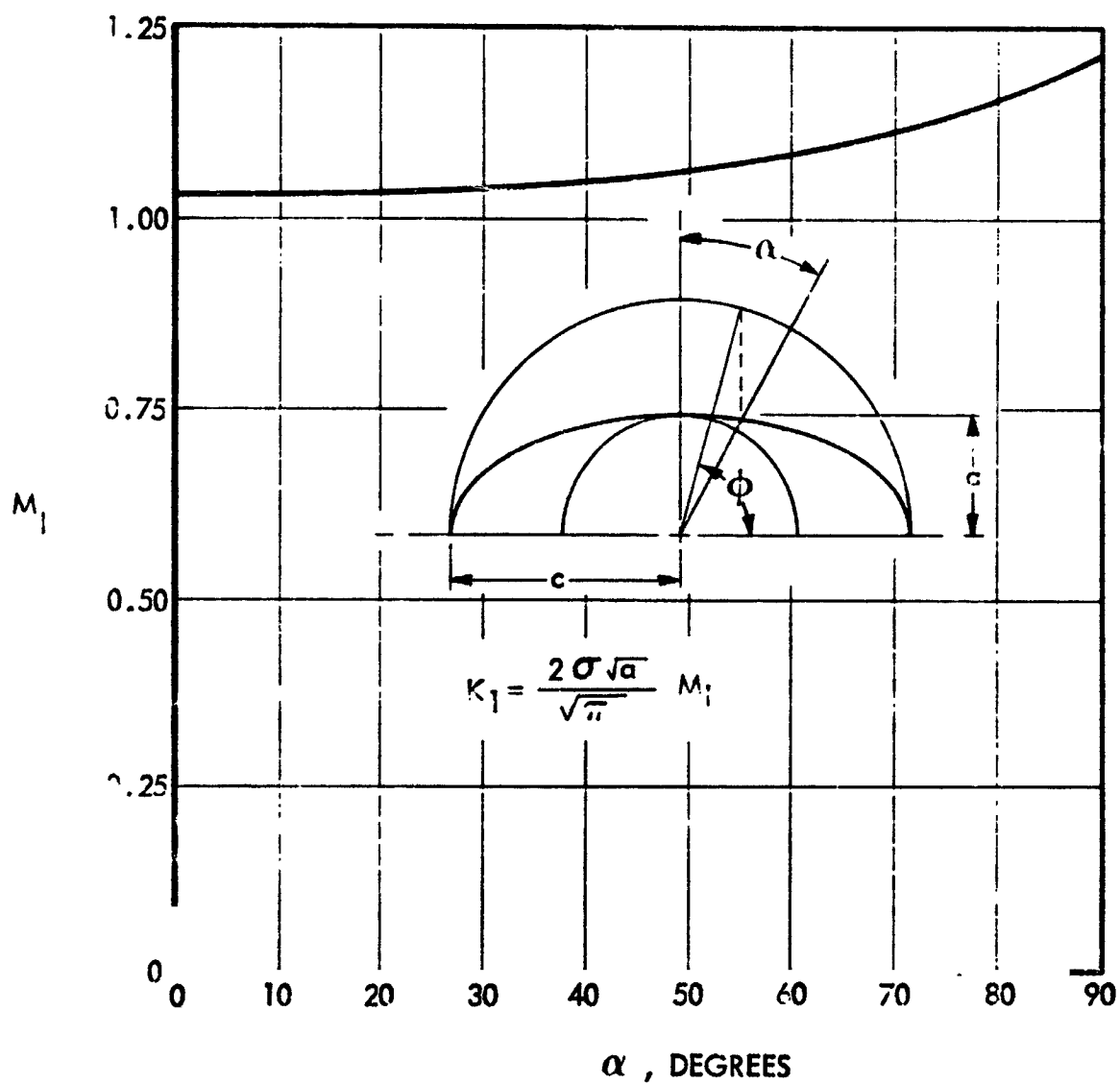
Figure 3 : STRESS INTENSITY FACTOR FOR A SEMI-CIRCULAR
SURFACE FLAW
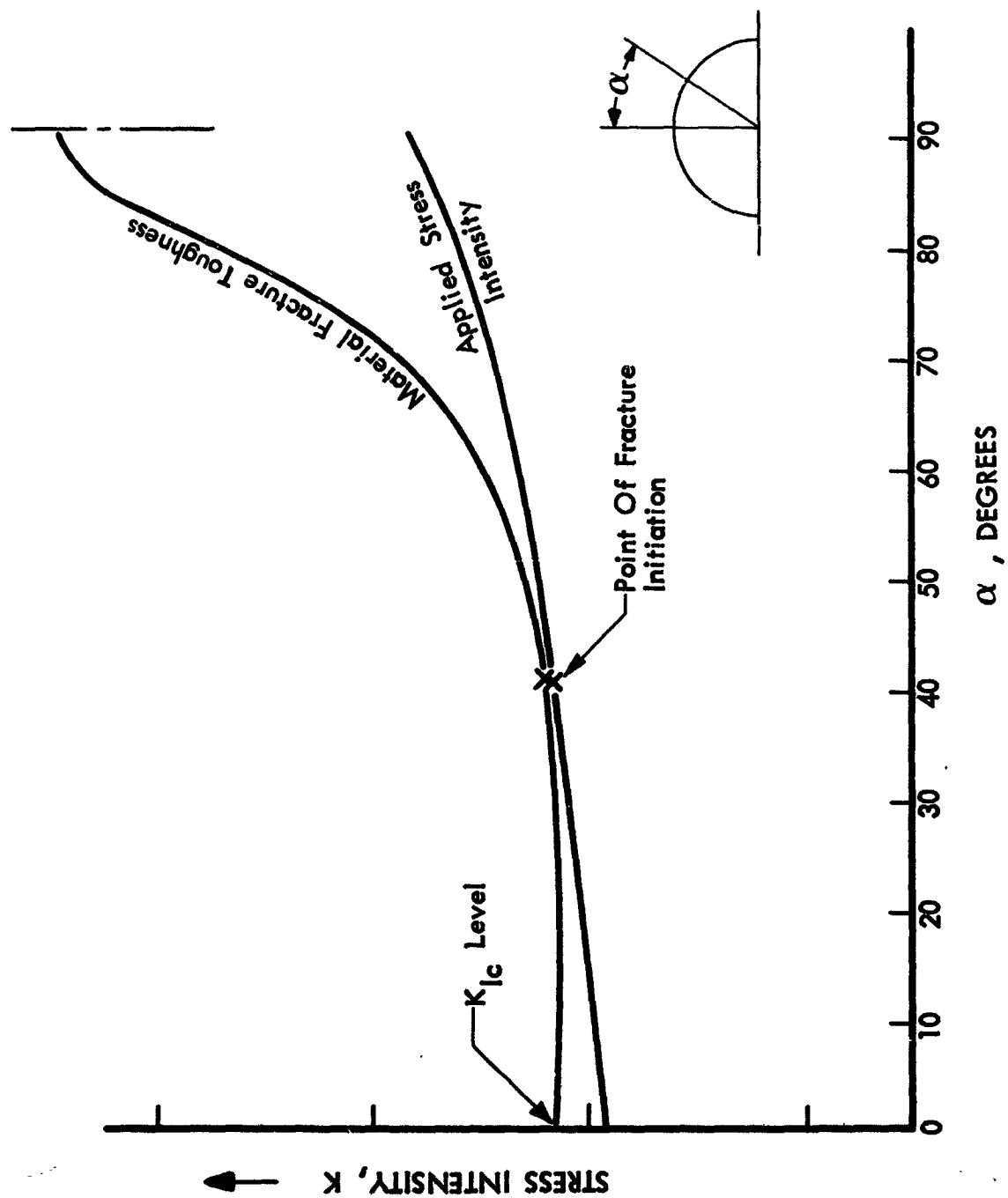
Figure 4 : SCHEMATIC REPRESENTATION OF POSSIBLE FRACTURE INITIATION
AT A SEMICIRCULAR SURFACE FLAW
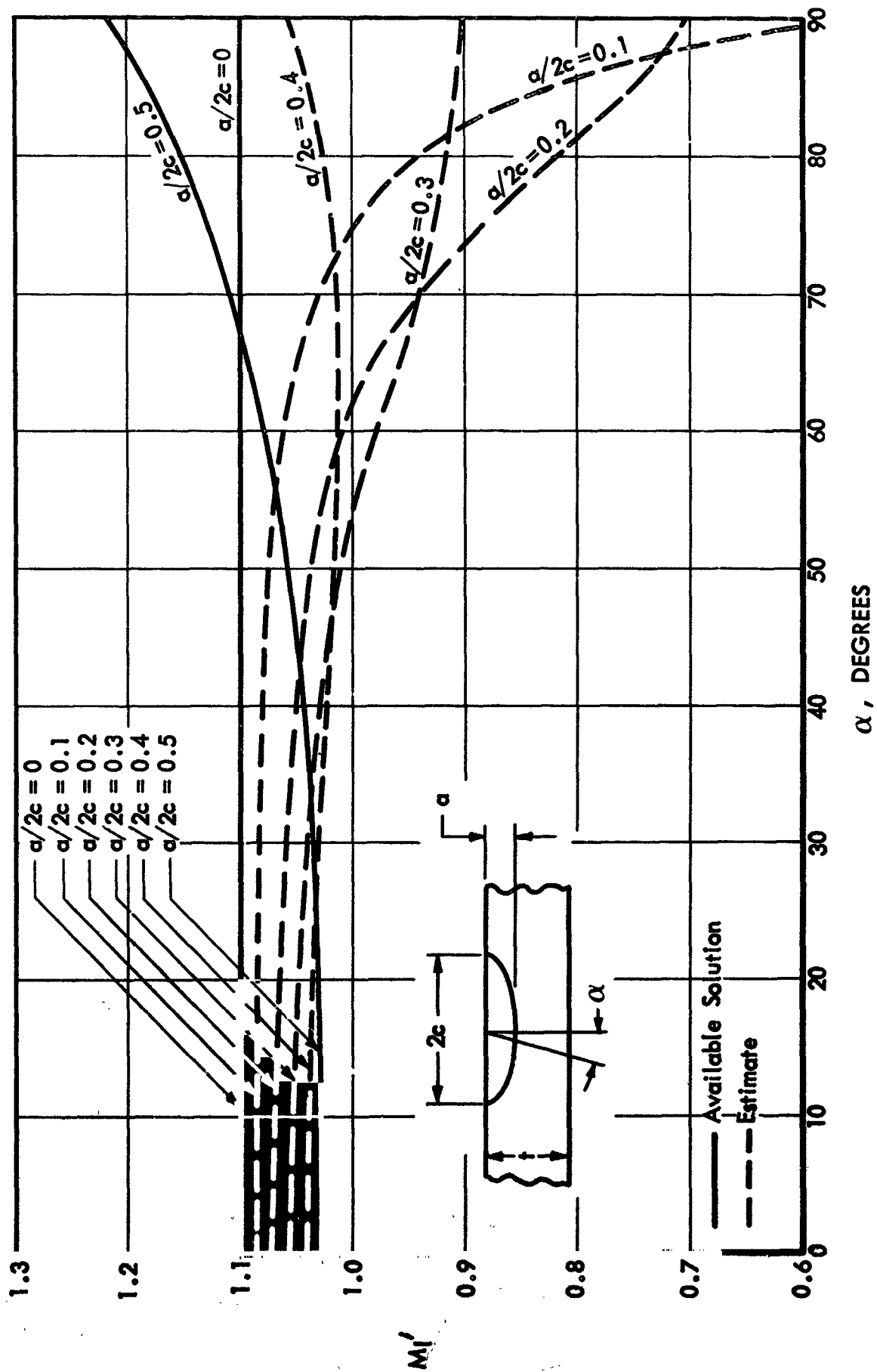
Figure 5 : STRESS INTENSITY FACTOR FOR A SEMI-ELLIPTICAL SURFACE FLAW
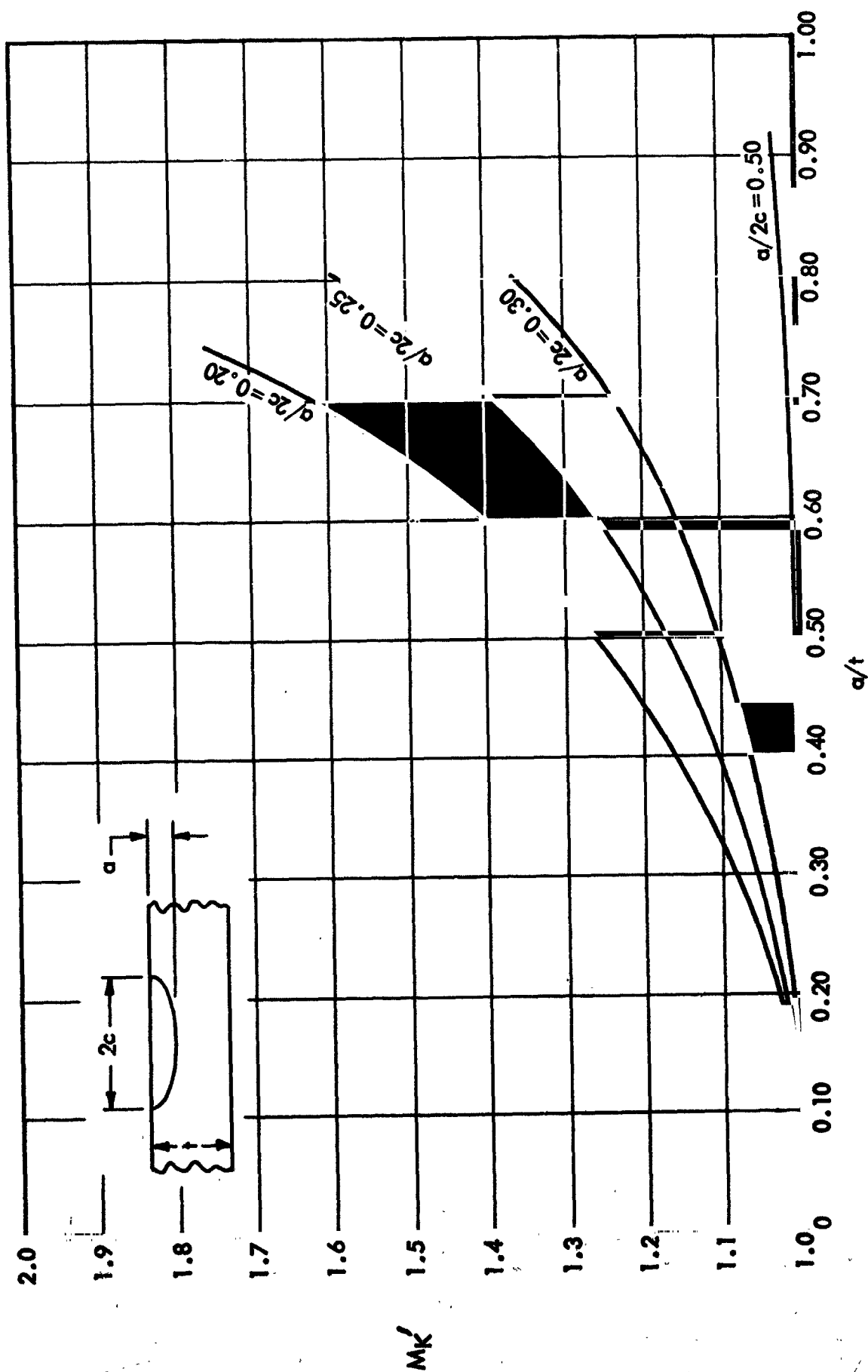
Figure 6 : ELASTIC STRESS INTENSITY MAGNIFICATION FACTORS FOR DEEP SURFACE FLAWS

74
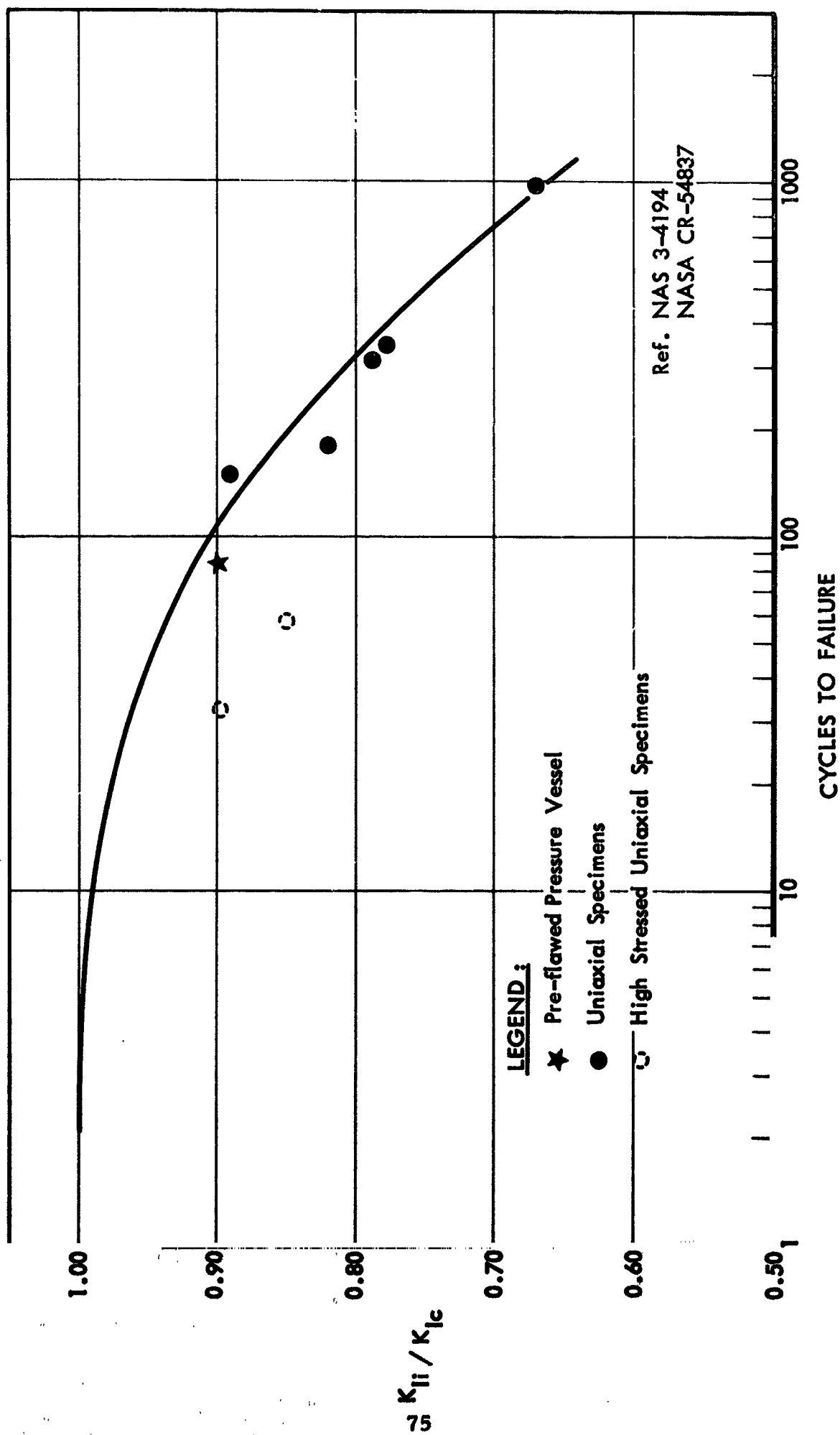
Figure 7 : CYCLIC LIFE DATA FOR 5 Al-2 1/2 Sn (ELI) TITANIUM
AT -320 °F (0-100-0 Load Profile, 1 CPM)

LEGEND :

★ Pre-flawed Pressure Vessel
● Uniaxial Specimens
○ High Stressed Uniaxial Specimens

Ref. NAS 3-4194
NASA CR-54837

CYCLES TO FAILURE

K_{Ii} / K_{Ic}

75
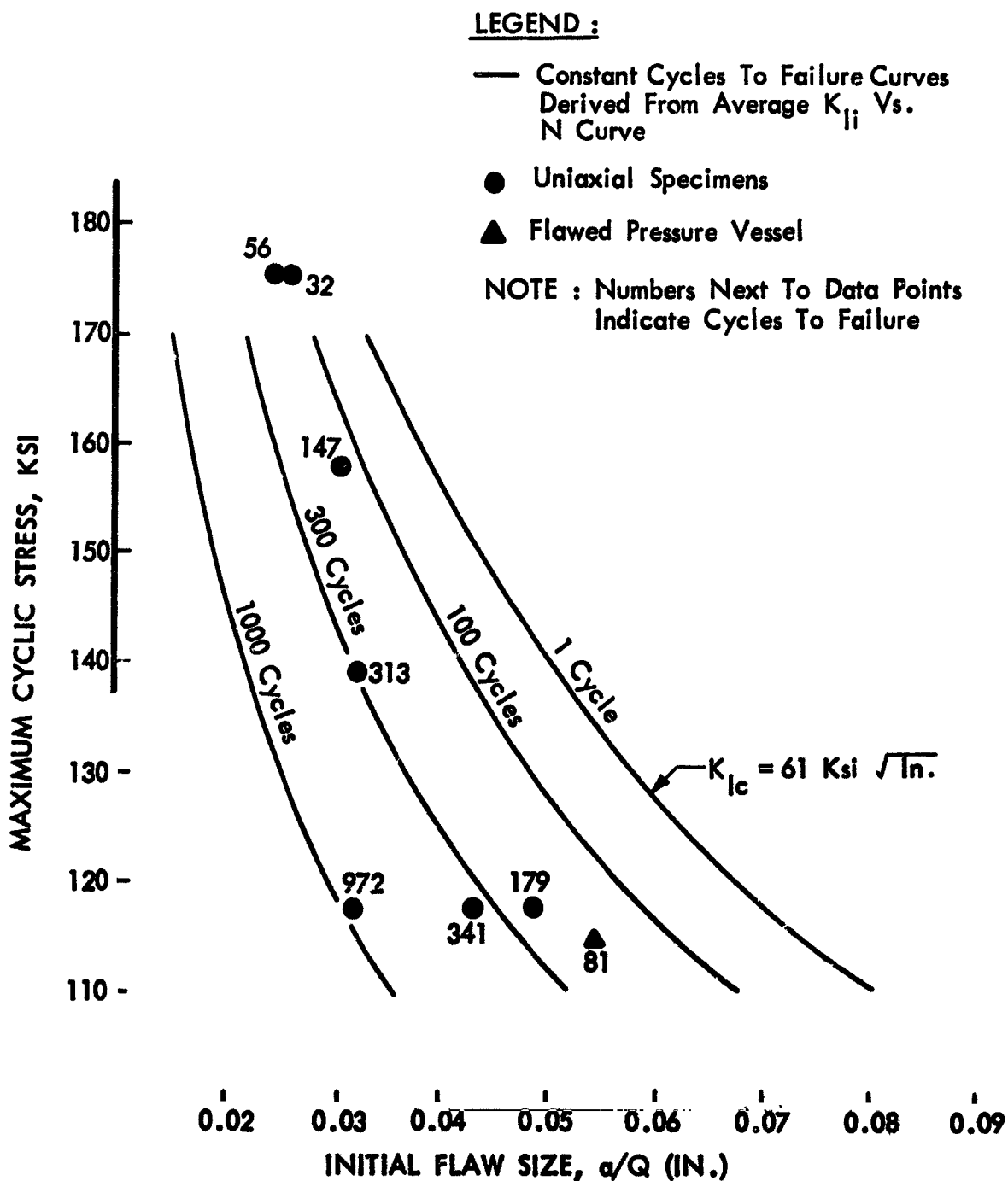
Figure 8 : CYCLIC FLAW GROWTH DATA FOR 5 Al-2 1/2 Sn (ELI) TITANIUM AT -320 °F (0-100-0 Load Profile)
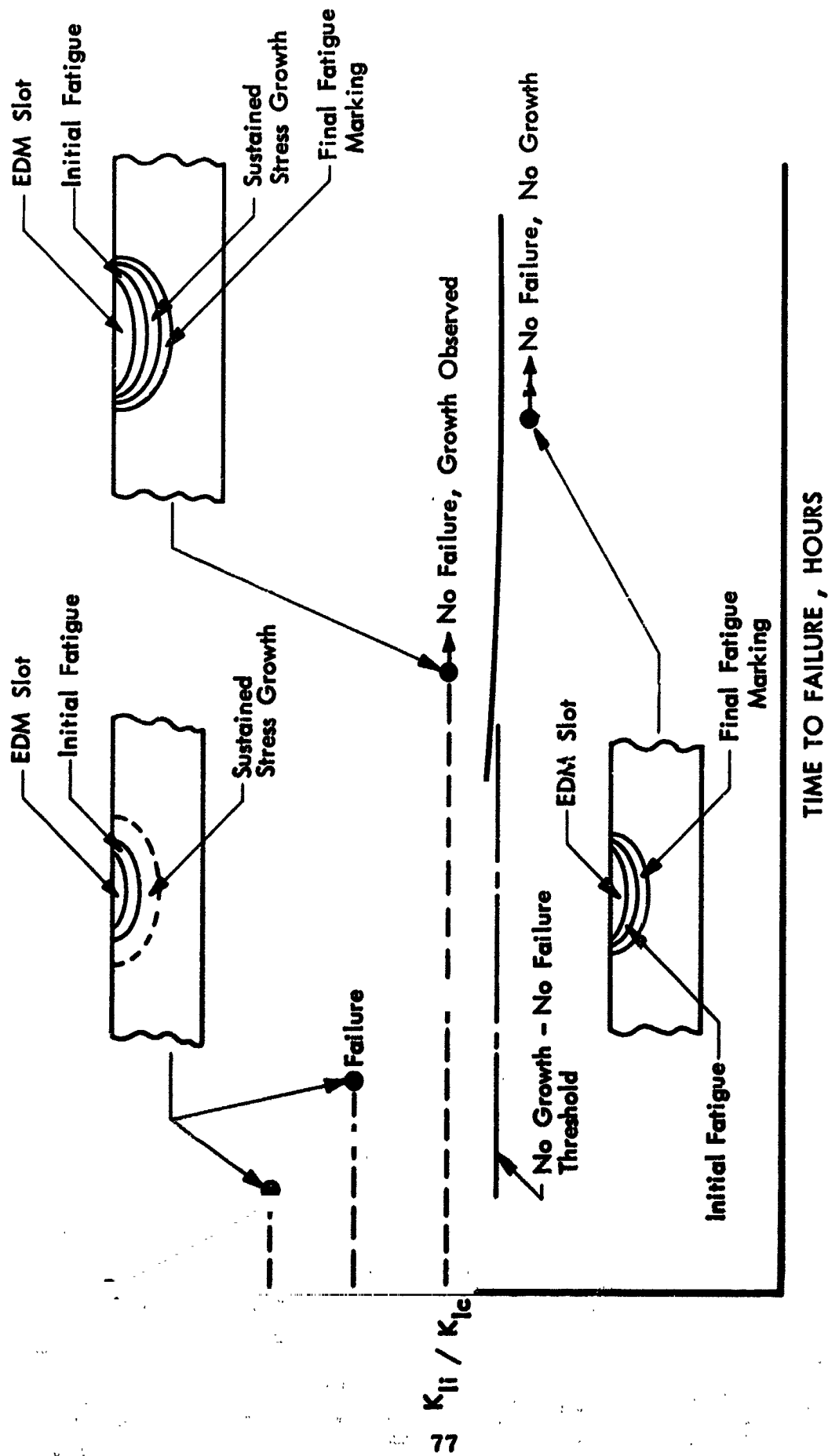
Figure 9: SUSTAINED STRESS FLAW GROWTH TEST APPROACH
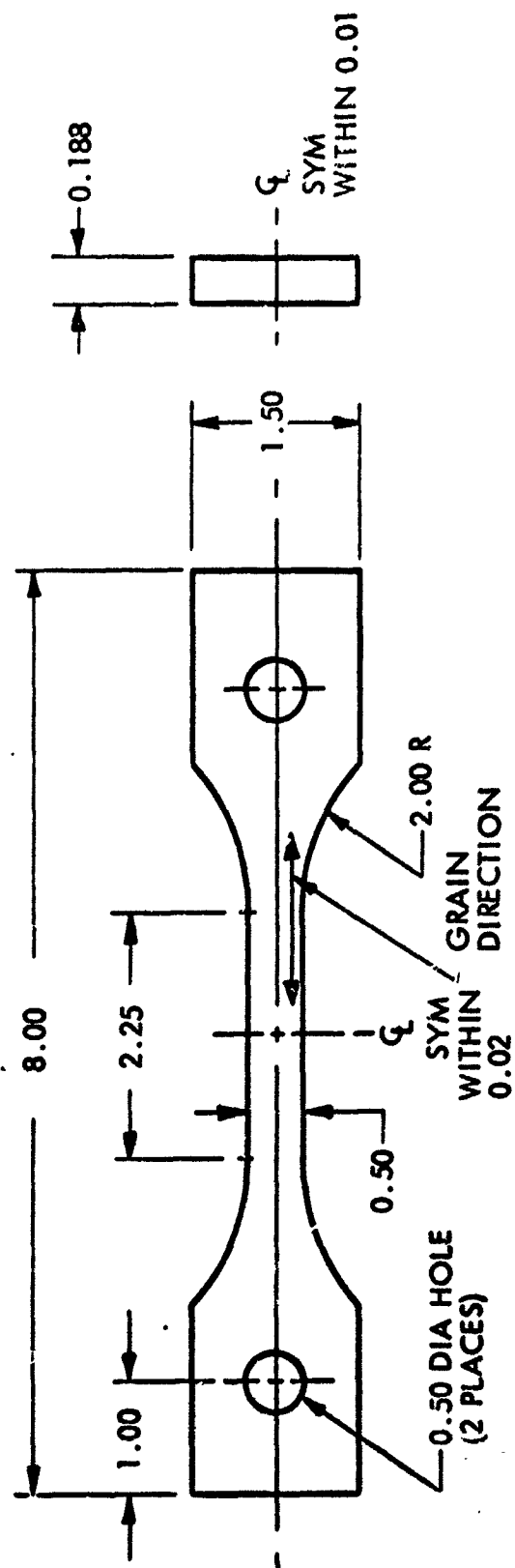
Figure 10 : TENSILE SPECIMEN (Titanium)

0.188

C̵ SYM WITHIN 0.01

1.50

8.00

2.25

1.00

0.50

2.00 R

GRAIN DIRECTION

SYM WITHIN 0.02

C̵

0.50 DIA HOLE (2 PLACES)
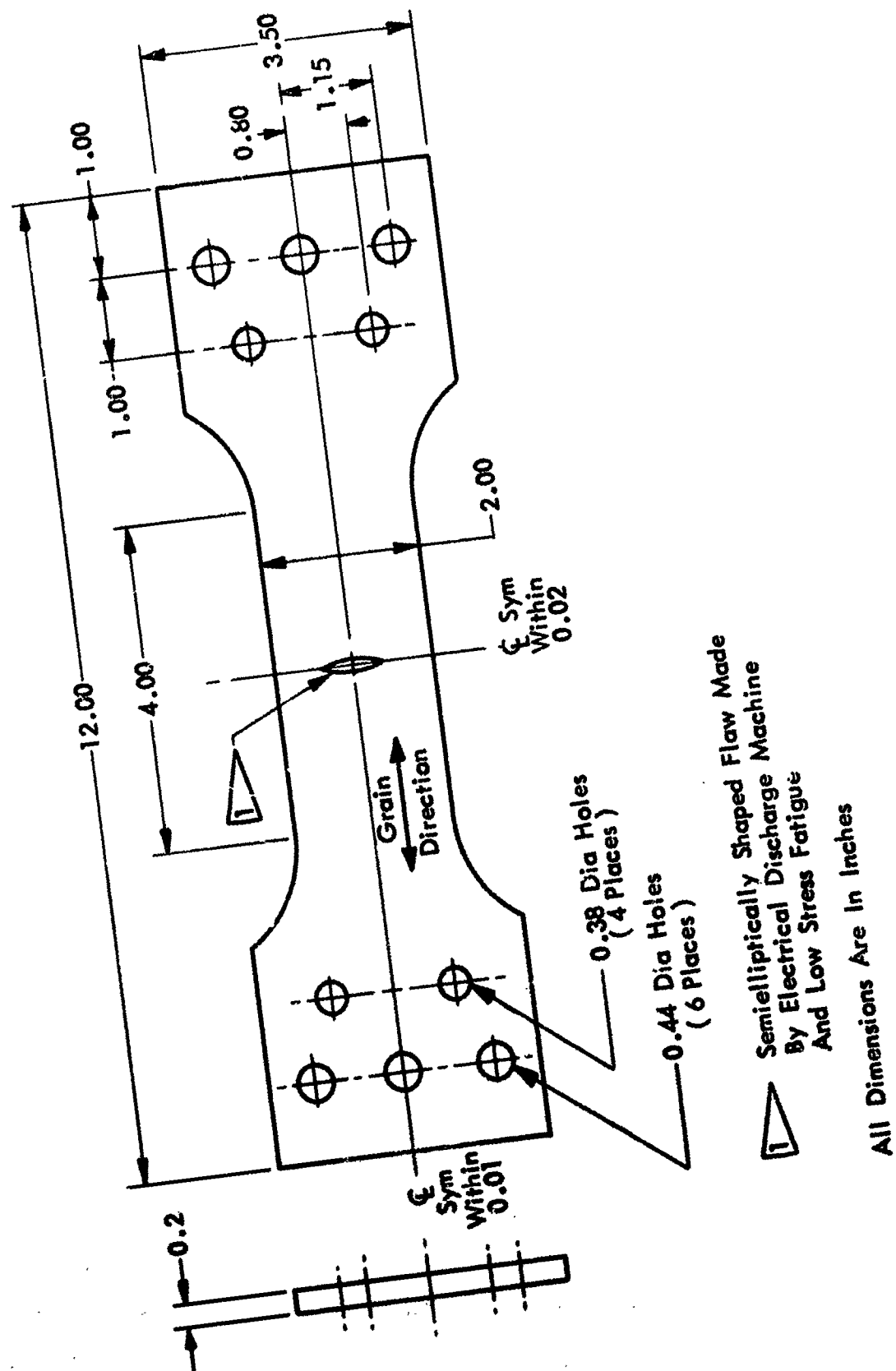
Figure 11 : SURFACE FLAWED TITANIUM SPECIMEN

3.50

1.15

0.80

1.00

1.00

2.00

4.00

12.00

0.2

€ Sym
Within
0.02

€ Sym
Within
0.01

Grain
Direction

0.38 Dia Holes
(4 Places)

0.44 Dia Holes
(6 Places)

Semielliptically Shaped Flaw Made
By Electrical Discharge Machine
And Low Stress Fatigue

All Dimensions Are In Inches

Figure 12 : TENSILE SPECIMEN (Aluminum)

5.50

2.25

1.00

GRAIN
DIRECTION

0.70 DIA

CHAMFER 45°
TO DEPTH OF THD

0.50
R

C_L SYM
WITHIN
0.02

0.50
DIA

THD 7/8-9NC-2

Figure 13 : SURFACE-FLAWED SPECIMEN FOR 0.60 IN. ALUMINUM

6.00

$\mathbb{C}_L$ SYM
WITHIN 0.01

1.2 (REF)

24.00

GRAIN
DIRECTION

10.00

3.00 R

0.60

$\mathbb{C}_L$ SYM
WITHIN 0.02

5.50

2.25

1.25

1.00 DIA
HOLE
(6 PLACES)

1 SEMIELLIPTICALLY SHAPED
FLAW MADE BY ELECTRICAL
DISCHARGE MACHINE AND
LOW-STRESS FATIGUE

25-53143-1 TITANIUM TEST TANK ASSY

Figure 14 : 5Al-2 1/2 Sn (ELI) TITANIUM TEST CYLINDER (-423 °F Tests)

Figure 15: 2219-T87 ALUMINUM TEST CYLINDER (R.T. And -423 Of Tests)

Figure 16 : INSTRUMENTATION FOR MEASURING FLAW
OPENING DISPLACEMENTS

Test Tank

Servovalve

Test-Cell Wall

Pressure
Accumulator

Oil Pressure Unit
(30 gpm Sprague)

| Sinusoidal Programmer | Load Controller | Trapezoidal Programmer | Recorder |

Hydraulic pressure gage
Hydraulic filter
Hydraulic pressure transducer
Instrumentation line
Hydraulic line
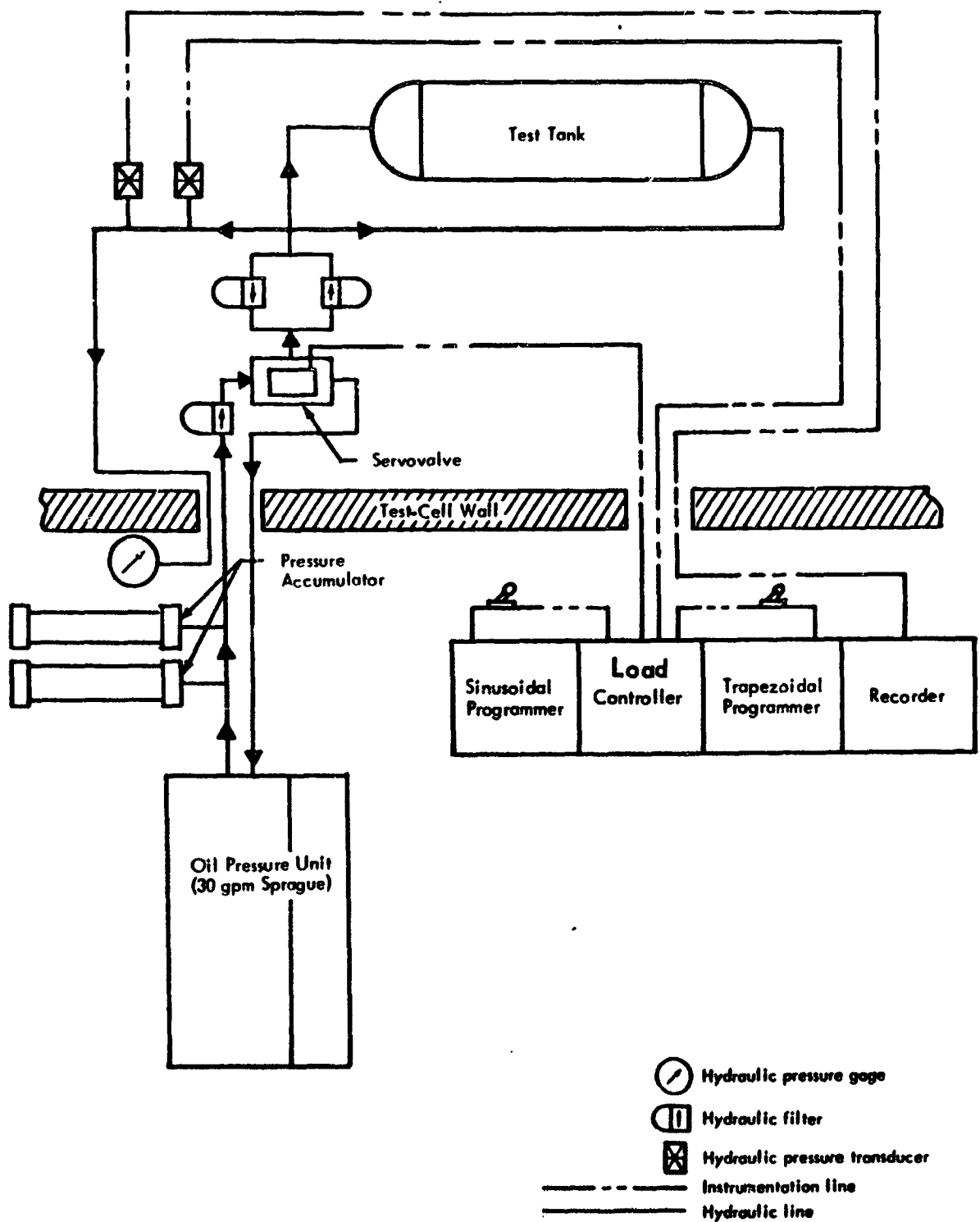
Figure 17: SCHEMATIC DIAGRAM OF PRESSURE AND
CONTROL SYSTEM USED FOR ROOM TEMP TANK TESTS
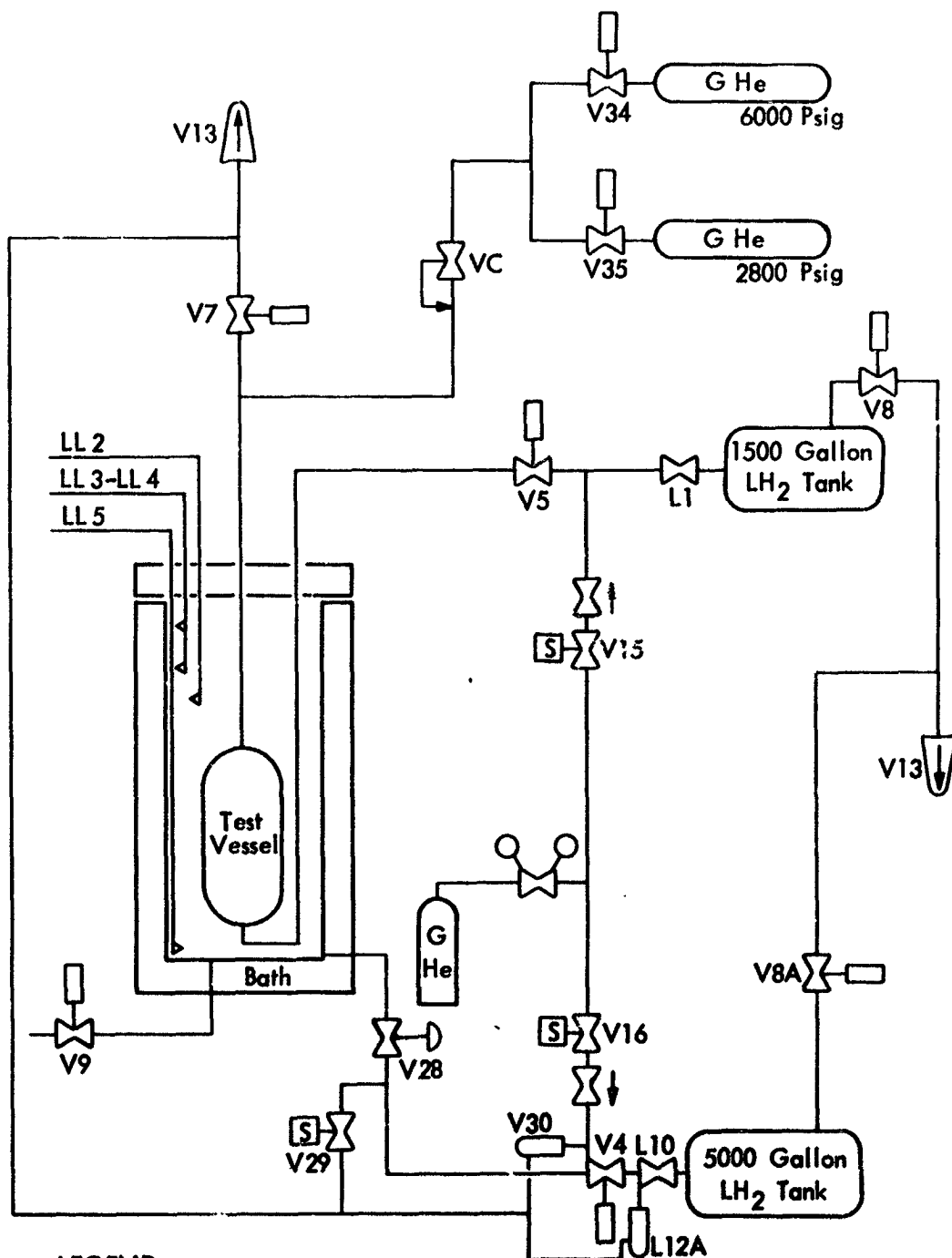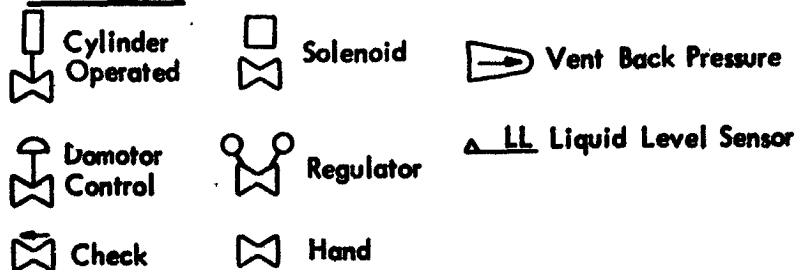
Figure 18: LIQUID HYDROGEN PRESSURIZATION SYSTEM
(Helium Boosters)

LEGEND :

Cylinder Operated
Damotor Control
Solenoid
Relief
Regulator
Check
Hand
Vent Back Pressure
Liquid Level Sensor
Burst Disc
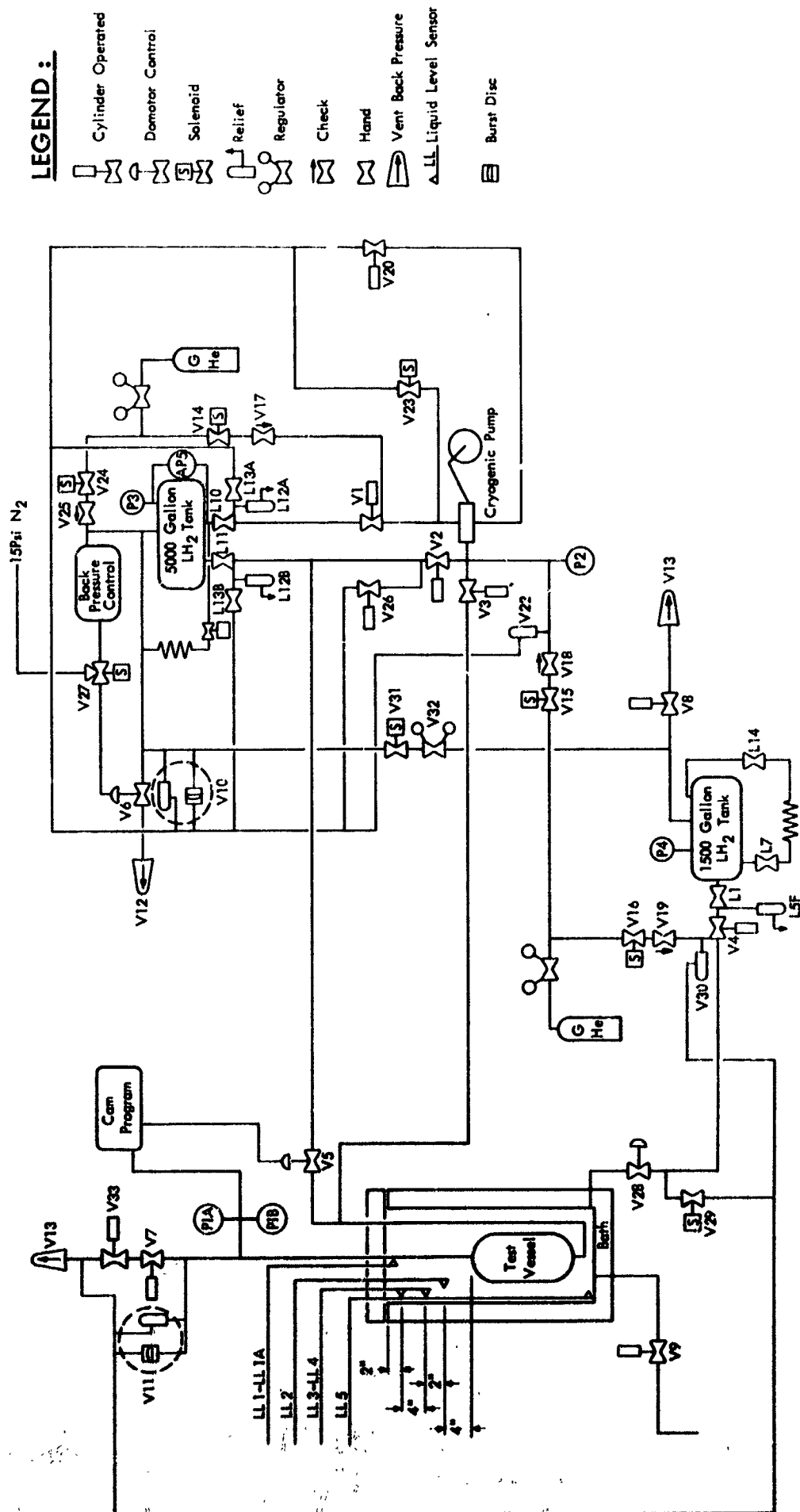
Figure 19 : LIQUID HYDROGEN PRESSURIZATION SYSTEM (Aft Servo Pickup)

87
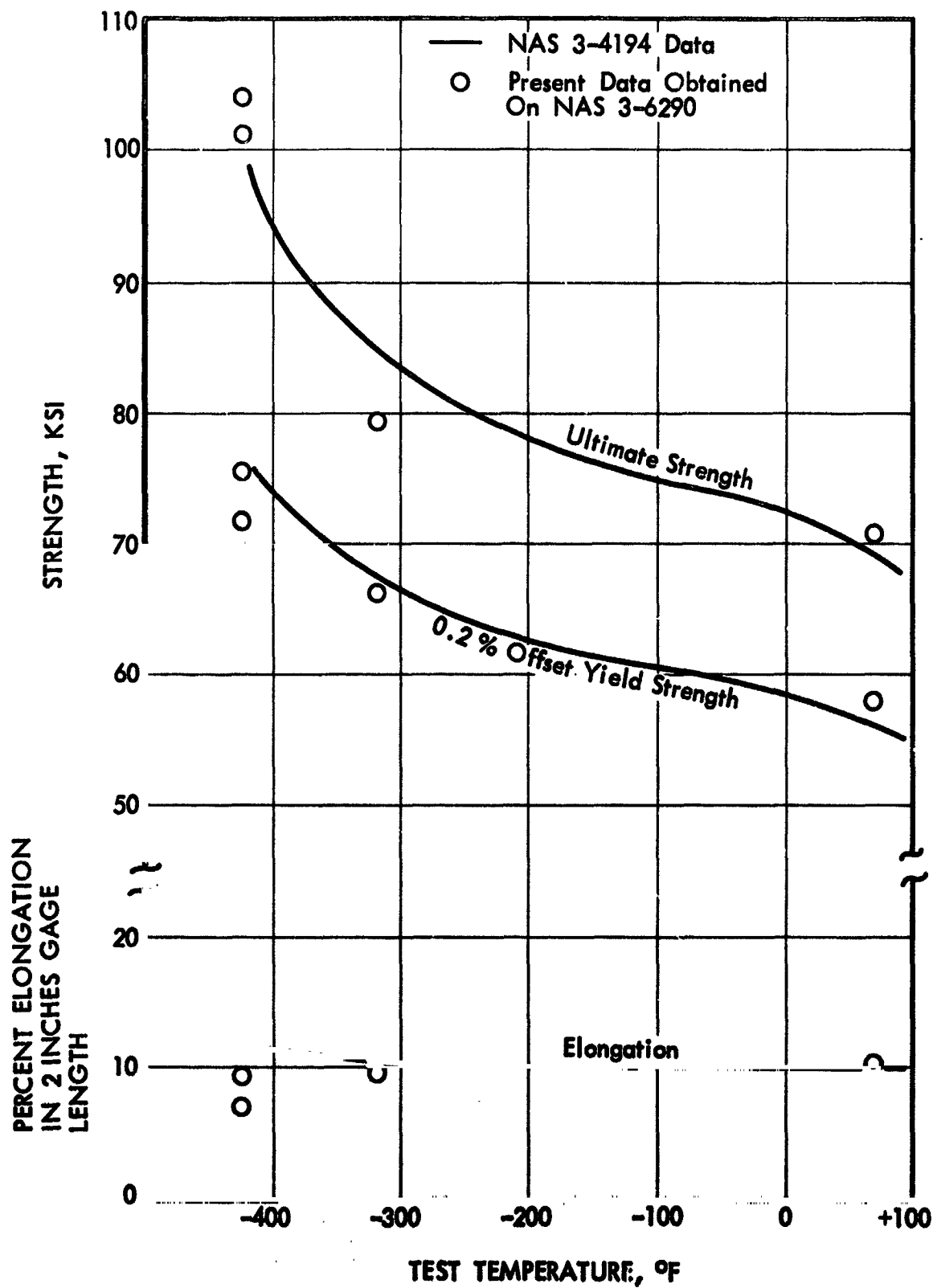
Figure 20: MECHANICAL PROPERTIES OF 2219-T87
ALUMINUM PLATE

Figure 21: STATIC FRACTURE TOUGHNESS OF 2219-T87 ALUMINUM

TEMPERATURE, °F

K_{Ic} , KSI $\sqrt{IN.}$

NAS 3-4194 Data , Static K_{Ic}
O Present Data Obtained
On NAS 3-6290
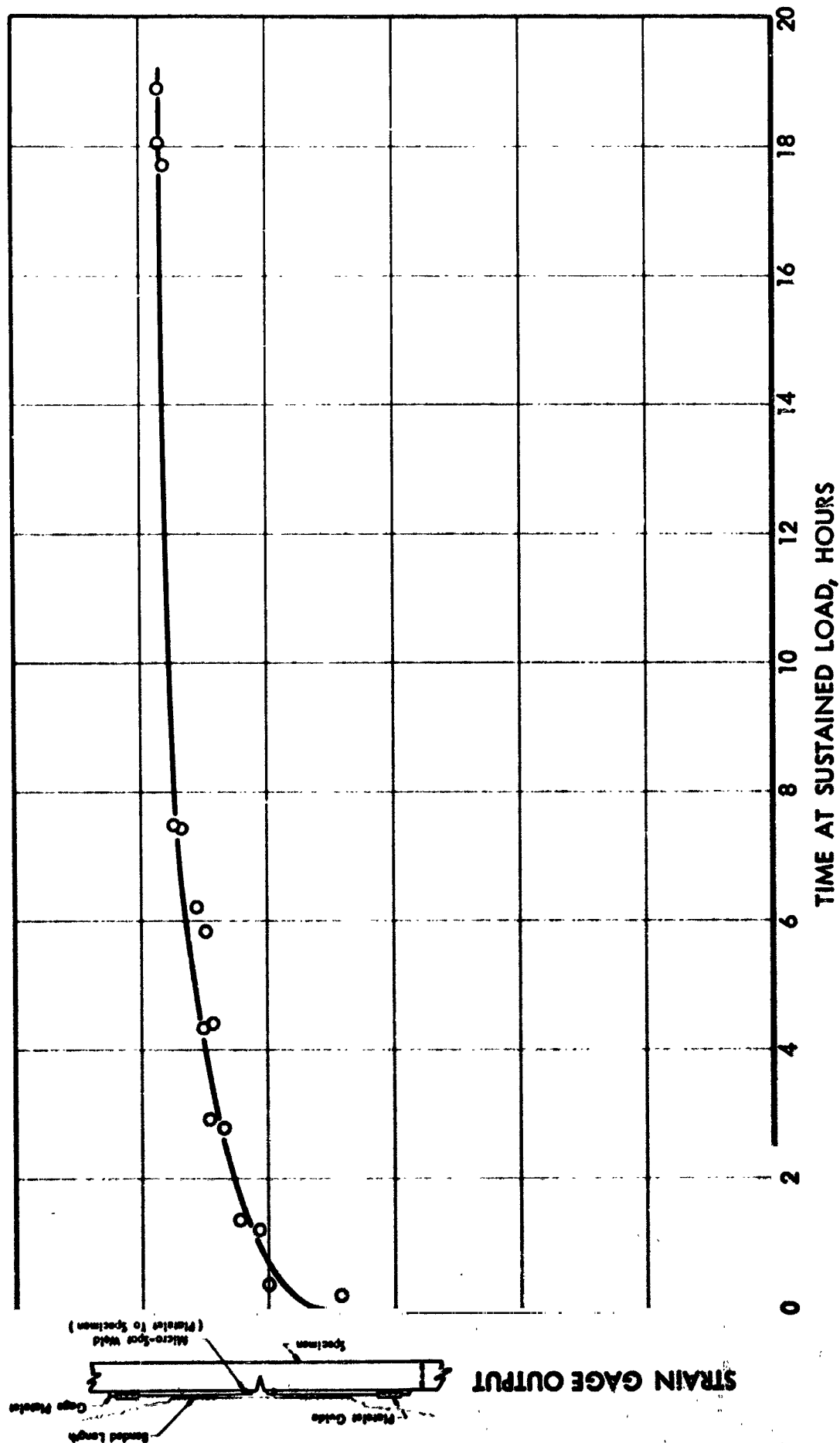
Figure 22: SUMMARY OF FLAW OPENING DISPLACEMENT
(2219-T87 Aluminum Specimen Number CA-34)

Figure 23: FLAW OPENING DISPLACEMENT UNDER SUSTAINED LOADING
(2219-T87 Aluminum Specimen DA-33, Beginning Of The
First Test Run)
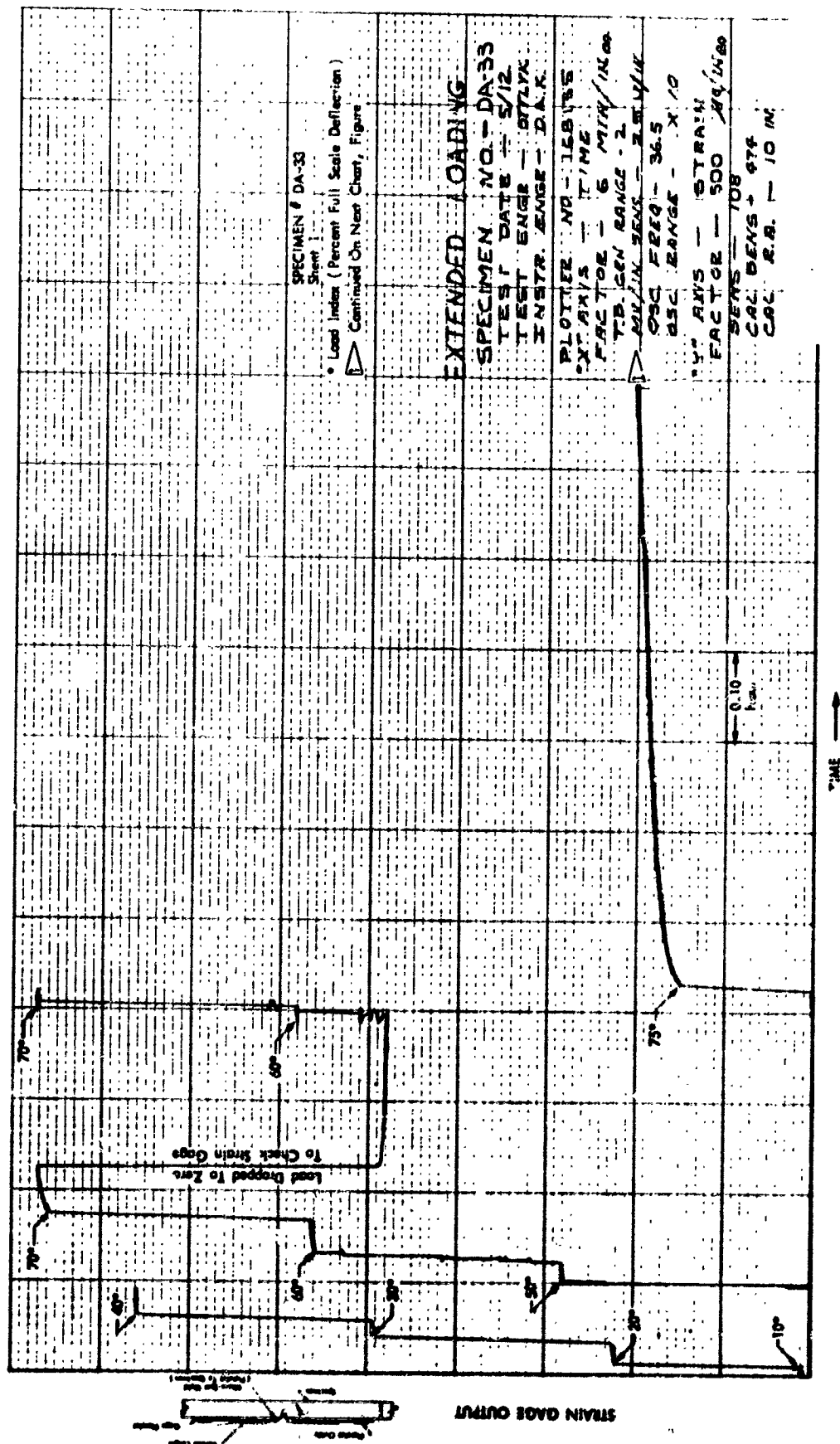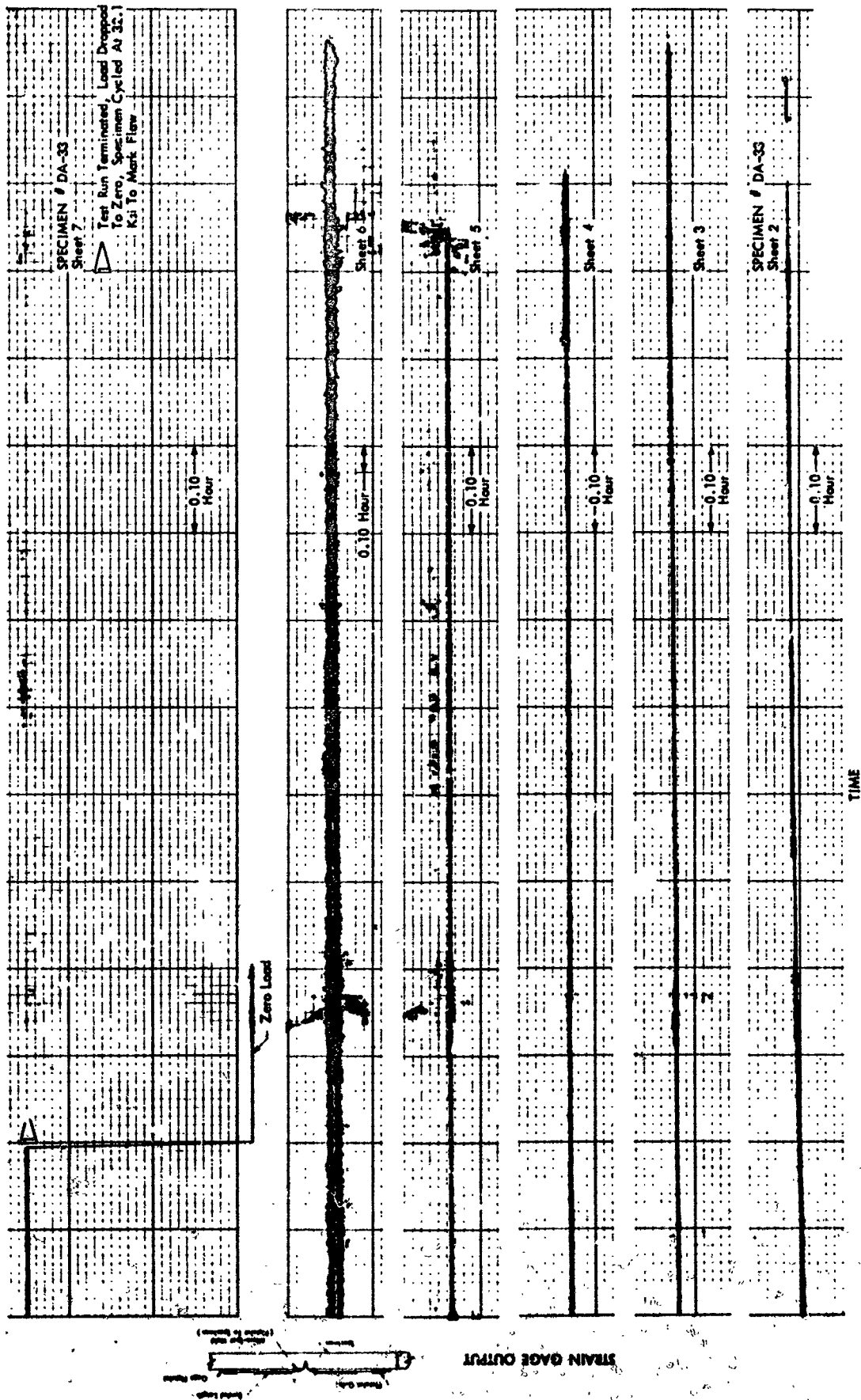
Figure 24: FLAW OPENING DISPLACEMENT UNDER SUSTAINED LOADING (2219-T87 Aluminum Specimen DA-33, Conclusion Of The First Test Run)
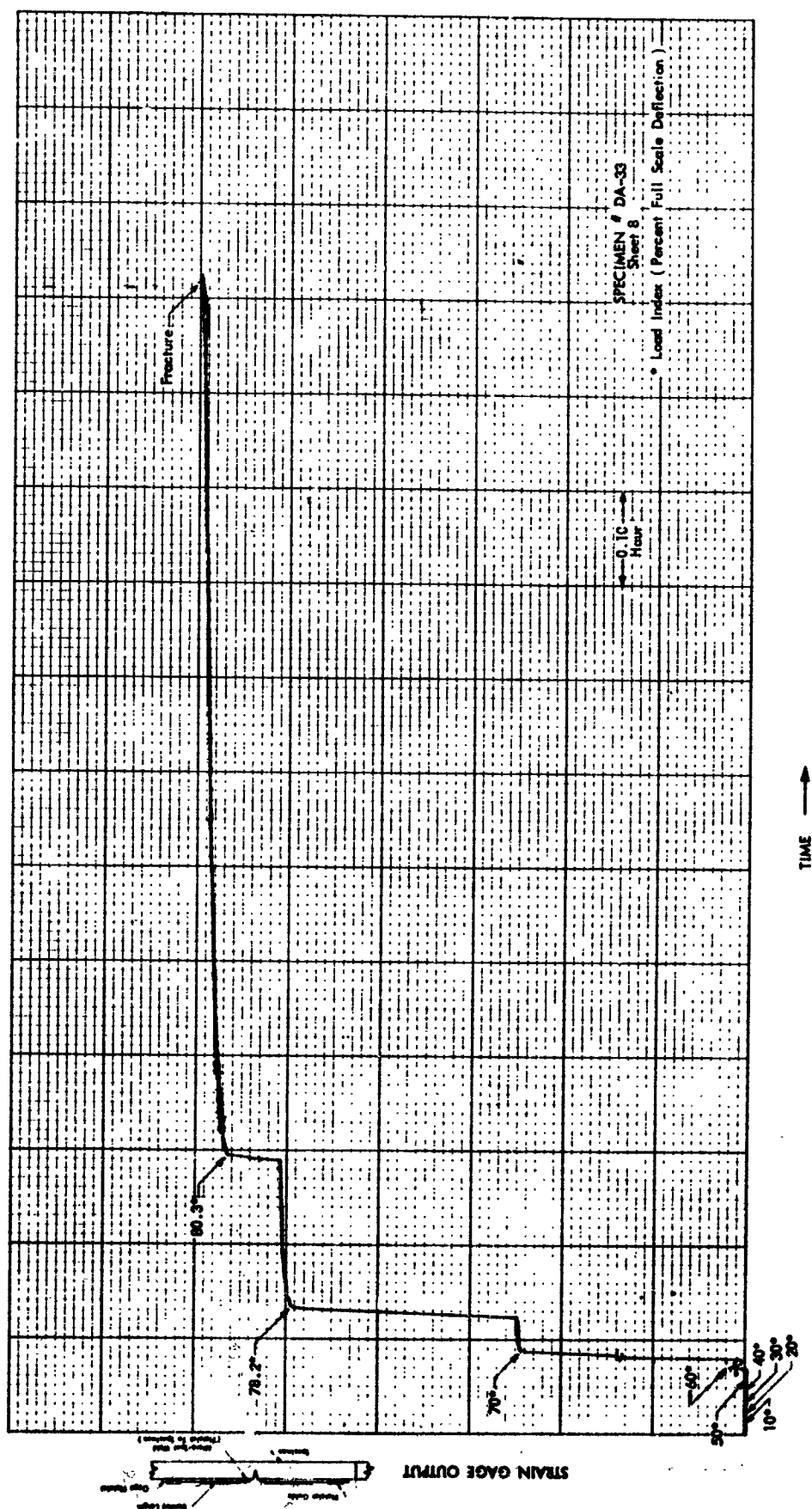
Figure 25 : FLAW OPENING DISPLACEMENT UNDER SUSTAINED LOADING
(2219-T87 Aluminum Specimen DA-33, Second Test Run)
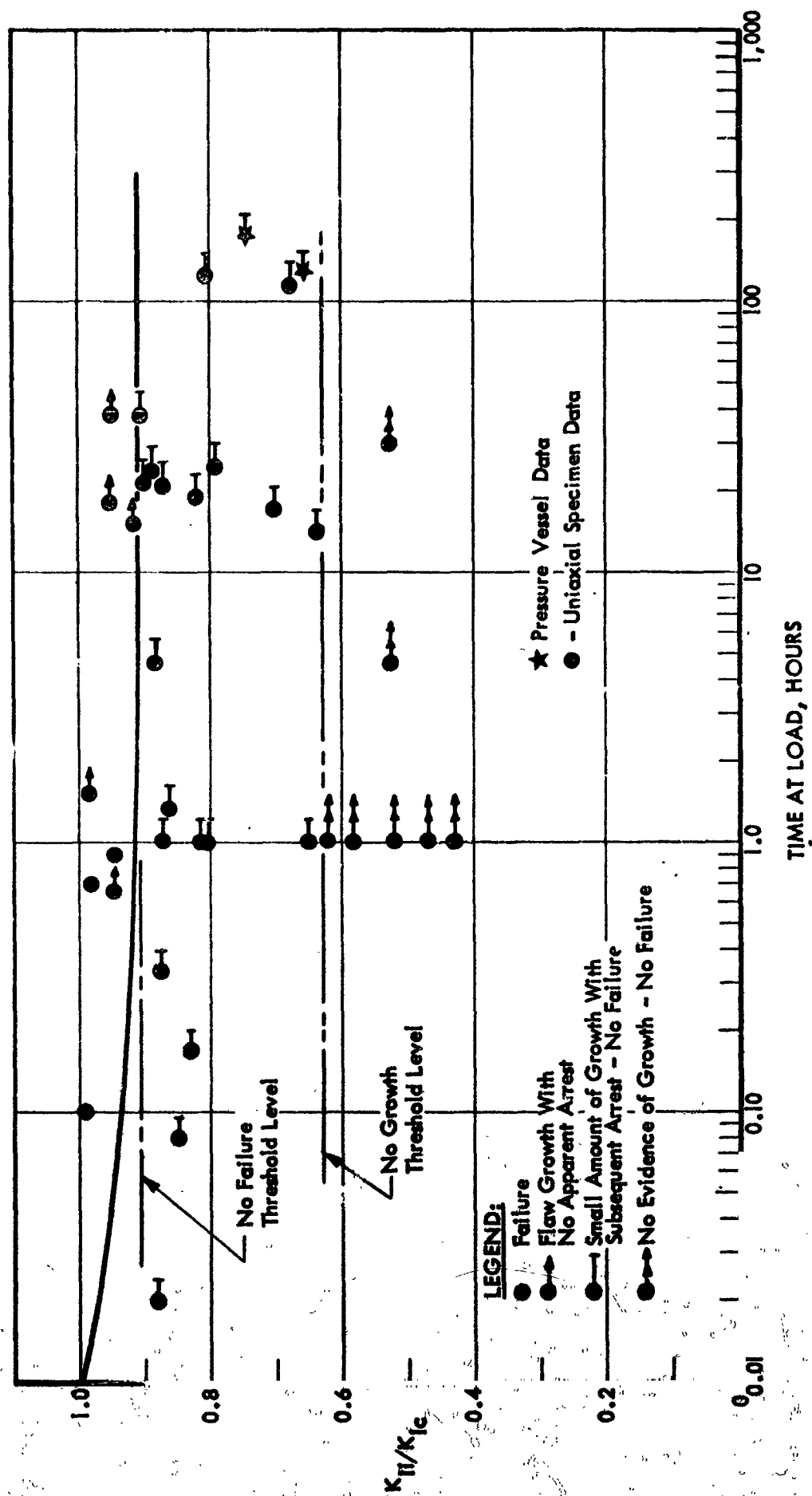
Figure 26: SUSTAINED STRESS LIFE DATA (2219 – T87 Aluminum @ Room Temperature)
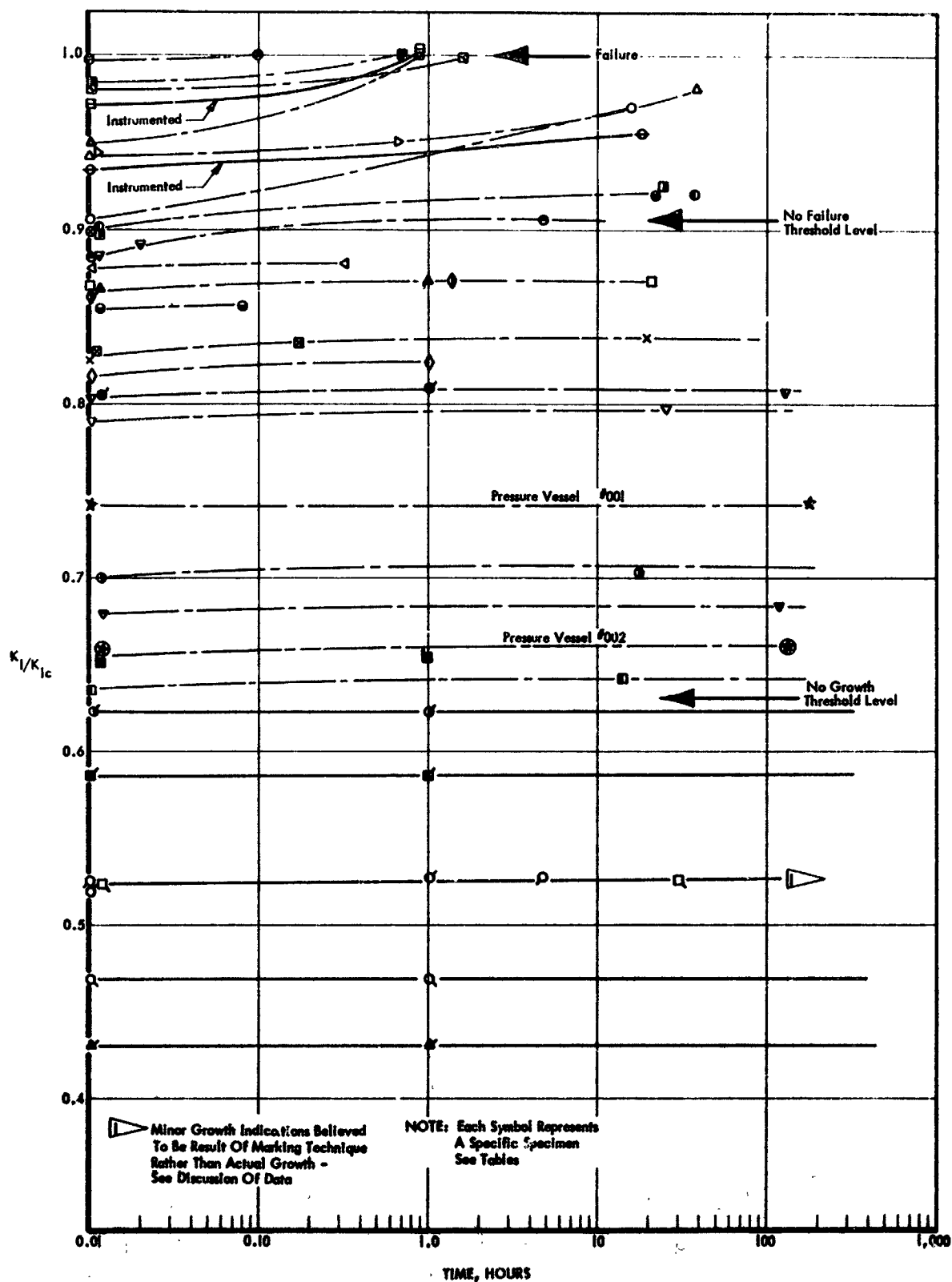
Figure 27: SUSTAINED STRESS FLAW GROWTH CURVES
(2219 - T87 Aluminum @ Room Temp.)

95
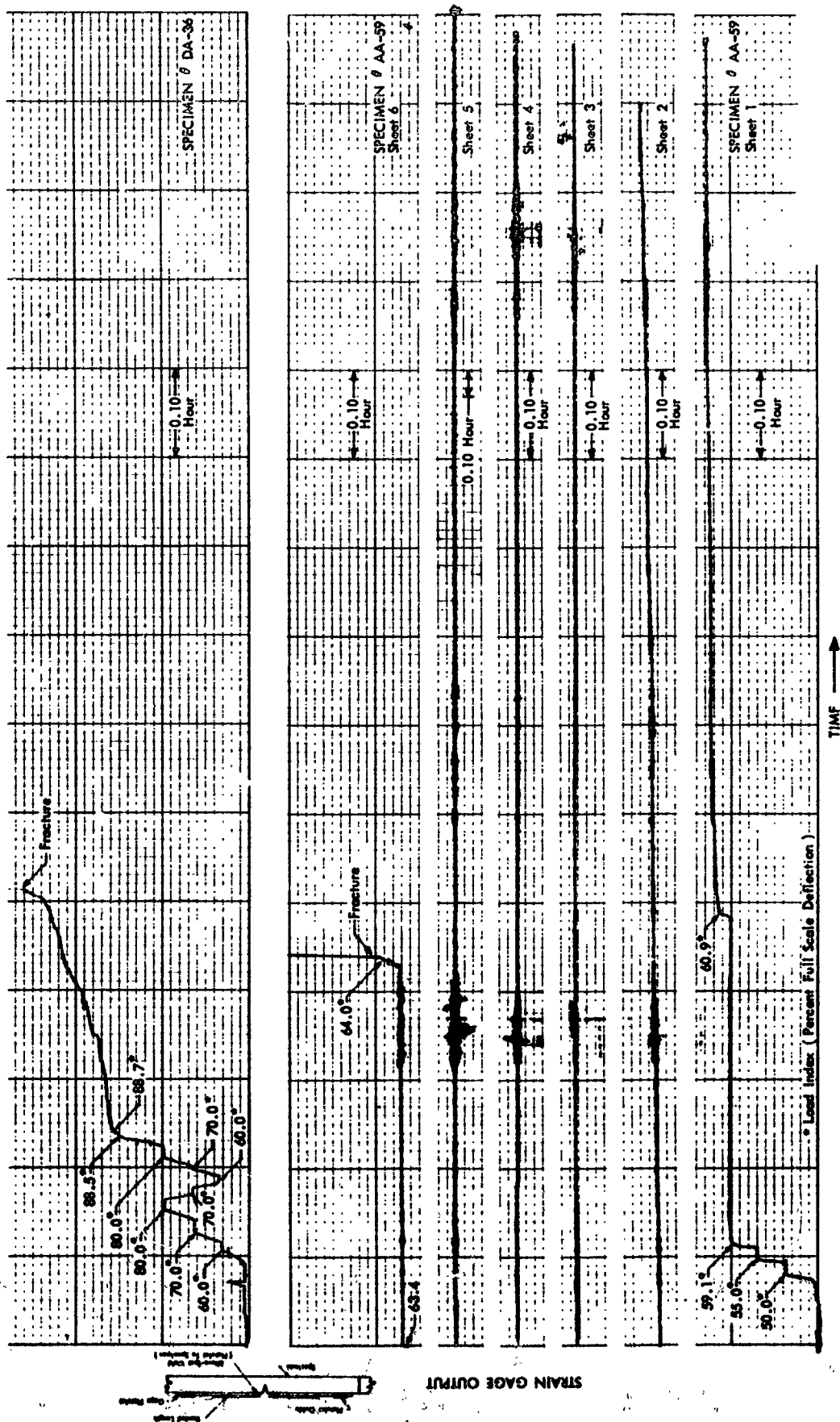
Figure 28 : FLAW OPENING DISPLACEMENT UNDER SUSTAINED LOADING
(2219-T87 Aluminum Specimens AA-59 And DA-36)
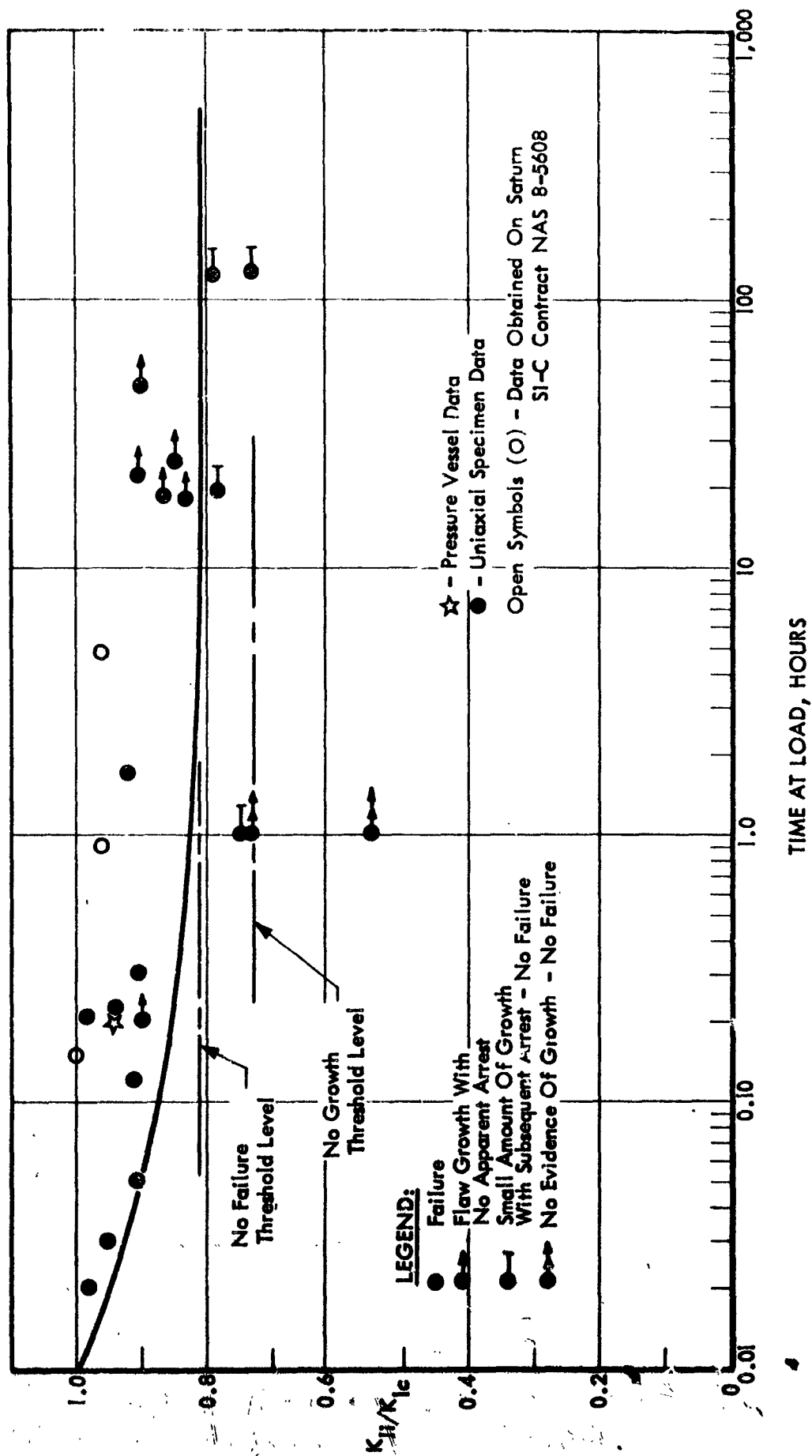
Figure 29: SUSTAINED STRESS LIFE DATA
(2219 - T87 Aluminum @ -320°F)
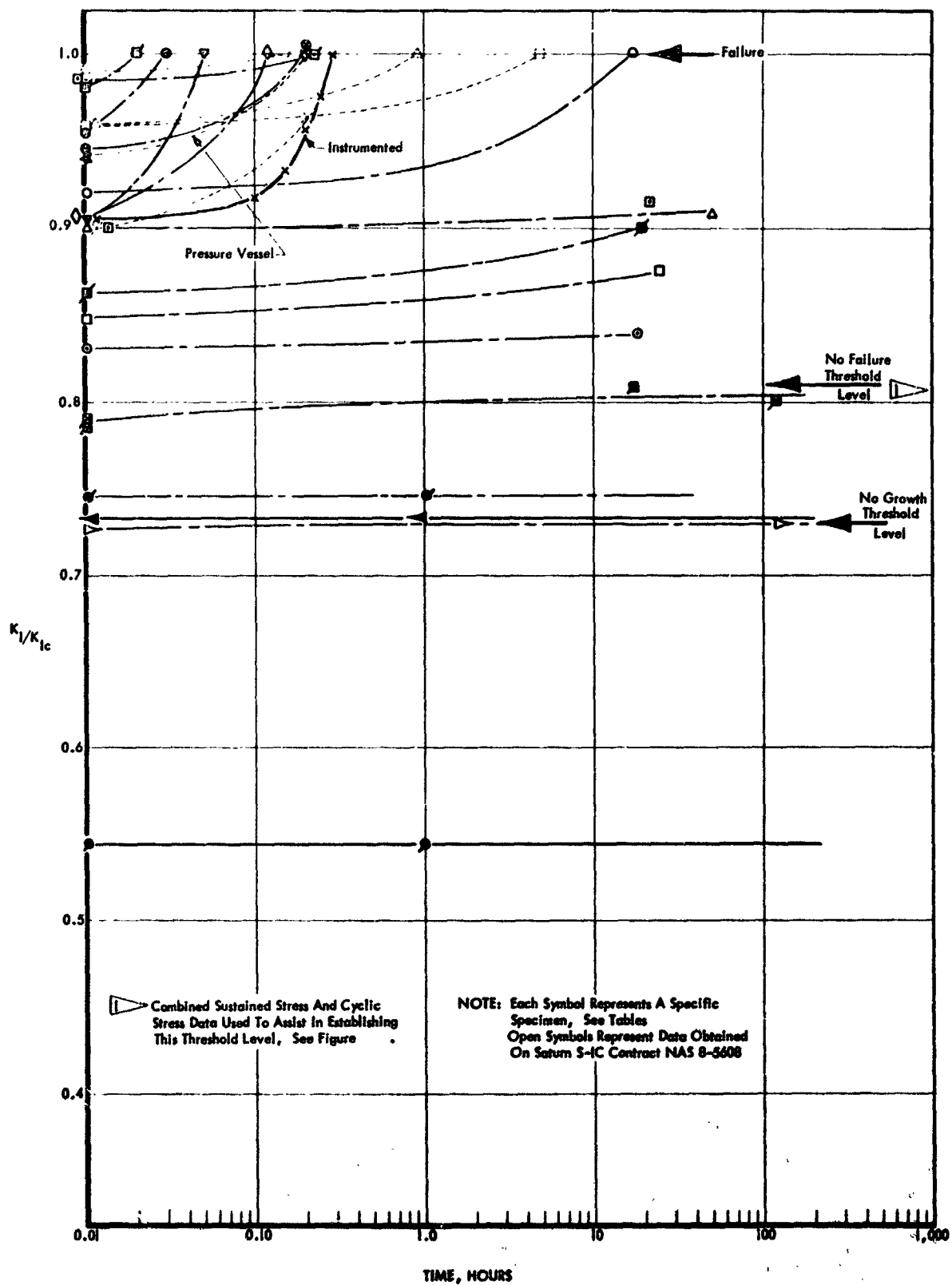
Figure 30: SUSTAINED STRESS FLAW GROWTH CURVES
(2219 - T87 Aluminum @ -320°F)

98
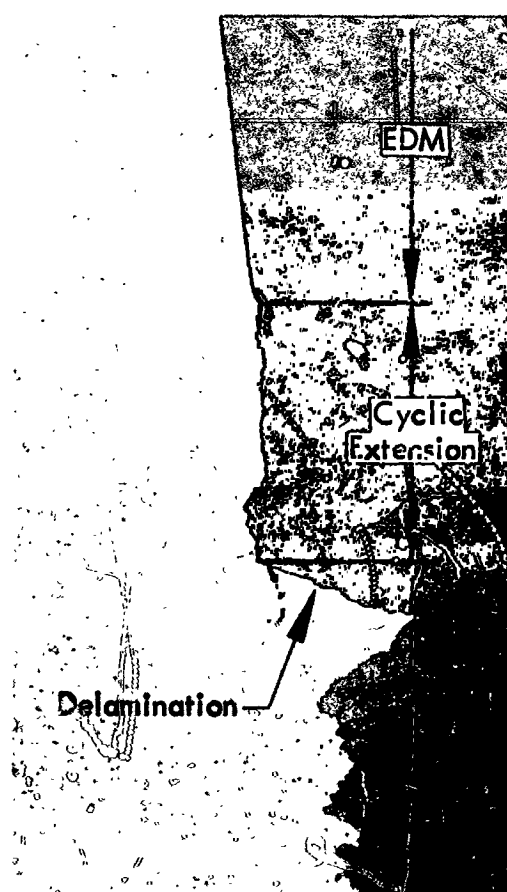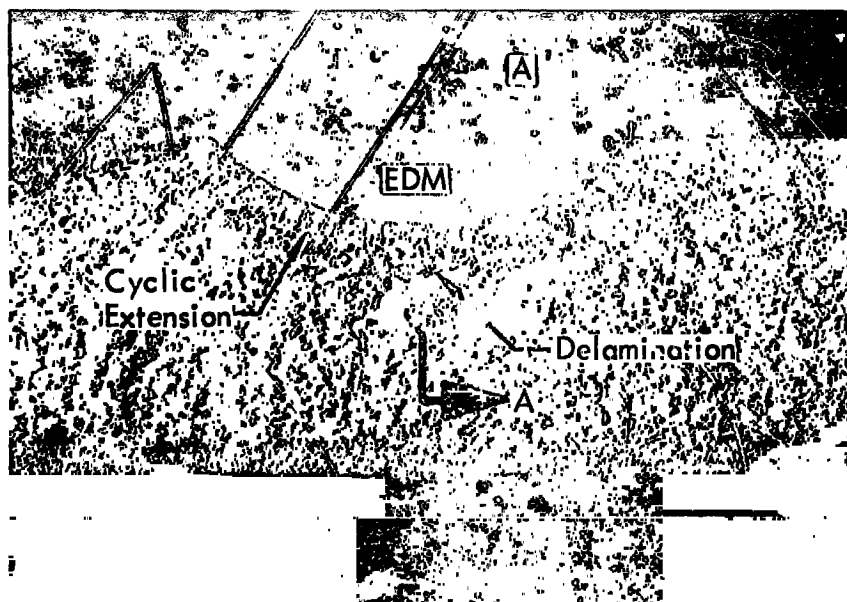
Section A-A

Figure 31: FRACTOGRAPH OF DELAMINATION (2219-T87 Aluminum Specimen No. CA-45)
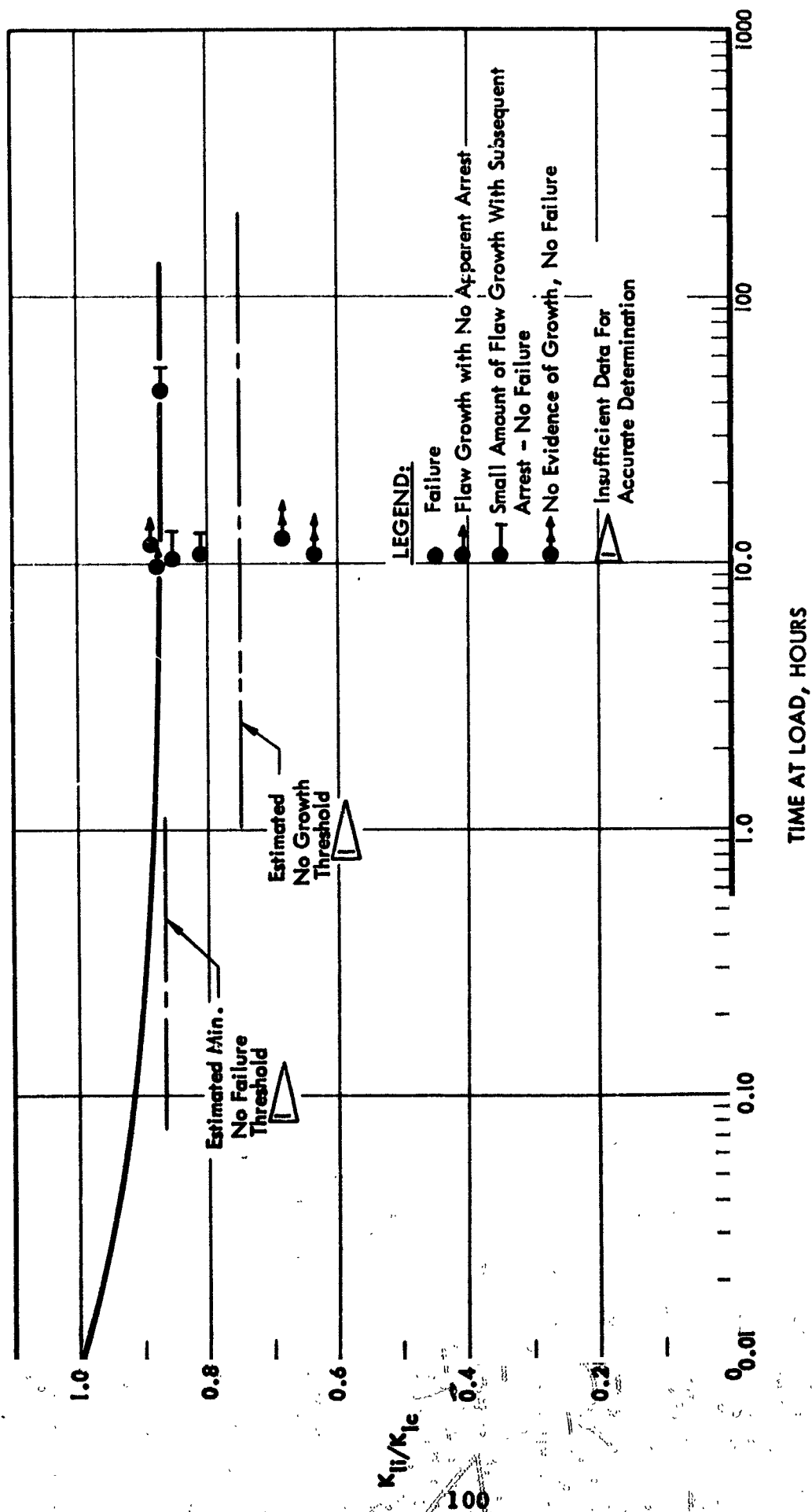
Figure 32 : SUSTAINED STRESS LIFE DATA (2219-T87 Aluminum At -423 °F)
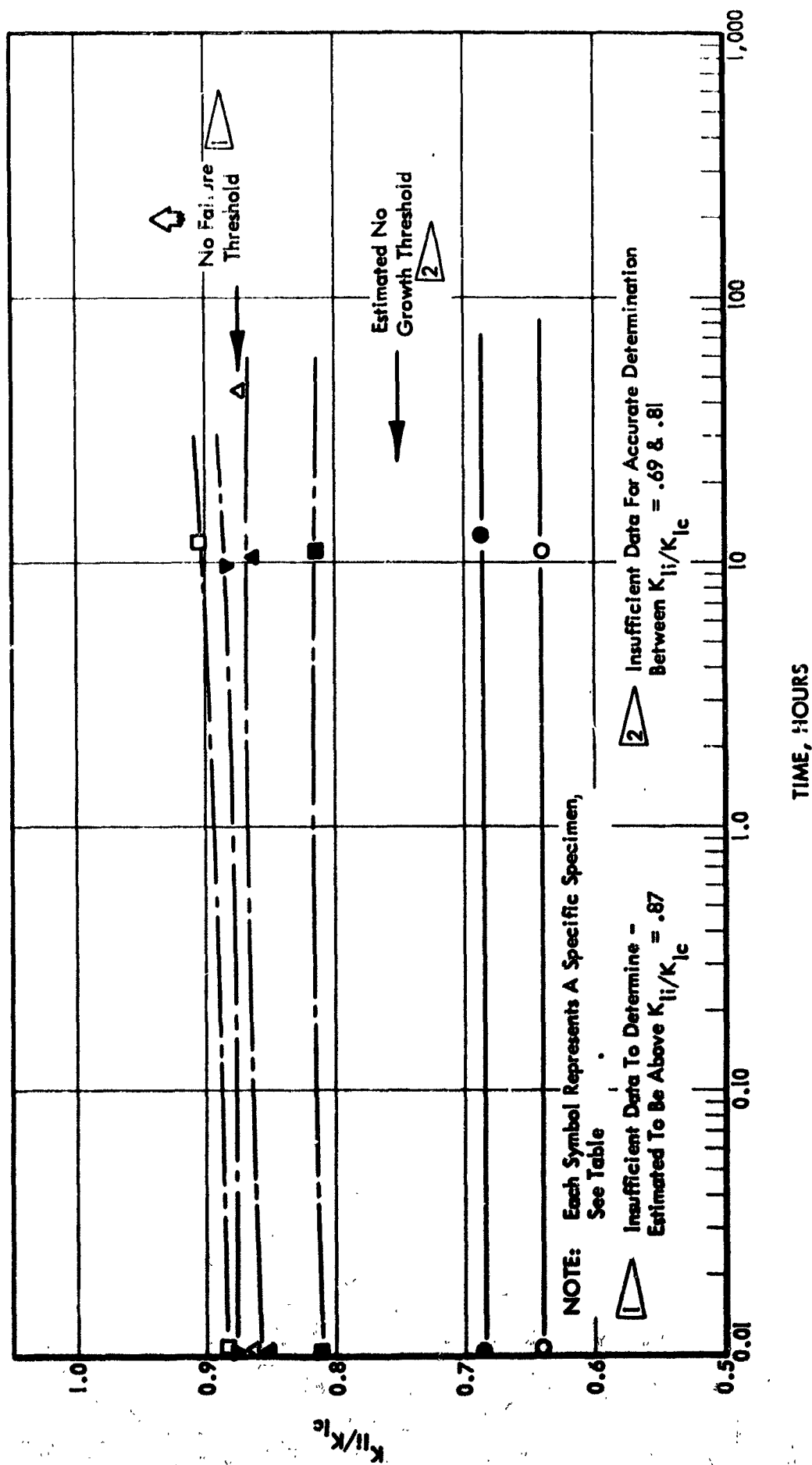
Figure 33: SUSTAINED STRESS FLAW GROWTH CURVES (2219 - T87 Aluminum @ -423°F)
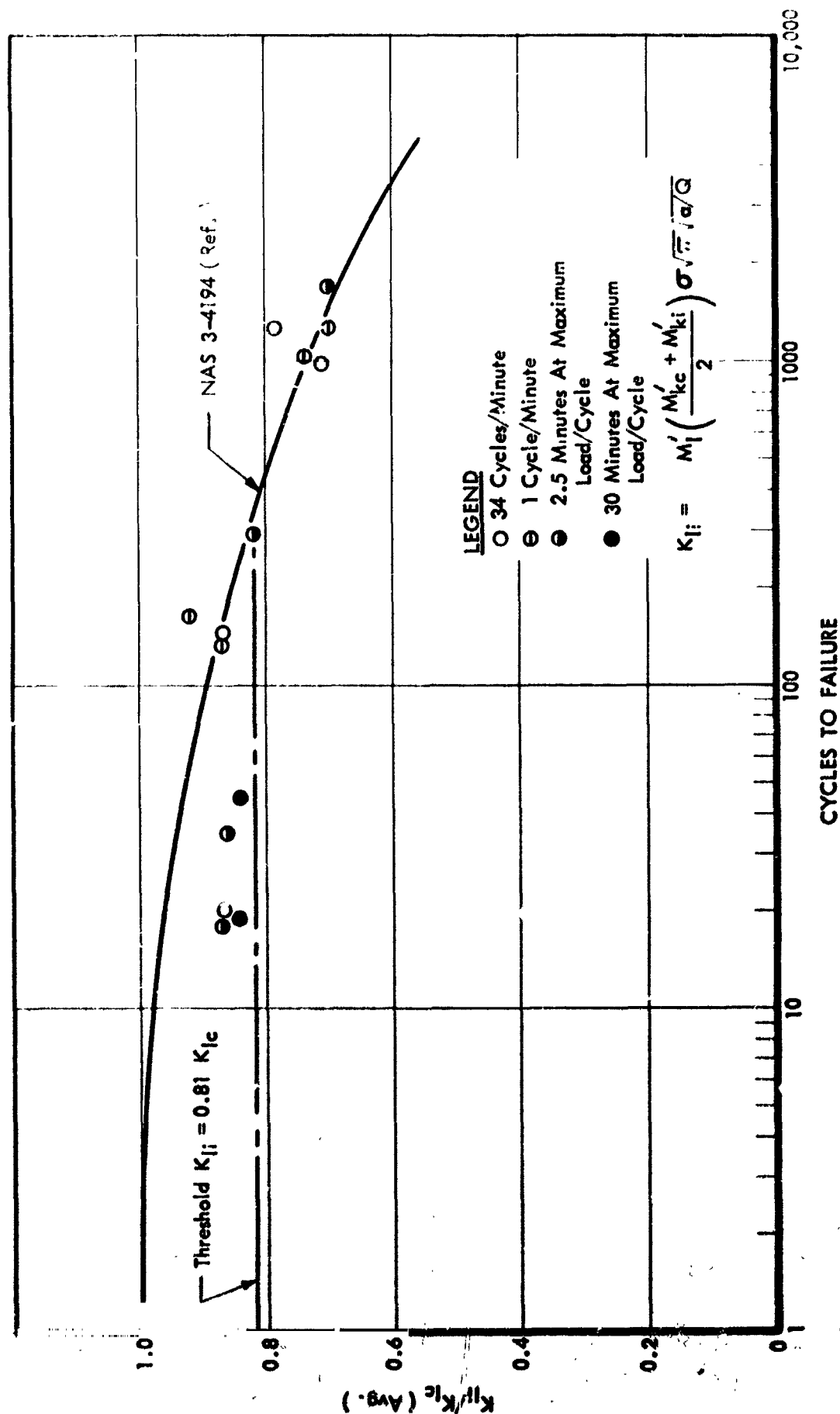
Figure 34 : COMBINED CYCLIC-SUSTAINED FLAW GROWTH IN 2219–T87 ALUMINUM AT –320 °F (End Point Analysis)

LEGEND

○ 34 Cycles/Minute
◐ 1 Cycle/Minute
◑ 2.5 Minutes At Maximum Load/Cycle
● 30 Minutes At Maximum Load/Cycle

$$K_{Ii} = M_I'\left(\frac{M_{kc}' + M_{ki}'}{2}\right)\sigma\sqrt{\pi}\,\sqrt{a/Q}$$

NAS 3–4194 (Ref.)

Threshold $K_{Ii} = 0.81\,K_{Ic}$

CYCLES TO FAILURE

K_{Ii}/K_{Ic} (Avg.)

Figure 35: COMBINED SUSTAINED STRESS AND CYCLIC FLAW GROWTH
(2219-T87 Aluminum At -320 °F)
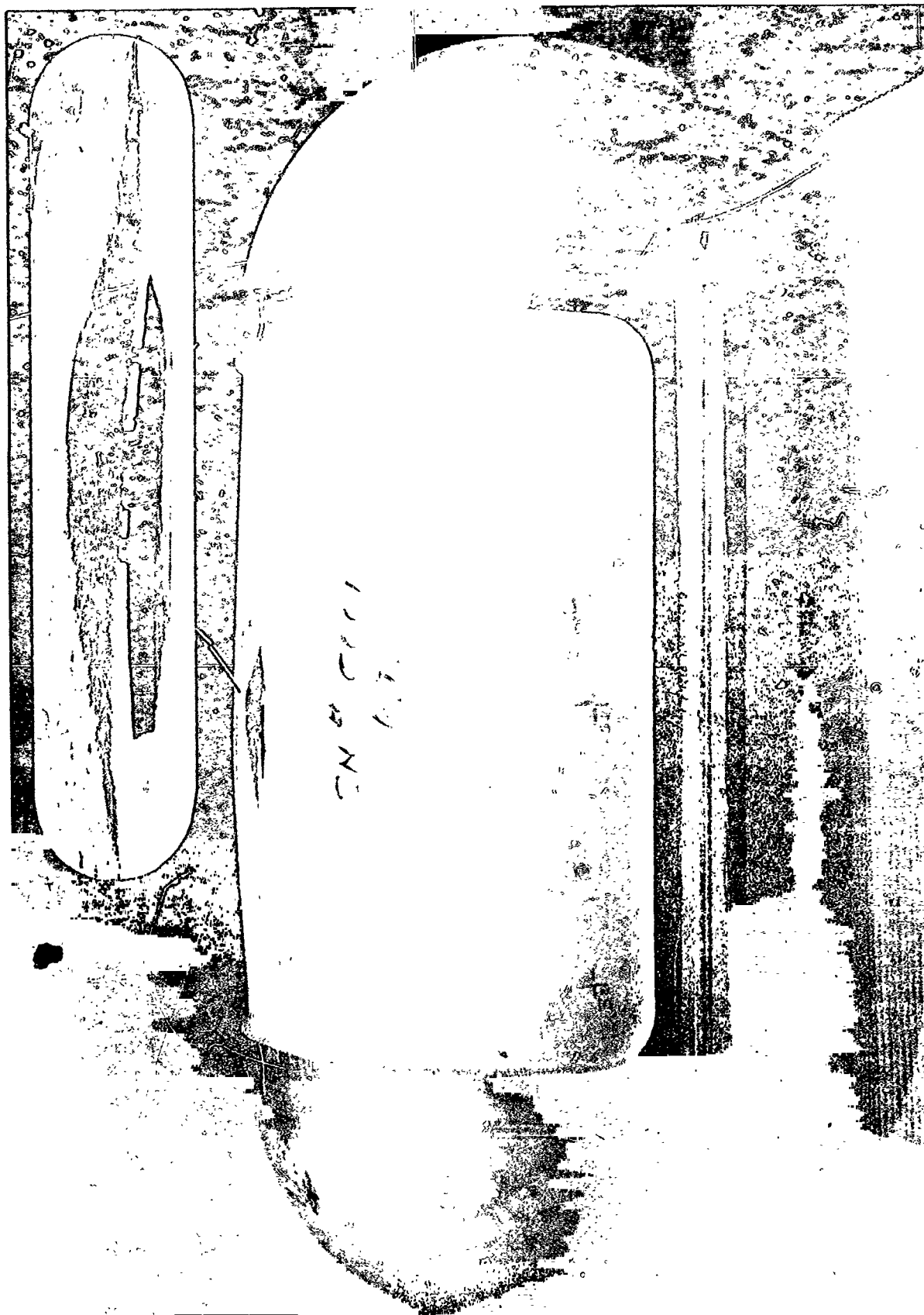
Figure 36: OVERALL VIEW OF FRACTURED 2219-T87 ALUMINUM TANK SERIAL NO. 0001 TESTED AT ROOM TEMPERATURE
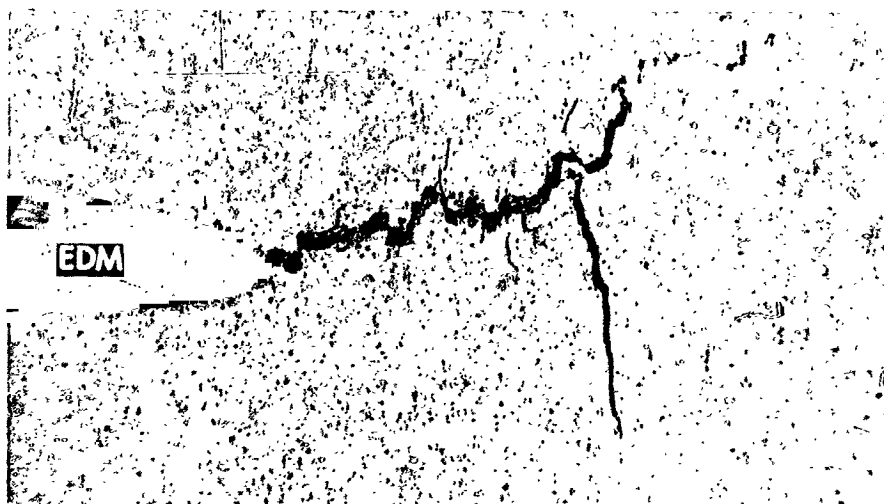
Photo # 2A240779   34 X

TANK NUMBER 0001
(Second Flaw)
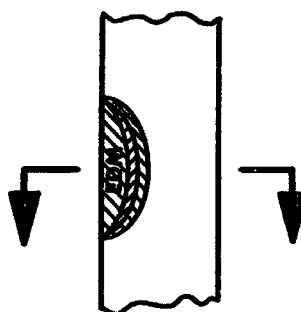
Photo # 2A240781   34 X

TANK NUMBER 0002
(Second Flaw)

Figure 37: DELAMINATION IN 2219-T87 ALUMINUM TANKS TESTED AT ROOM
           TEMPERATURE

Figure 38: OVERALL VIEW OF FRACTURED 2219-T87 ALUMINUM TANK SERIAL NO. 0003 TESTED AT -423 °F

106
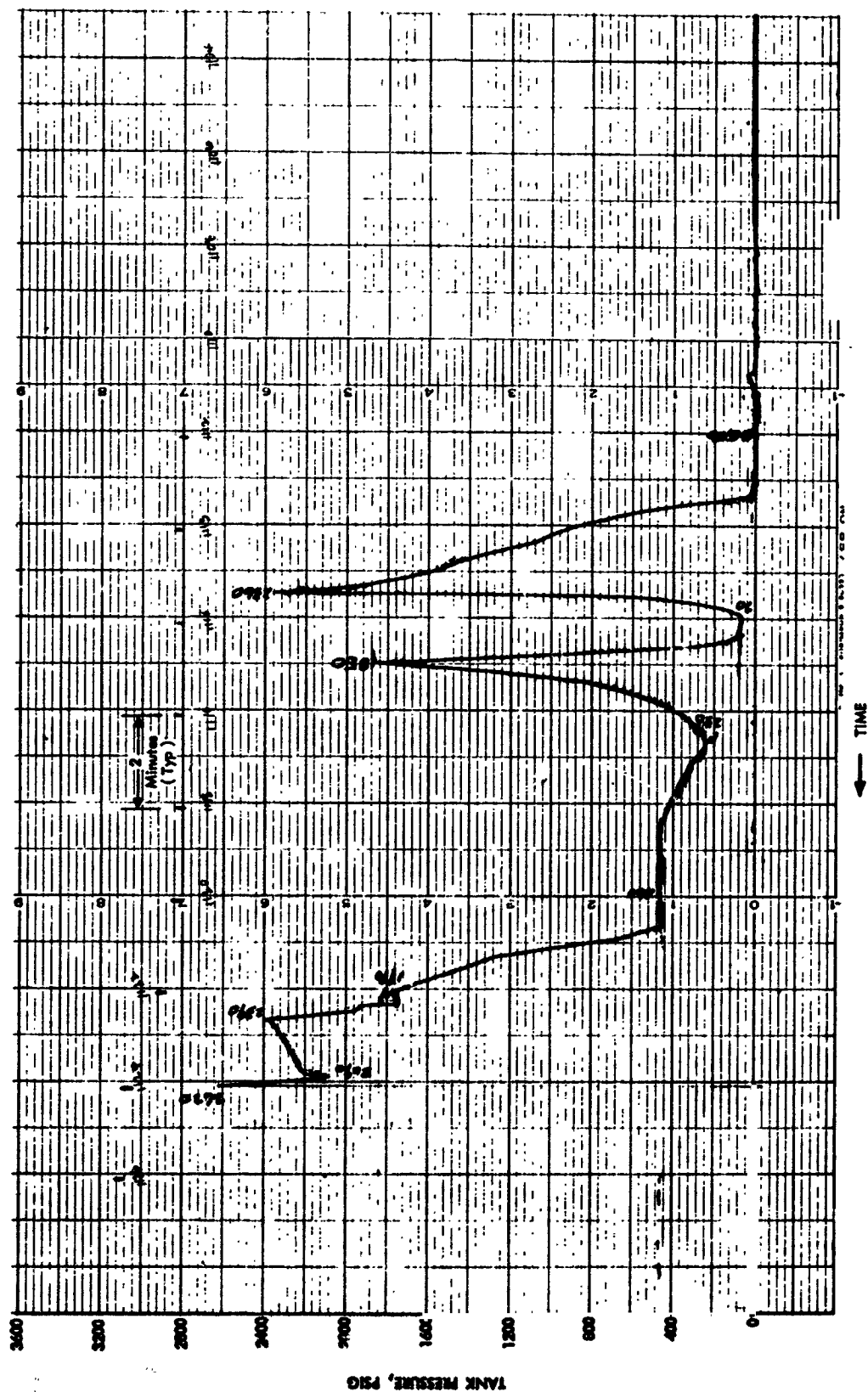
Figure 39: PRESSURE VS TIME CHART RECORD FOR 2219-T87 ALUMINUM TANK
SERIAL NO. 0004 TESTED AT -423 °F
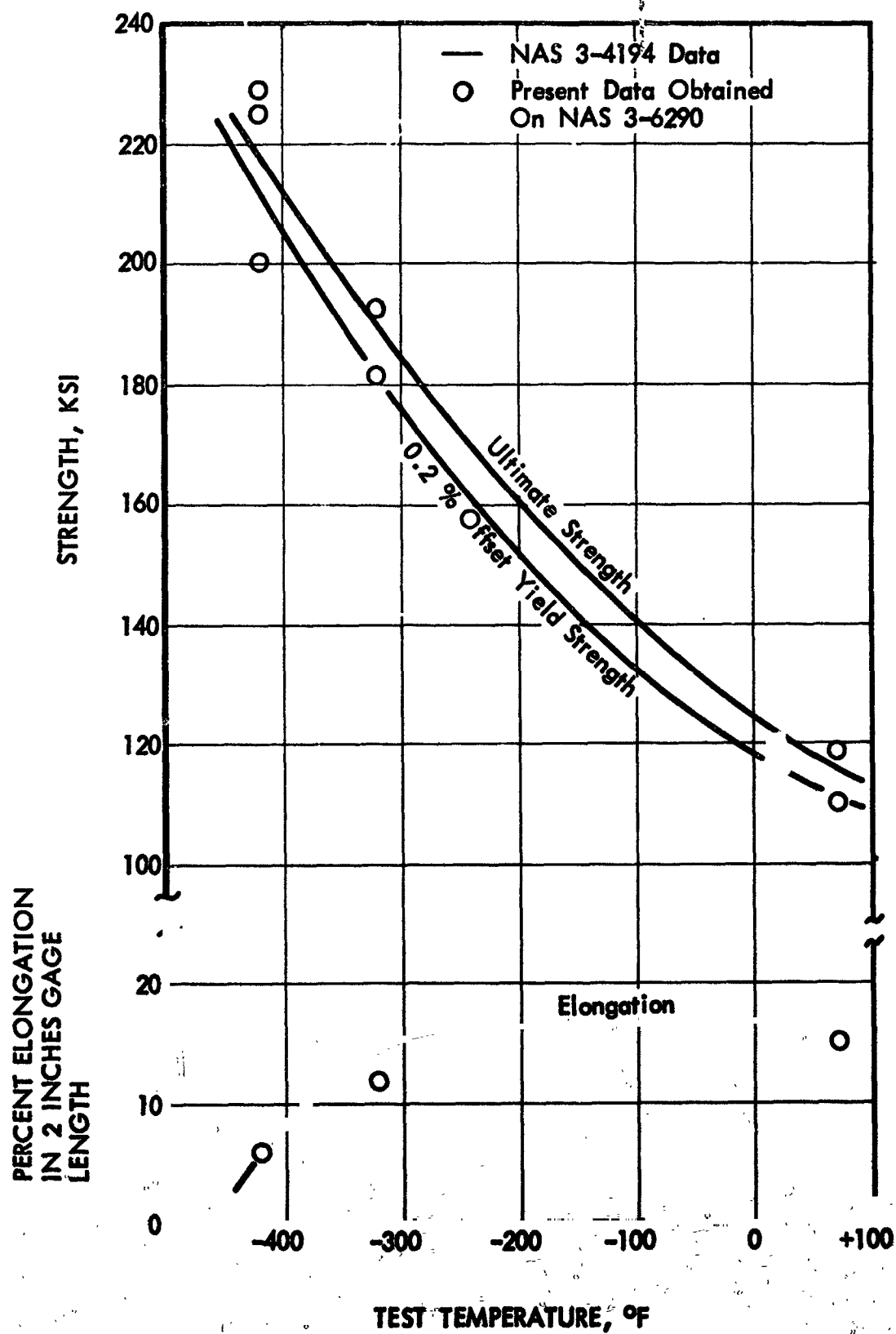
Figure 40: MECHANICAL PROPERTIES OF 5Al-2 1/2 Sn (ELI) TITANIUM PLATE
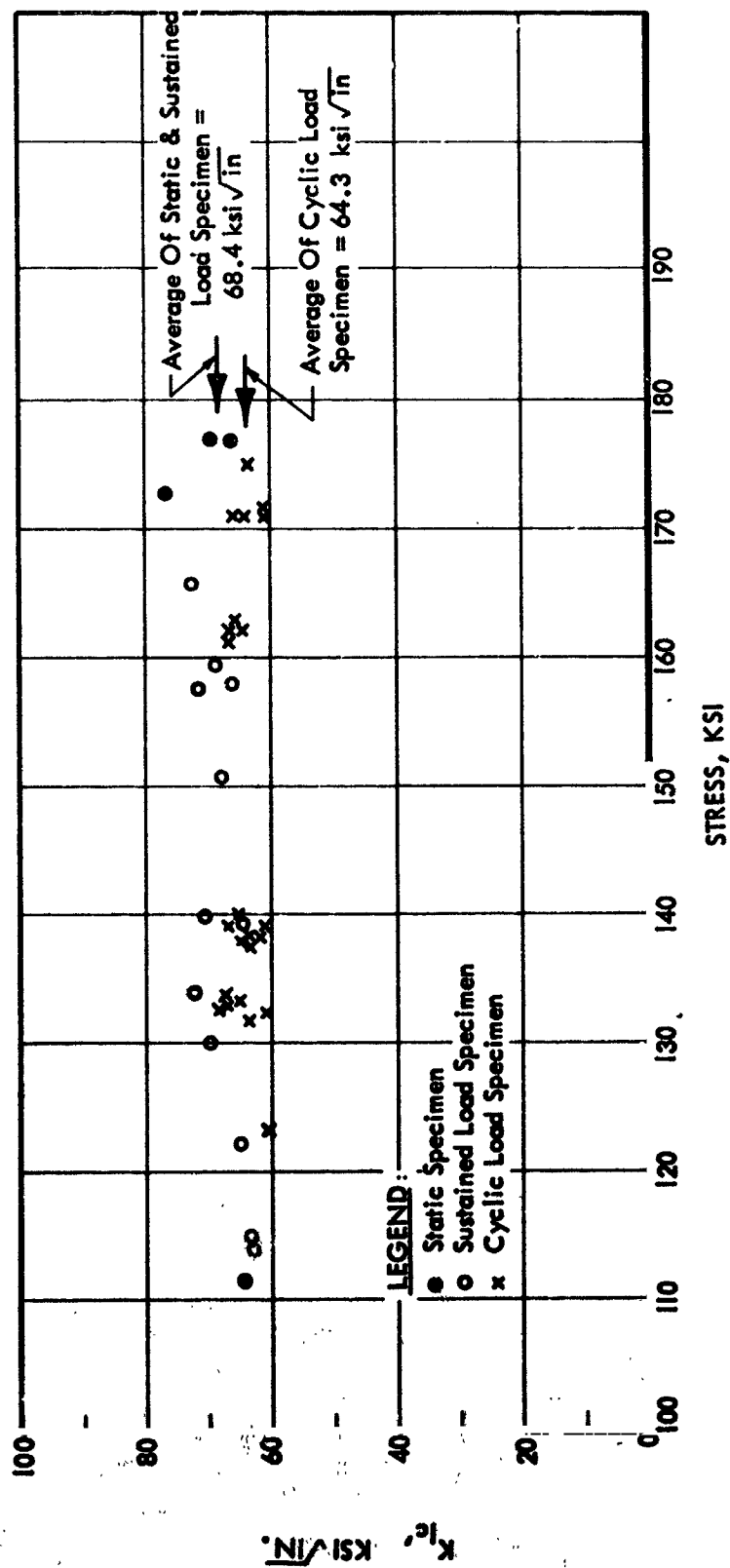
Figure 41: K_{Ic} VS FRACTURE STRESS (5 AL – 2 1/2 Sn (ELI) Titanium @ –320°F)
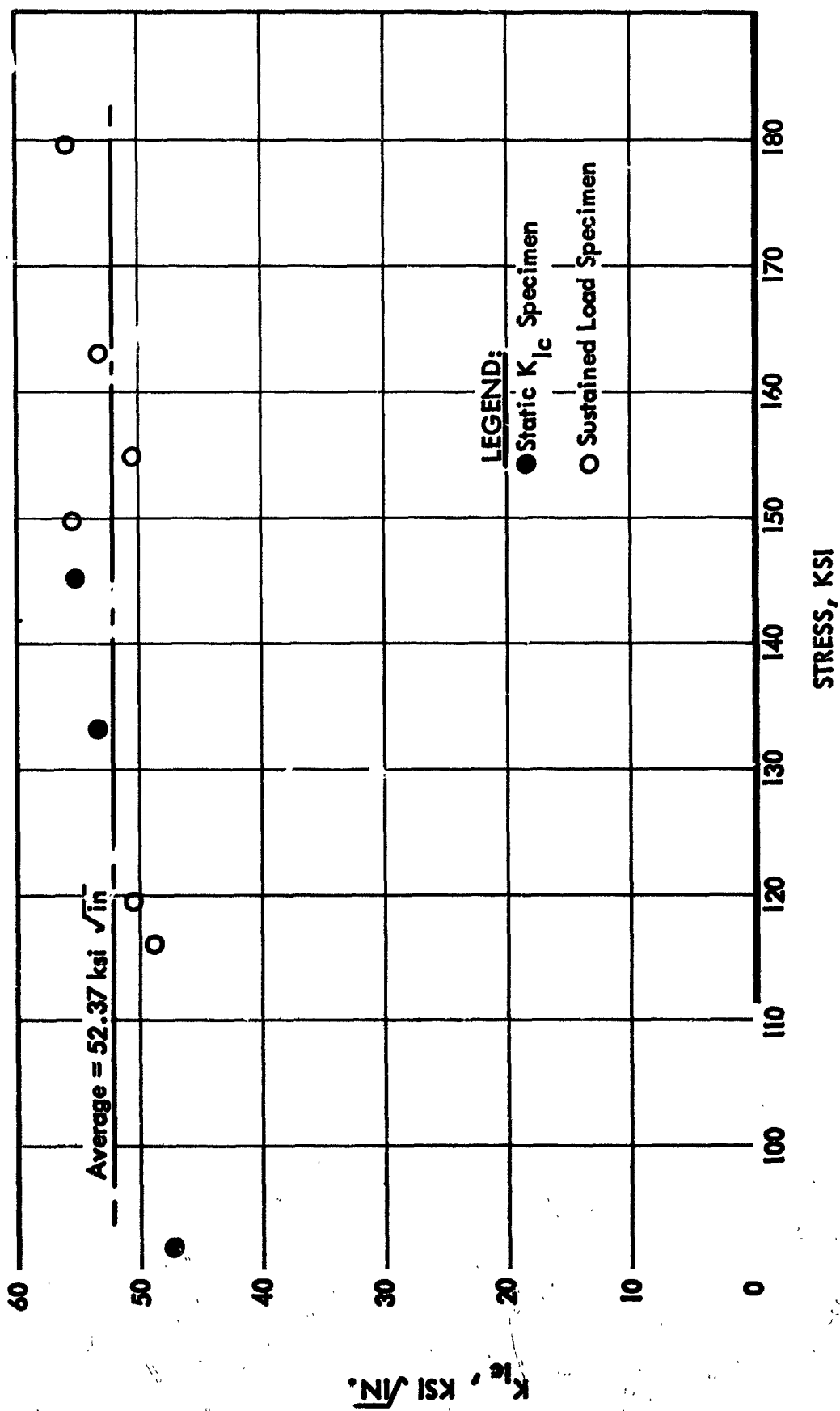
Figure 42: K_{Ic} VS FRACTURE STRESS (5 AL – 2 1/2 Sn (ELI) Titanium @ -423°F)
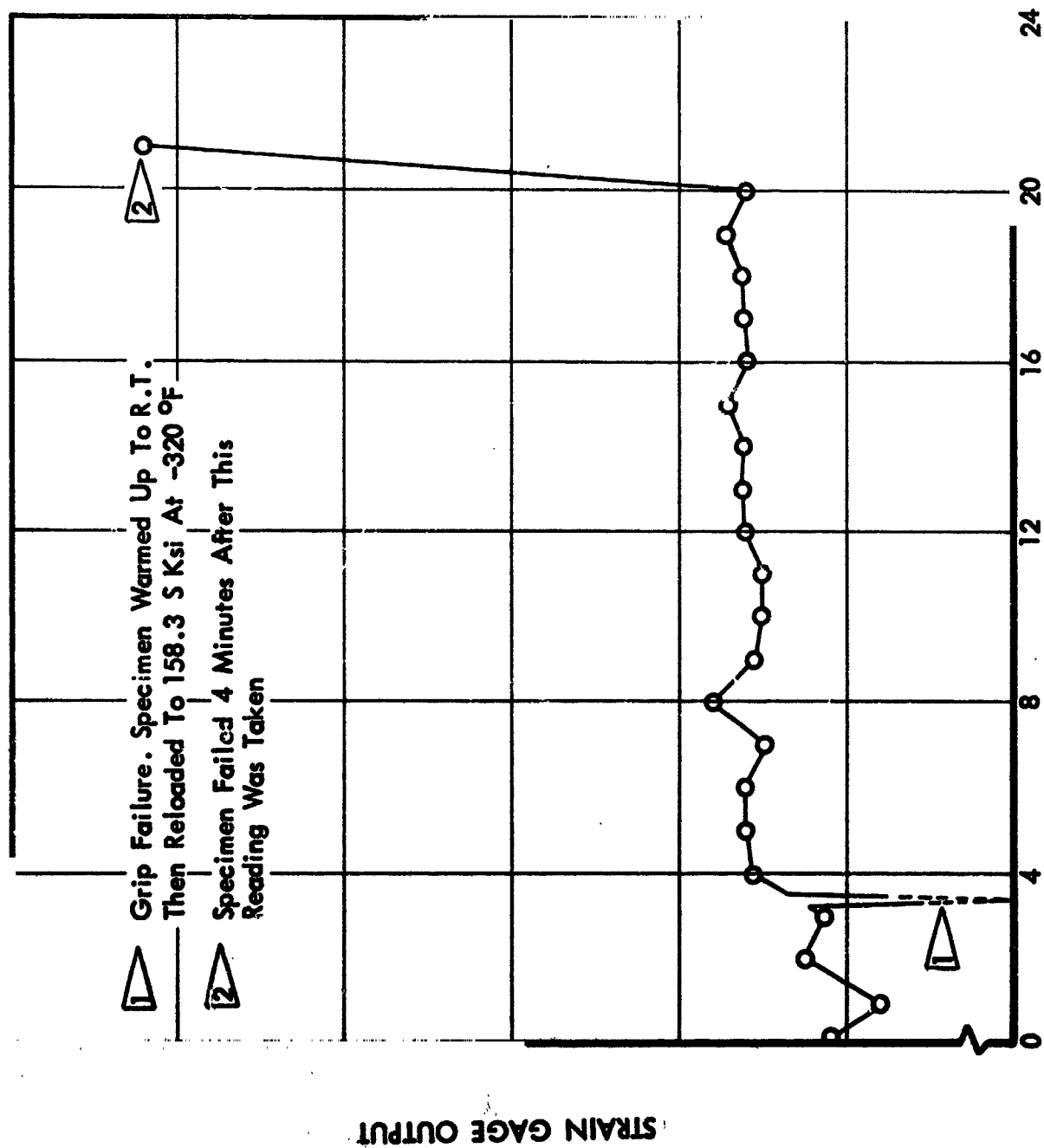
Figure 43 : FLAW OPENING DISPLACEMENT FOR 5Al-21/2 Sn (ELI) TITANIUM (Specimen Number 4T-15)
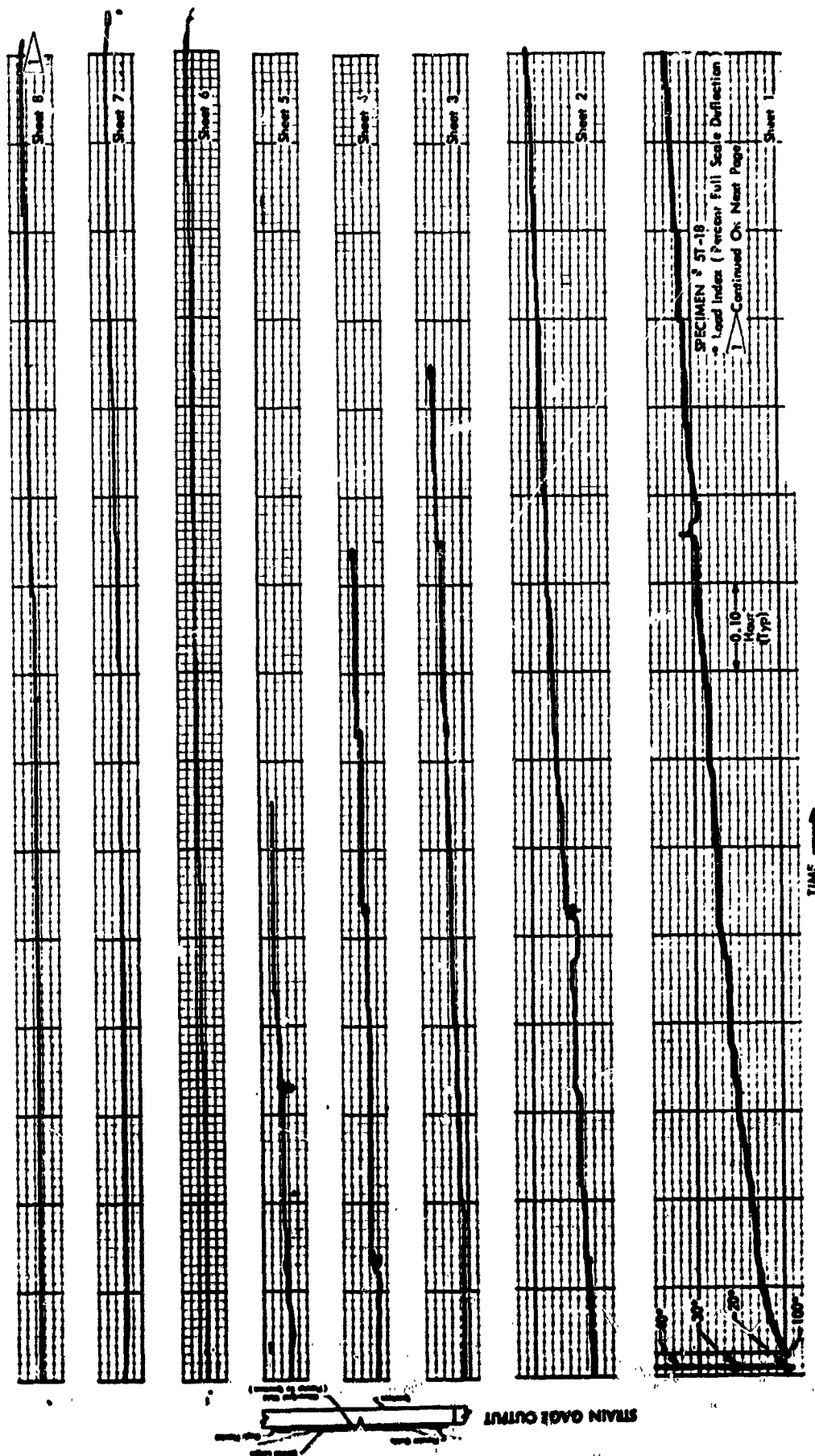
Figure 44 : FLAW OPENING DISPLACEMENT UNDER SUSTAINED LOADING
(5 Al-2 1/2 Sn (ELI) Titanium Specimen 5T-18, Beginning Of
The Test Run)
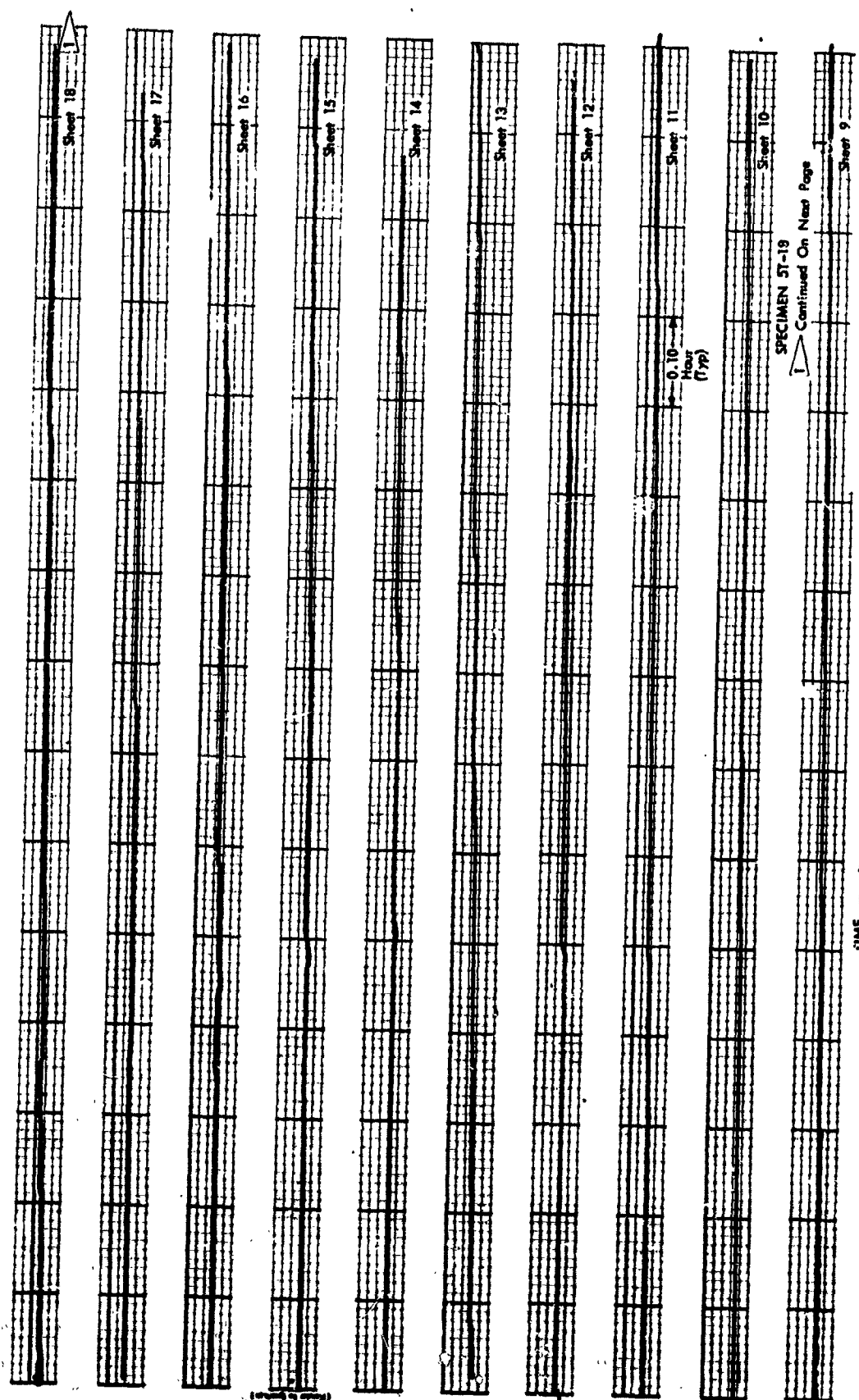
Figure 45 : FLAW OPENING DISPLACEMENT UNDER SUSTAINED LOADING
(5 Al-2 1/2 Sn (ELI) Titanium Specimen 5T-18, Continuation
Of The Test Run)

113
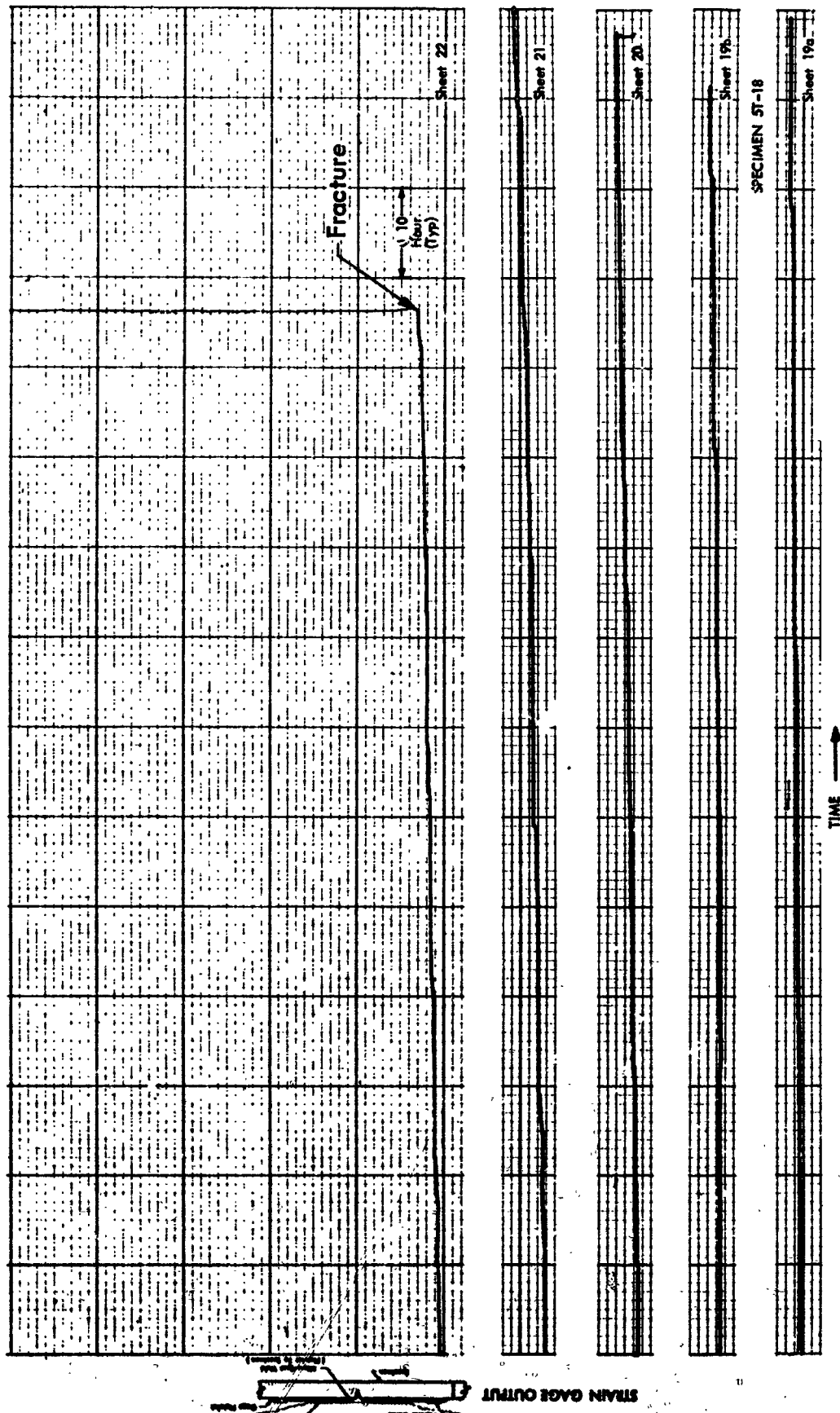
Figure 46: FLAW OPENING DISPLACEMENT UNDER SUSTAINED LOADING
(5 Al-2 1/2 Sn (ELI) Titanium Specimen 5T-18, Conclusion
Of The Test Run)
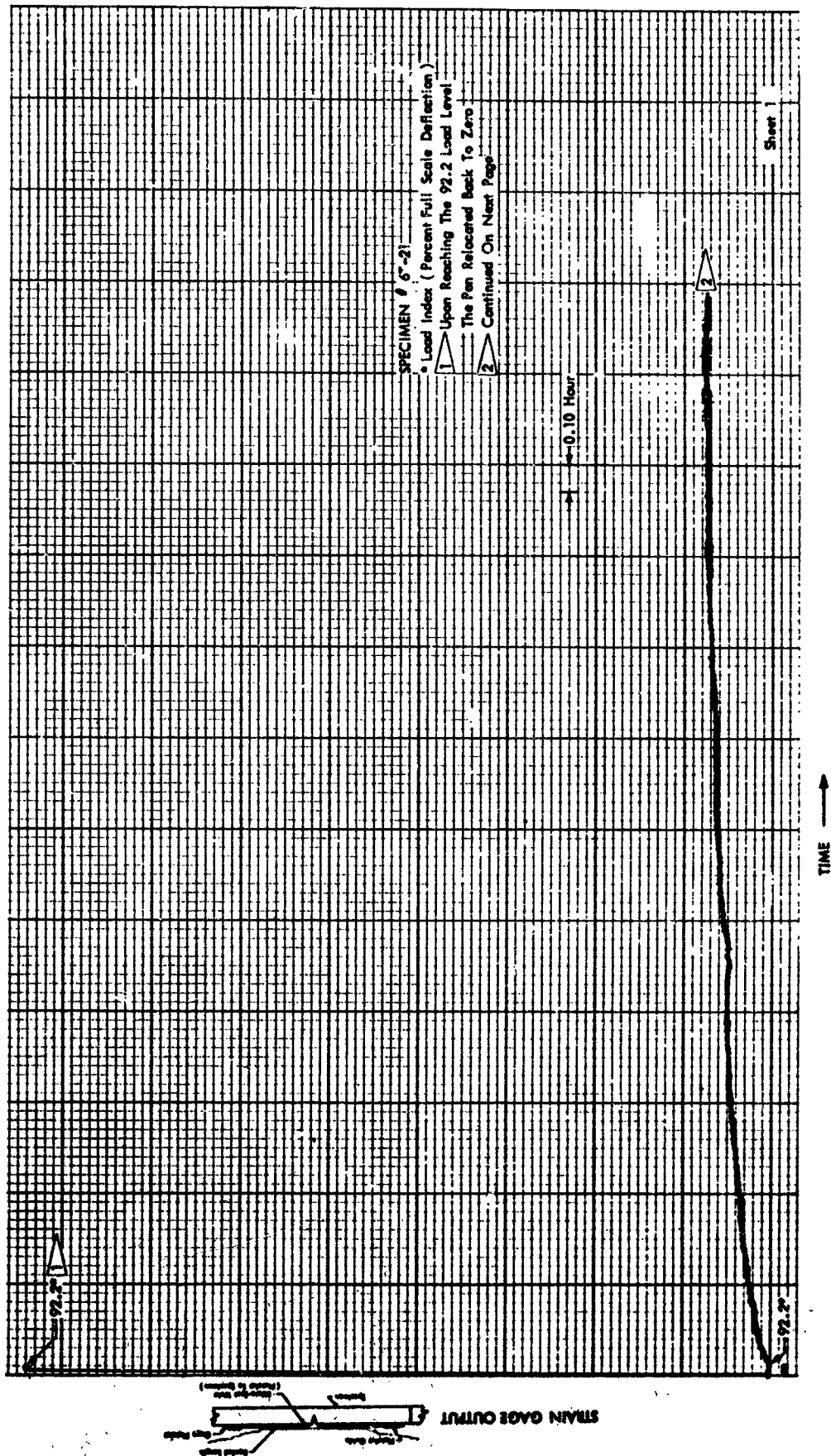
Figure 47: FLAW OPENING DISPLACEMENT UNDER SUSTAINED LOADING (5 Al-2 1/2 Sn (ELI) Titanium Specimen 6T-21, Beginning Of The First Test Run)
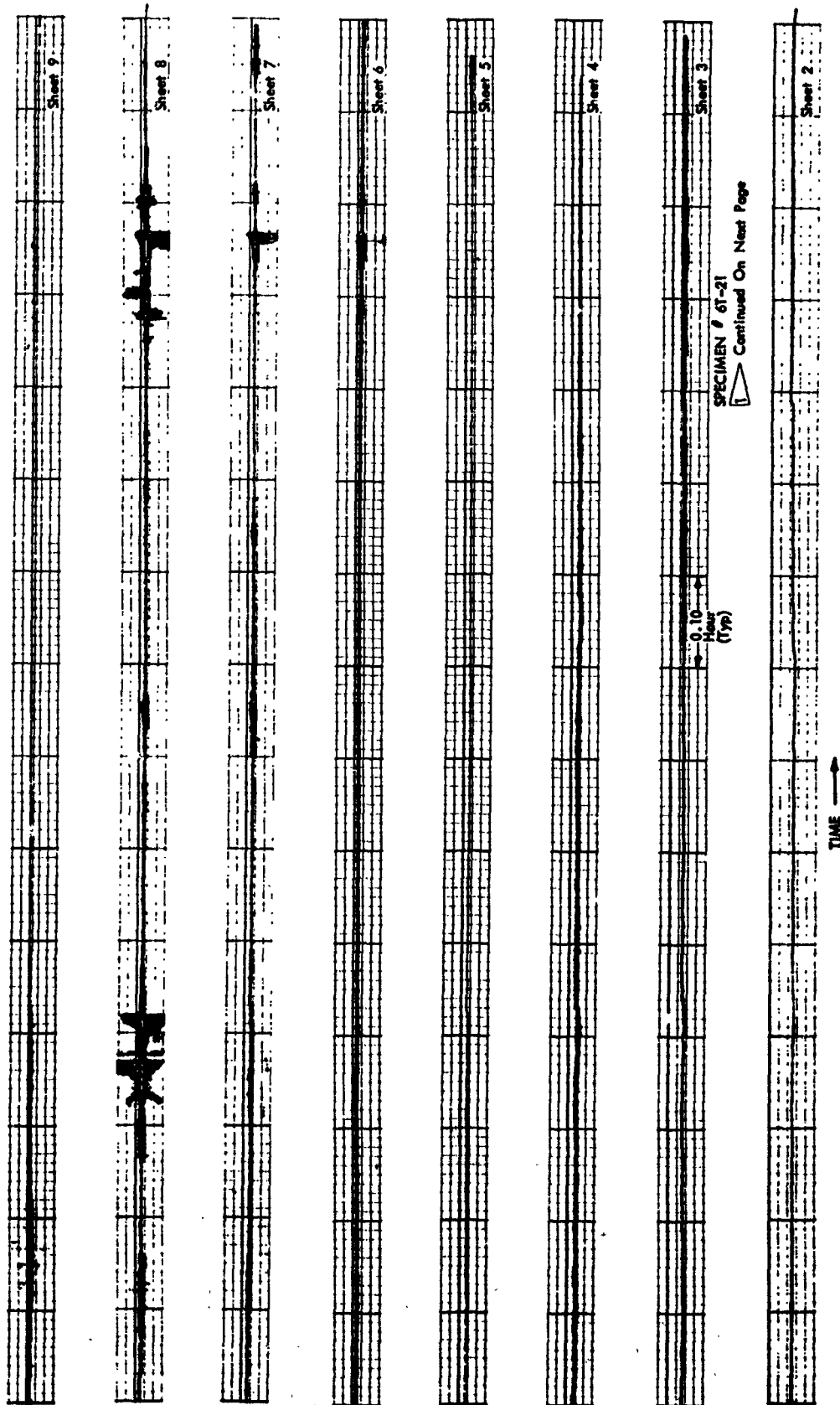
Figure 48: FLAW OPENING DISPLACEMENT UNDER SUSTAINED LOADING
(5 Al-2 1/2 Sn (ELI) Titanium Specimen 6T-21, Continuation
Of The First Test Run)

116
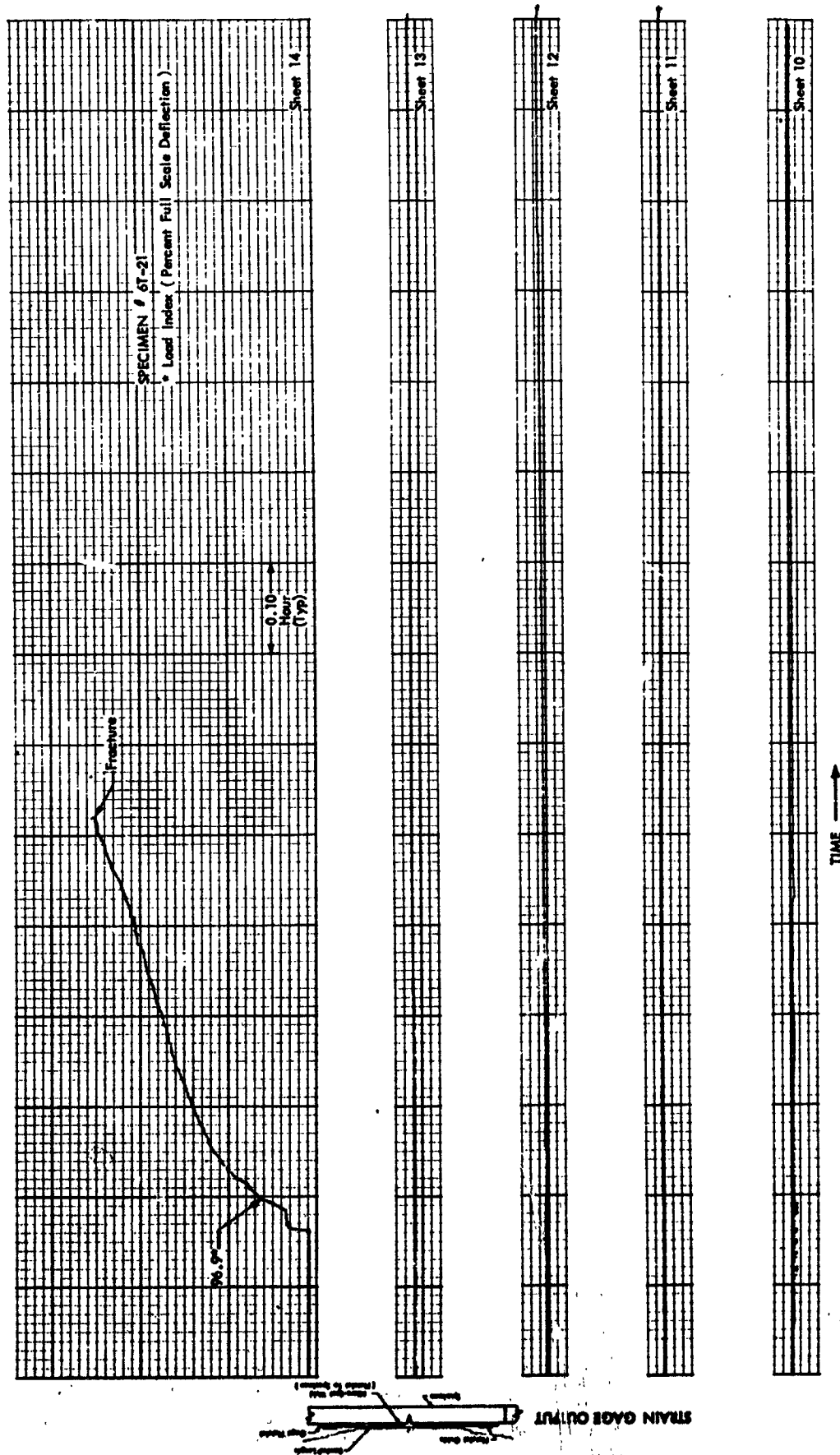
Figure 49: FLAW OPENING DISPLACEMENT UNDER SUSTAINED LOADING
(5 Al-2 1/2 Sn (ELI) Titanium Specimen 6T-21, Completion Of
The First Test Run And The Second Test Run)
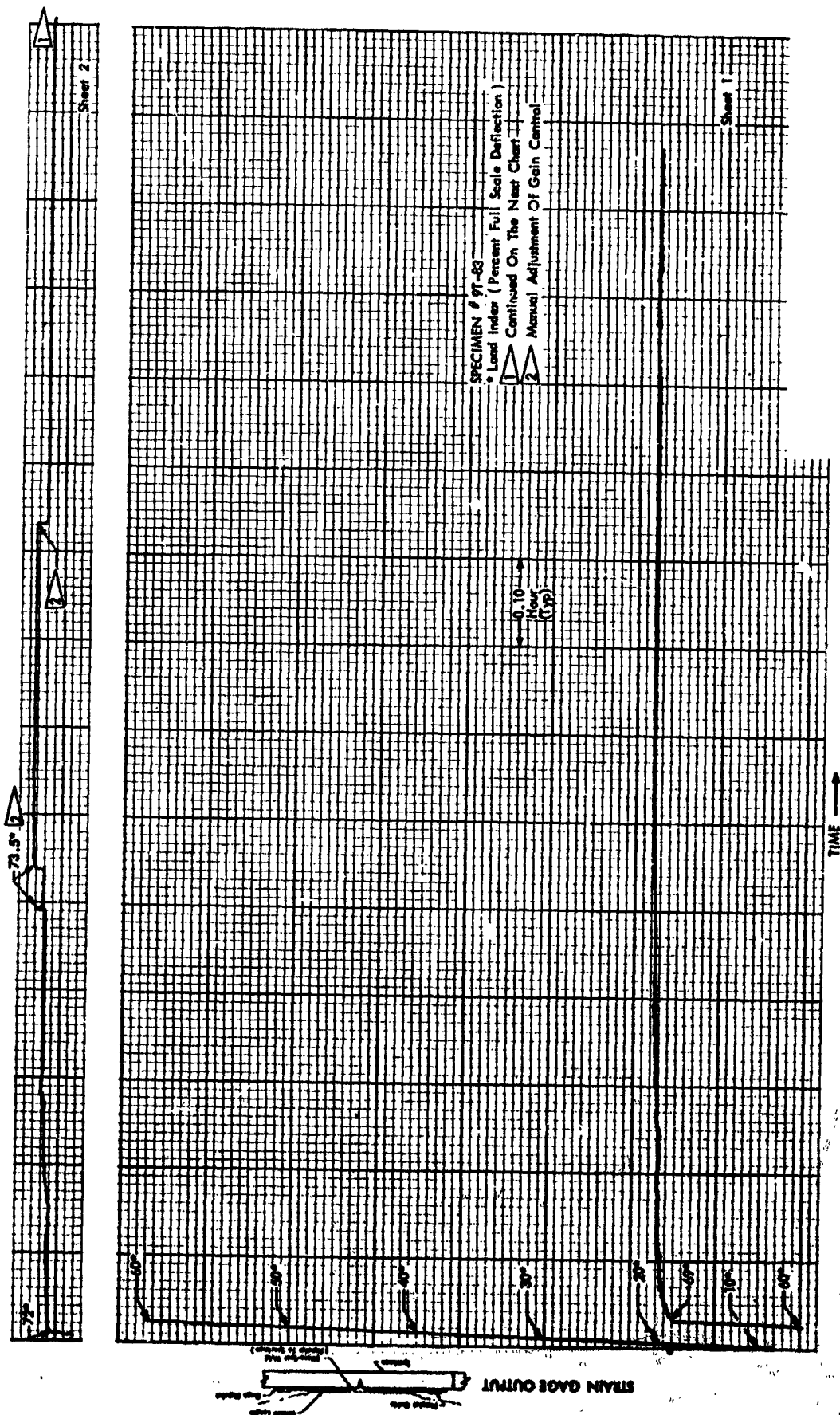
Figure 50: FLAW OPENING DISPLACEMENT UNDER SUSTAINED LOADING
(5 Al–2 1/2 Sn (ELI) Titanium Specimen 9T-83, Beginning Of
The Test Run)

Figure 51: FLAW OPENING DISPLACEMENT UNDER SUSTAINED LOADING
(5 Al-2 1/2 Sn (ELI) Titanium Specimen 9T-83, Continuation
Of The Test Run, Sheets 3 Thru 12)
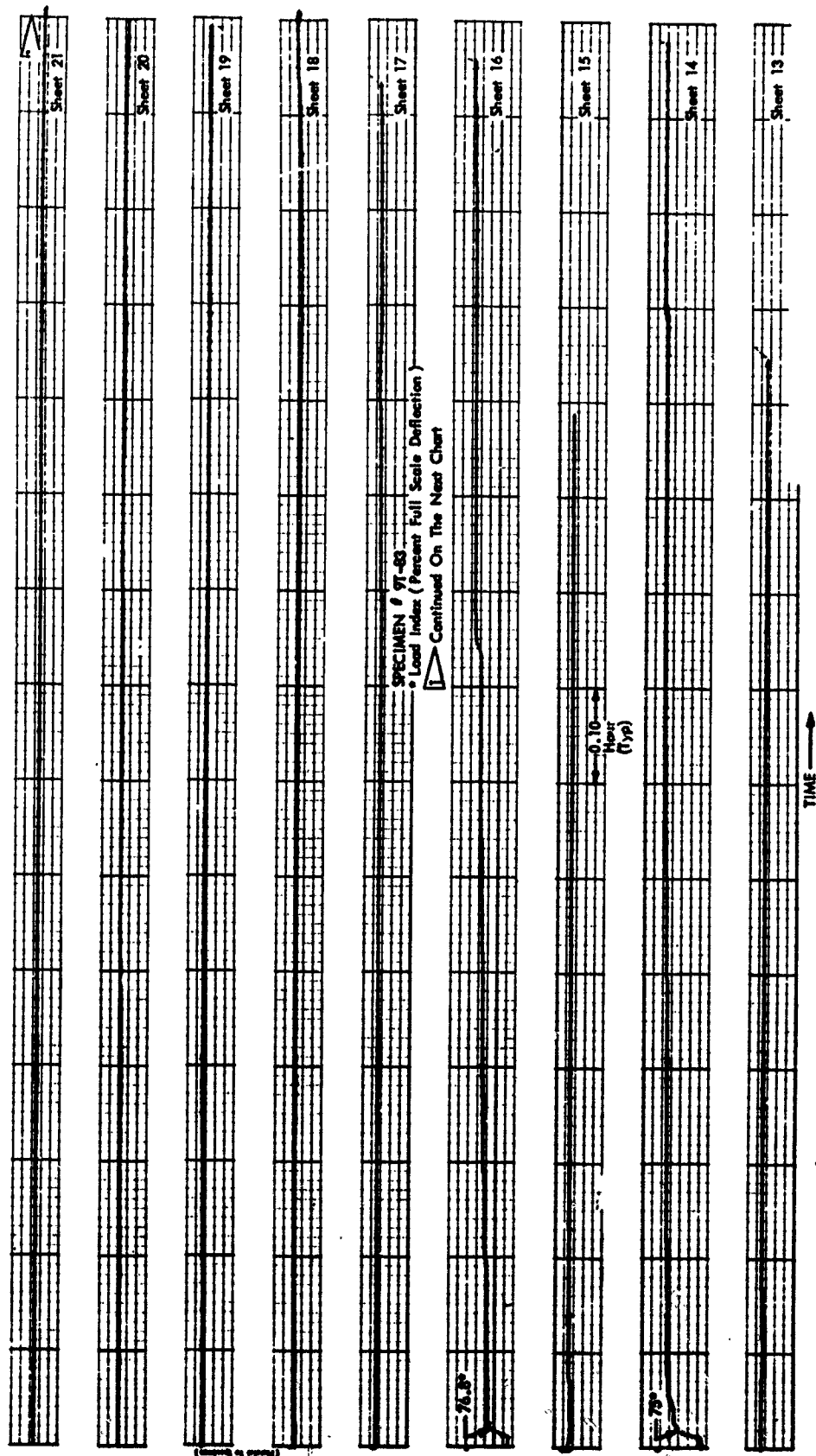
Figure 52: FLAW OPENING DISPLACEMENT UNDER SUSTAINED LOAD
(.5 Al-2 1/2 Sn (ELI) Titanium Specimen 9T-83, Continuation
Of The Test Run, Sheets 13 Thru 21)
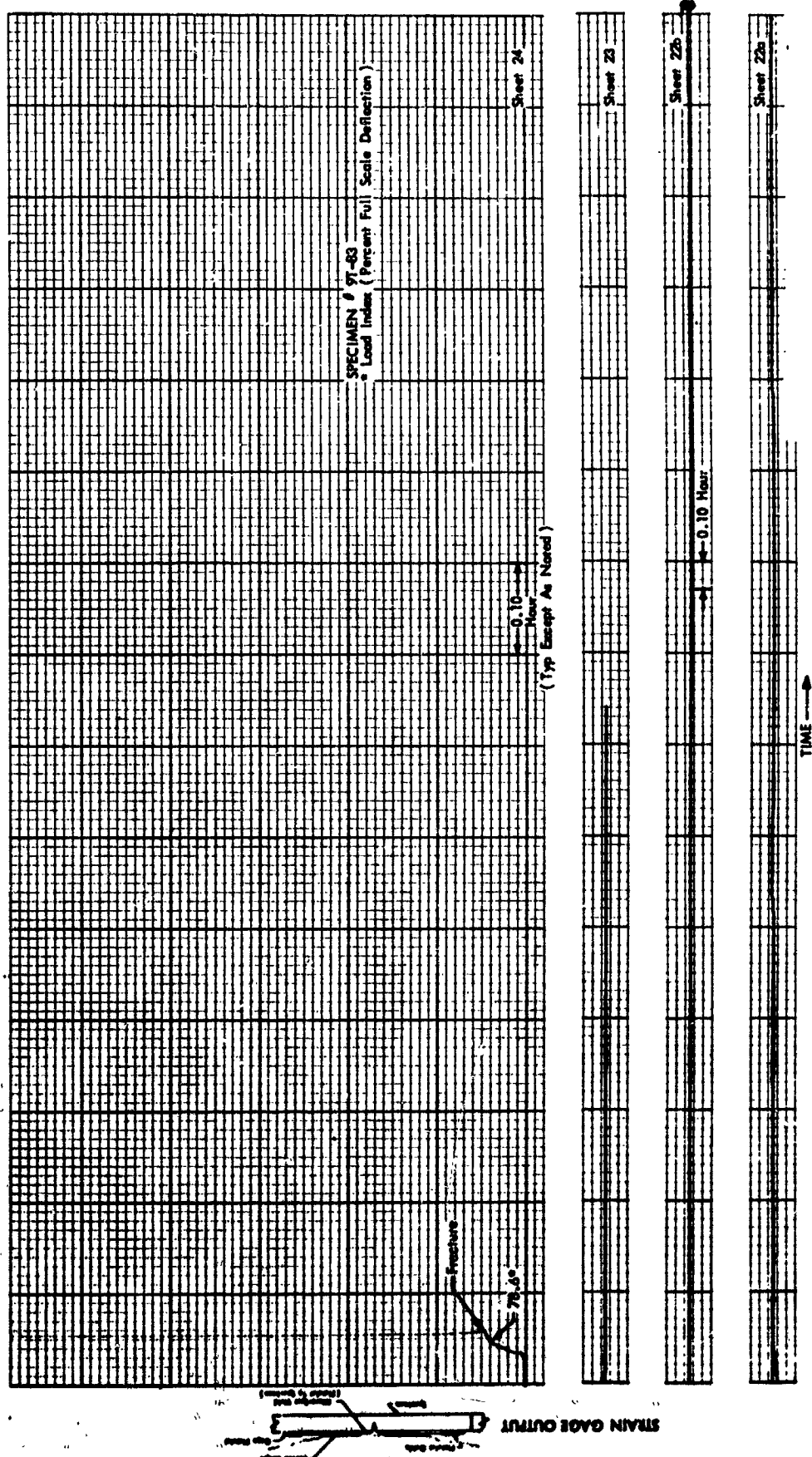
Figure 53: FLAW OPENING DISPLACEMENT UNDER SUSTAINED LOADING
(5 Al-2 1/2 Sn (ELI) Titanium Specimen 9T-83, Conclusion
Of The Test Run)

121
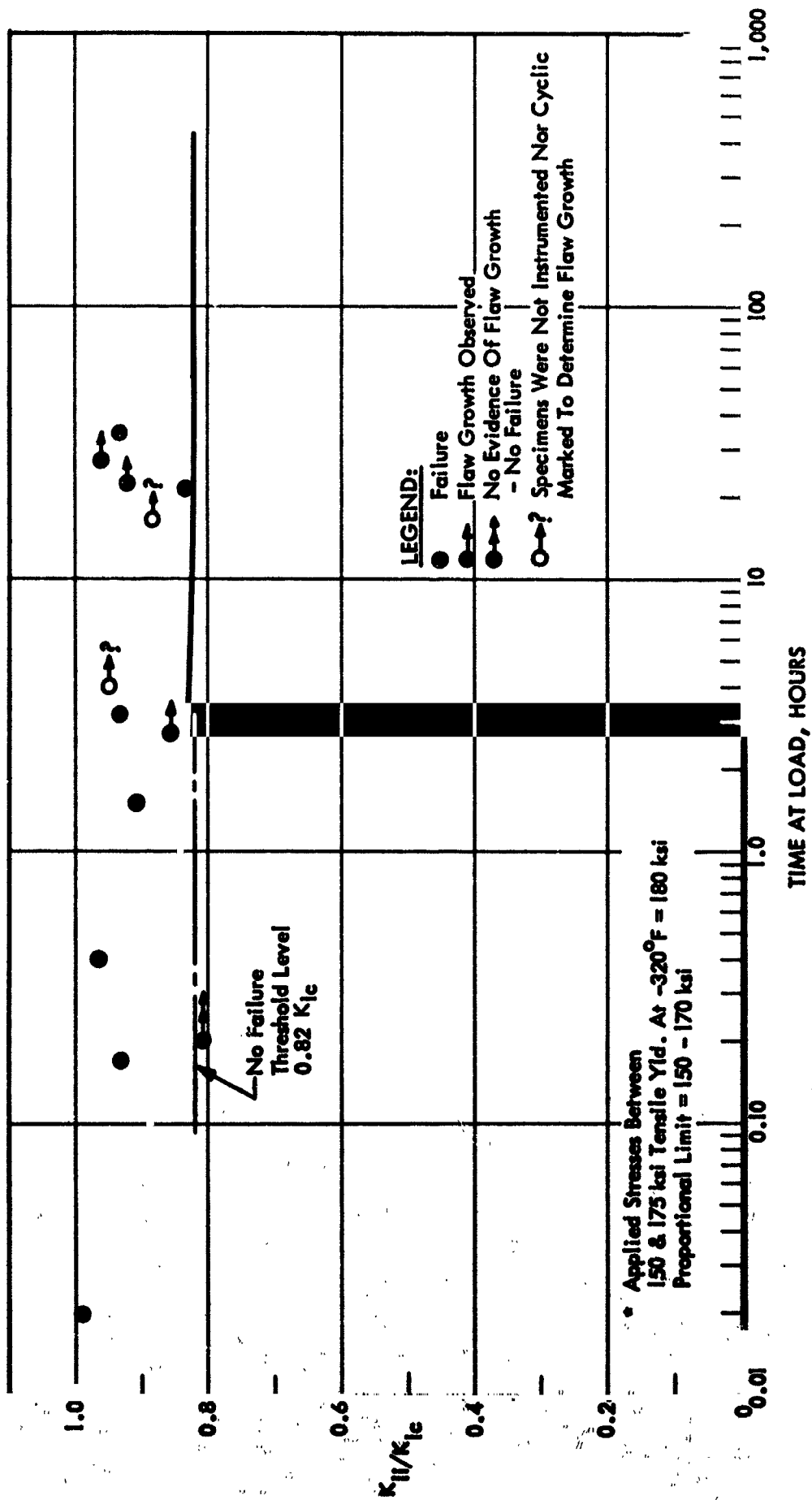
Figure 54: SUSTAINED STRESS LIFE DATA (5AL - 2 1/2 Sn (ELI) Titanium @ -320°F, High Stress Data*)
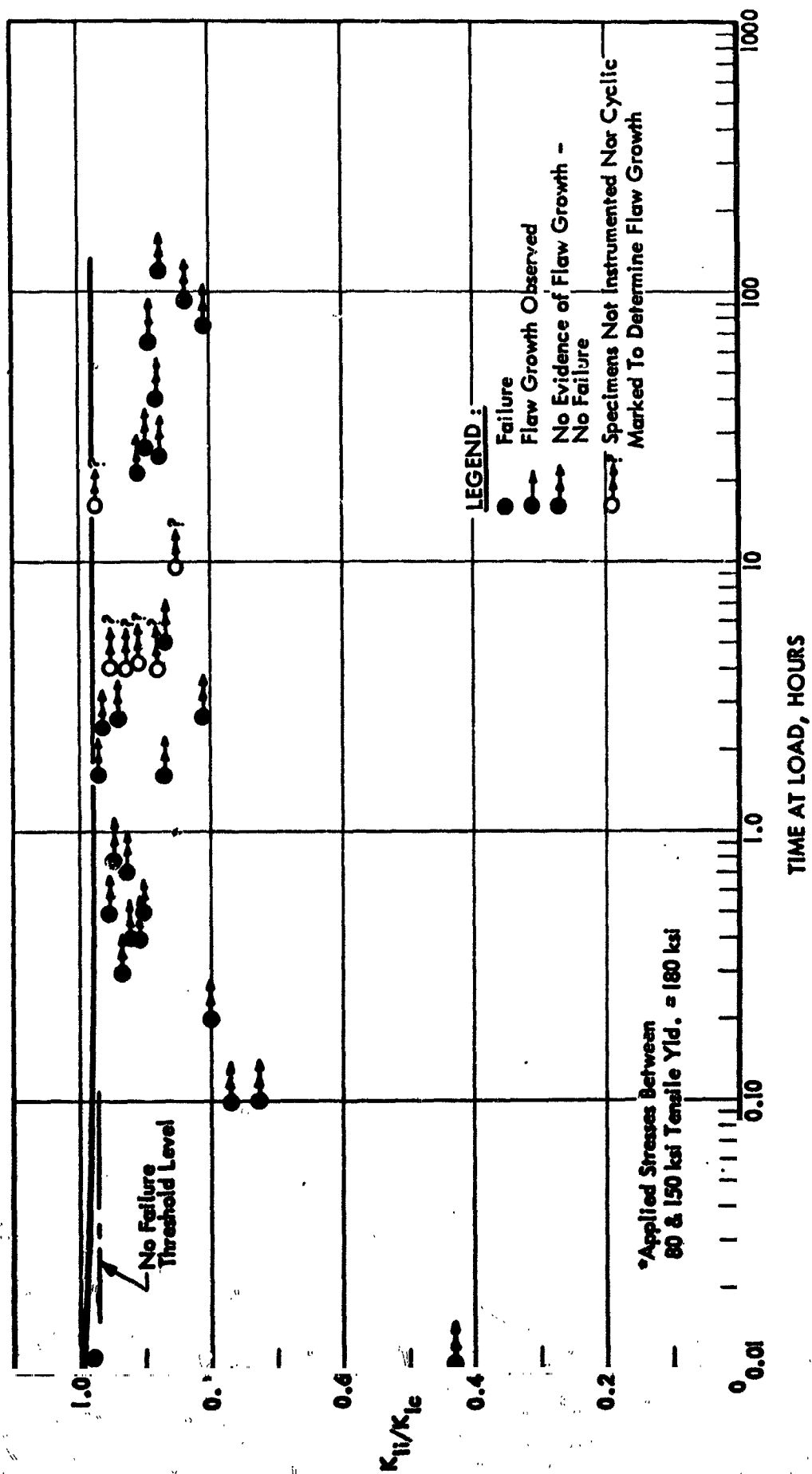
Figure 55 : SUSTAINED STRESS LIFE DATA
(5AL-2 1/2 Sn (ELI) Titanium @ -320°F
Low to Medium Stress Data*)

123
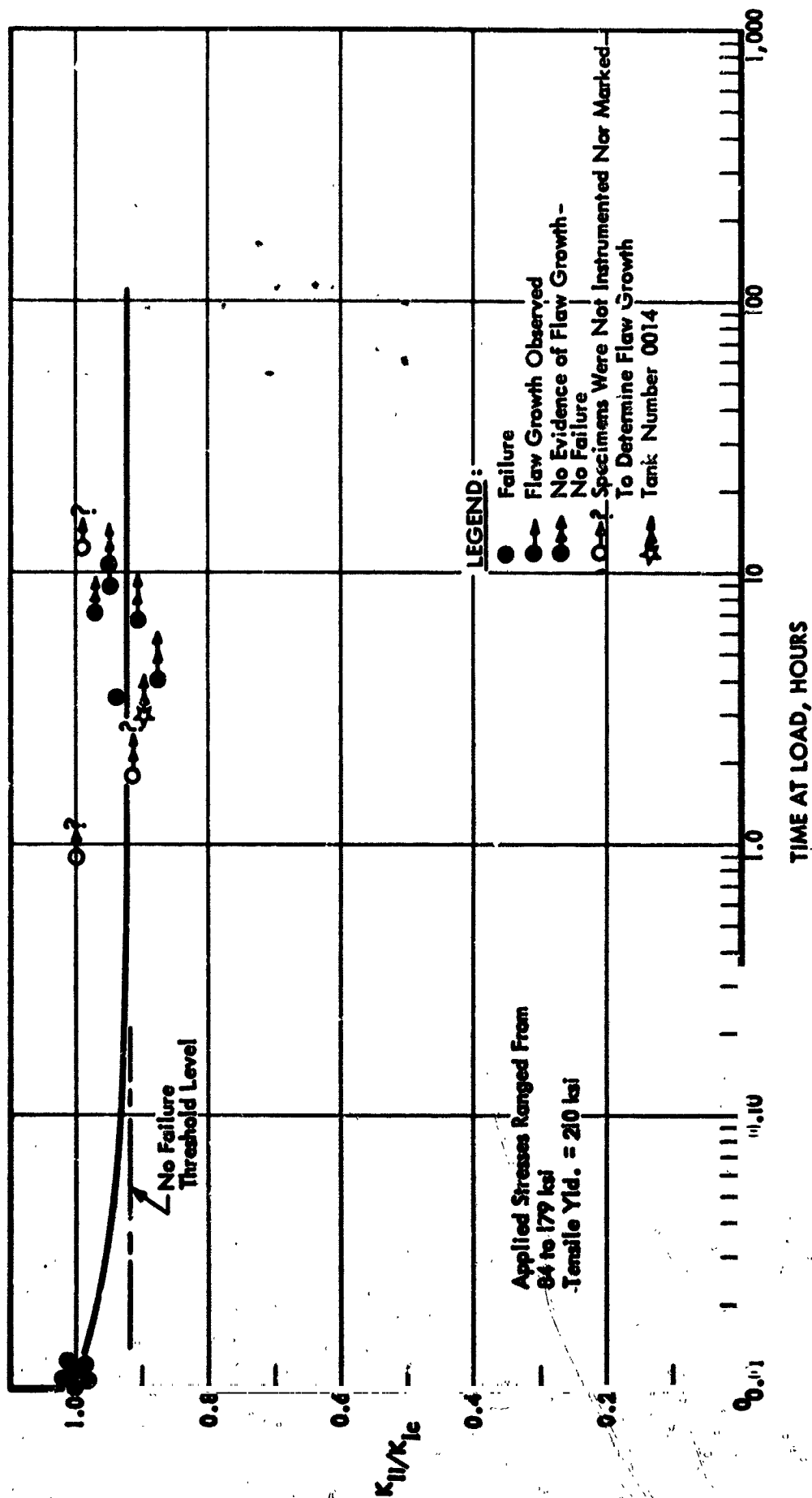
Figure 56: SUSTAINED STRESS LIFE DATA (5AL-2 I/2 Sn (ELI) Titanium @ -423°F)

124
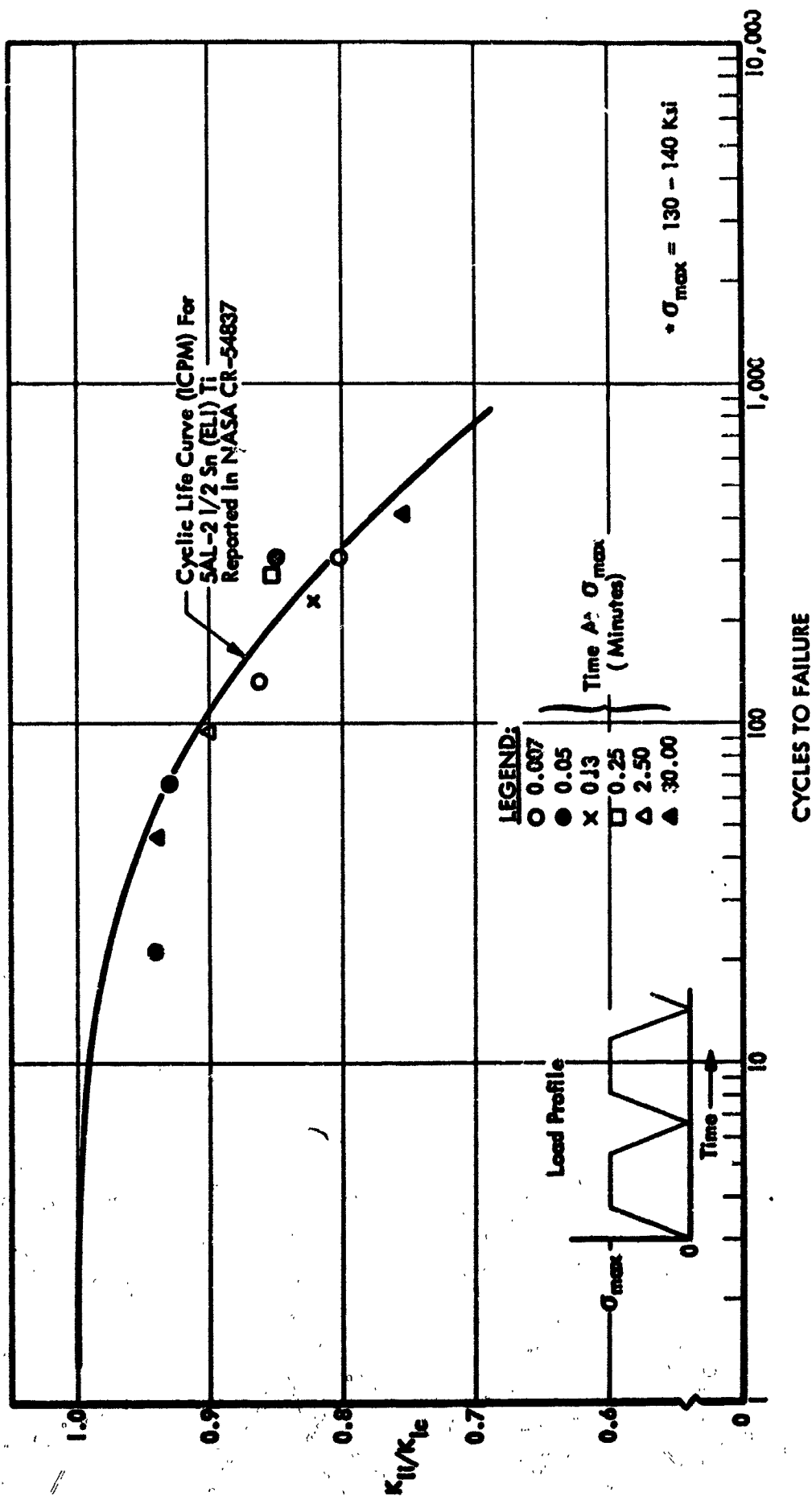
Figure 57: COMBINED SUSTAINED & CYCLIC STRESS LIFE DATA
(5 AL-2 1/2 Sn (ELI) Titanium @ -320°F, Low to Medium Stress Data*)
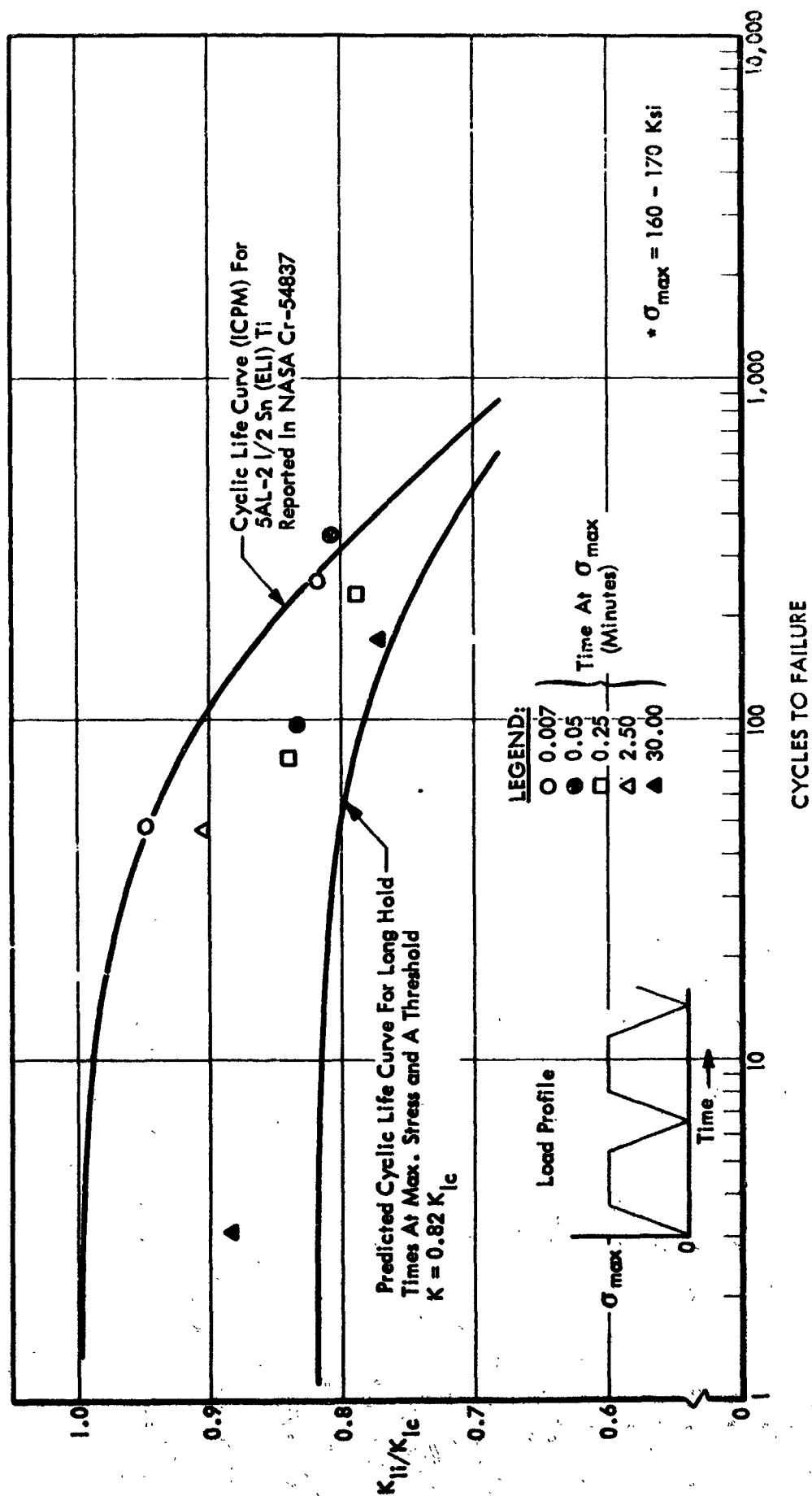
Figure 58: COMBINED SUSTAINED & CYCLIC STRESS LIFE DATA
(5AL-2 1/2 Sn (ELI) Titanium @ –320°F,
High Stress Data*)

R.T.   7.1x
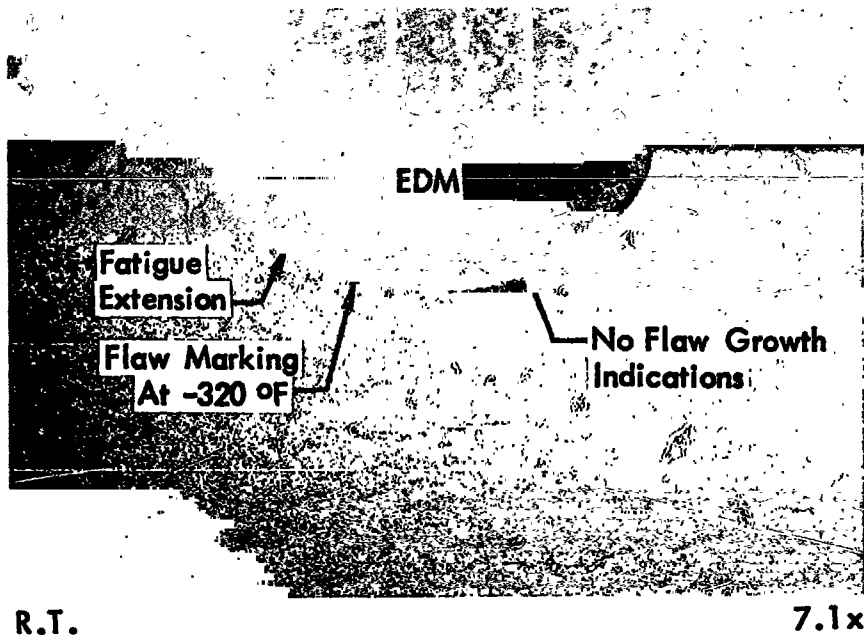
SPECIMEN NO. C-7
MARKED AT ROOM TEMPERATURE

R.T.   2.6x
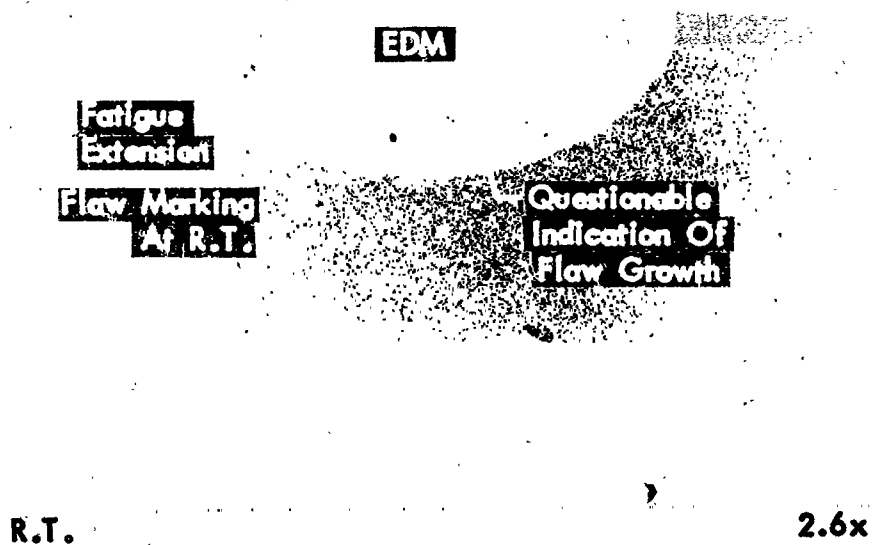
SPECIMEN NO. C6-1
MARKED AT -320 °F

Figure 59: ILLUSTRATION OF THE EFFECTS OF FLAW
MARKING TECHNIQUE

127
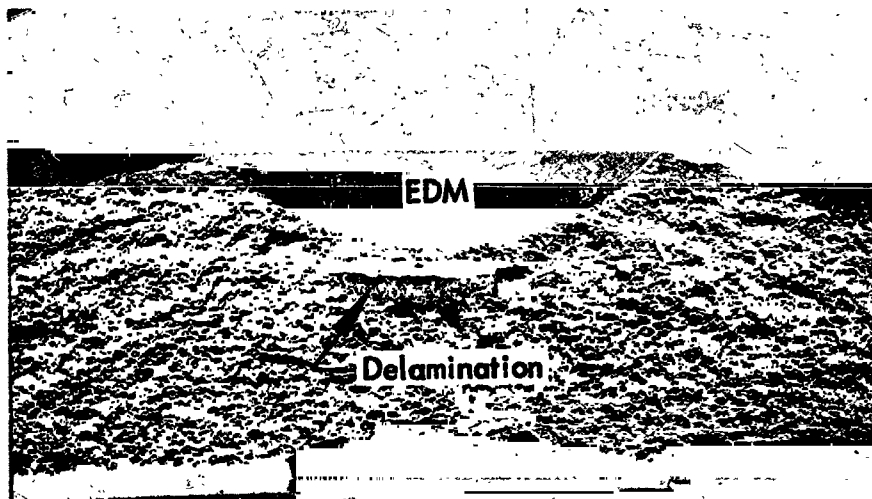
R.T.   2.8x

TANK NO. 0001, FLAW NO. 1
(White Light Illumination)
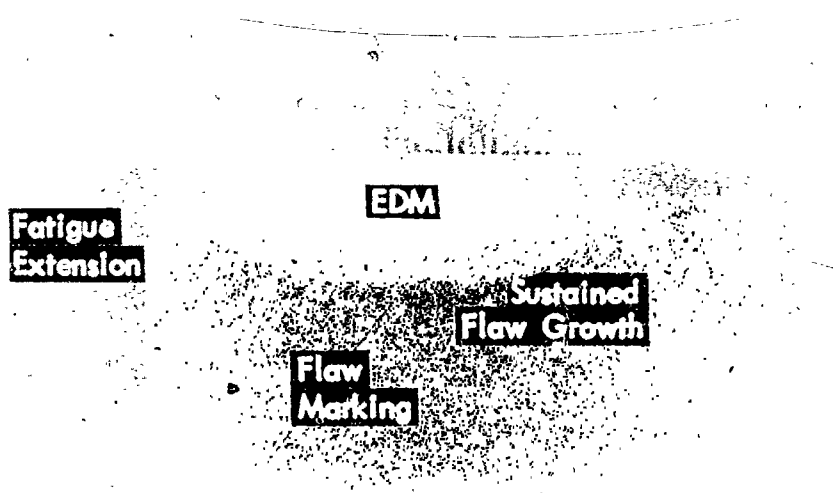
R.T.   2.8x

TANK NO. 0001, FLAW NO. 1
(Polarized Light Illumination)

Figure 60 : FRACTOGRAPHS OF 2219-T87 ALUMINUM TANK TESTED AT
ROOM TEMPERATURE (Tank No. 0001)
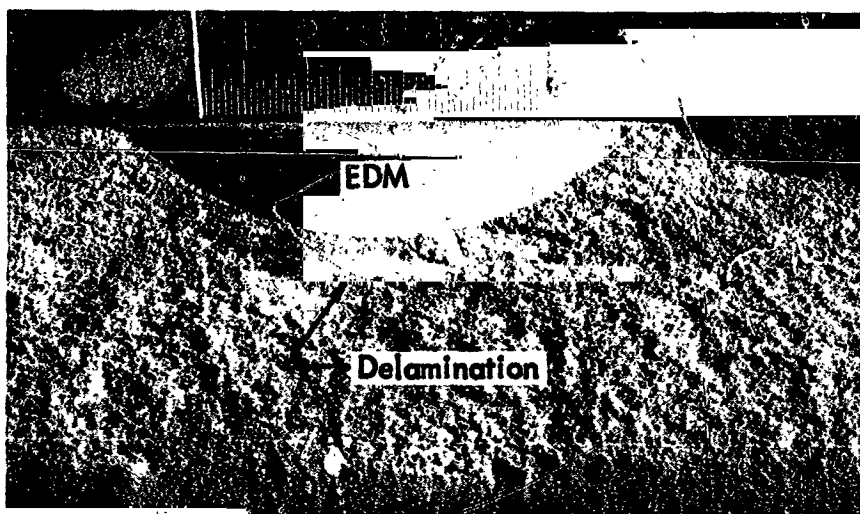
R.T.   3.3x

TANK NO. 0002, FLAW NO. 1
(White Light Illumination)
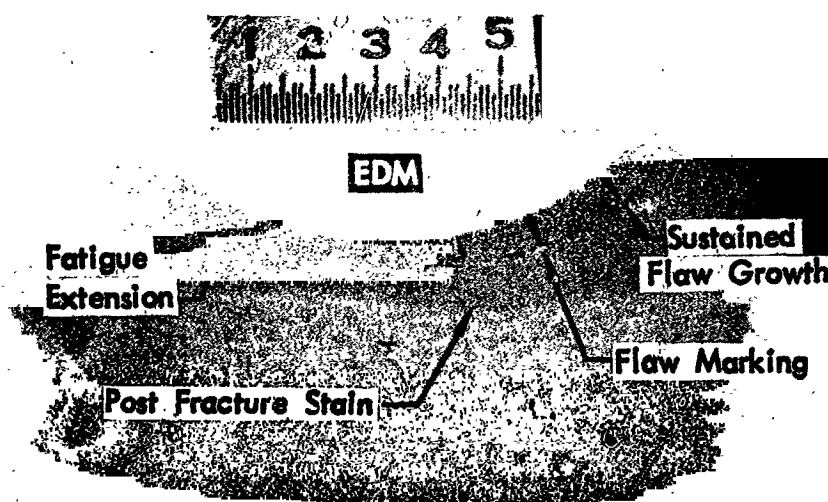
R.T.   3.2x

TANK NO. 0002, FLAW NO. 1
(Polarized Light Illumination)

Figure 61: FRACTOGRAPHS OF 2219-T87 ALUMINUM TANK TESTED AT
ROOM TEMPERATURE (Tank No. 0002)
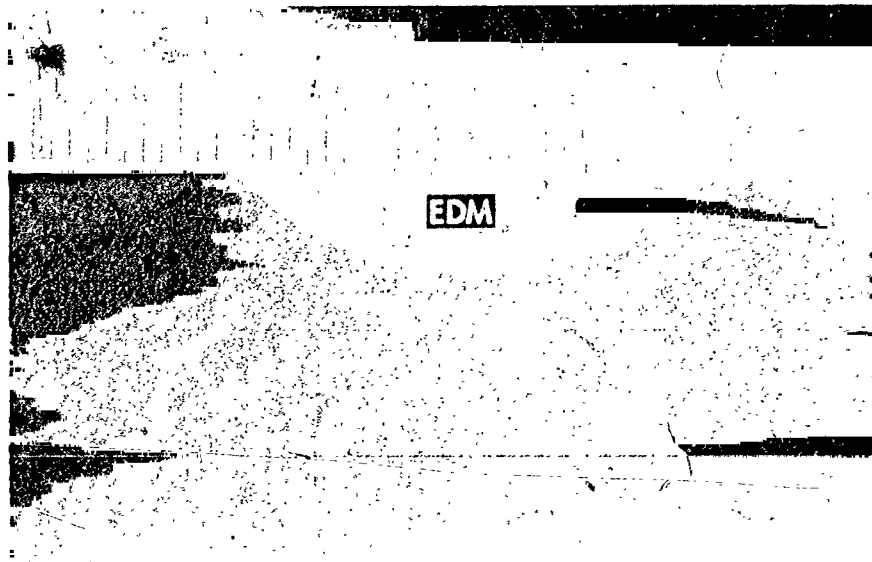
R.T.   3.0x

SPECIMEN NO. CA-41
(White Light Illumination)

EDM

Fatigue
Extension

Sustained
Flow Growth

Flow Marking
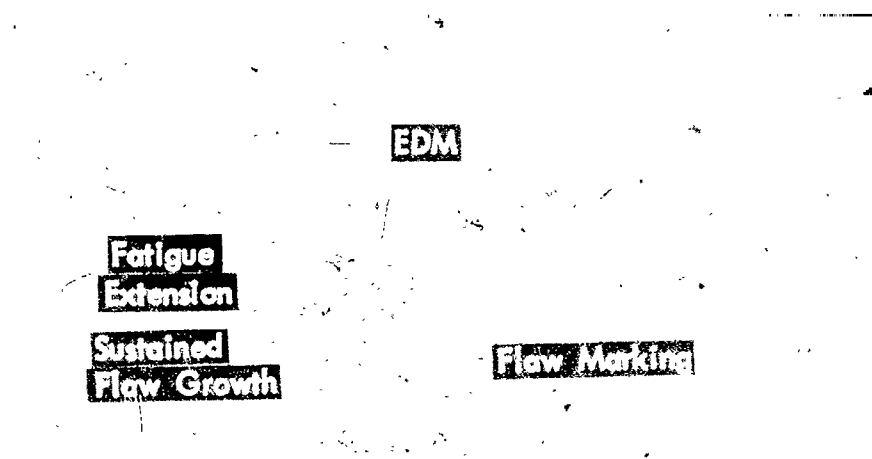
R.T.   3.0x

SPECIMEN NO. CA-41
(Polarized Light Illumination)

Figure 62: FRACTOGRAPHS OF 2219-T87 ALUMINUM SPECIMEN
TESTED AT ROOM TEMPERATURE (Specimen No. CA-41)

130

R.T.   2.9x
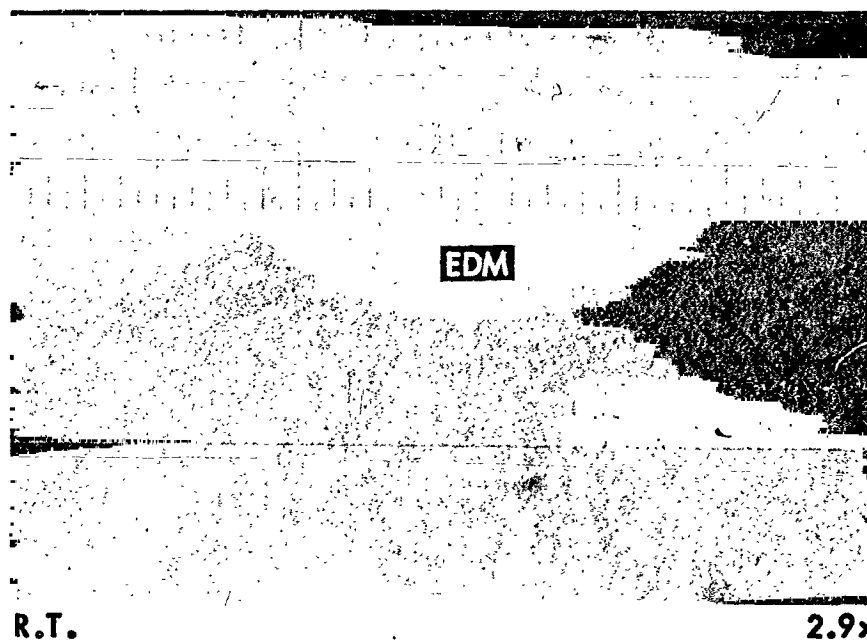
SPECIMEN NO. CA-43
(White Light Illumination)

R.T.   3.6x
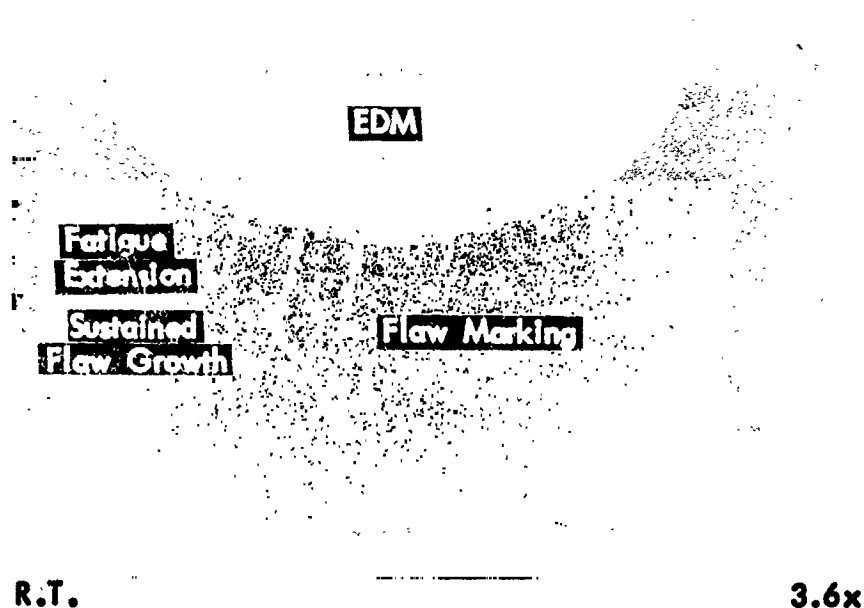
SPECIMEN NO. CA-43
(Polarized Light Illumination)

Figure 63: FRACTOGRAPHS OF 2219-T87 ALUMINUM SPECIMEN
TESTED AT ROOM TEMPERATURE (Specimen No. CA-43)

EDM

Sustained
Flaw Growth

Fatigue
Extension

Cyclic
Marking

R.T.   3.4x

SPECIMEN NO. C-1

EDM

Sustained
Flaw Growth

Fatigue Extension

Cyclic Marking

R.T.   3.4x
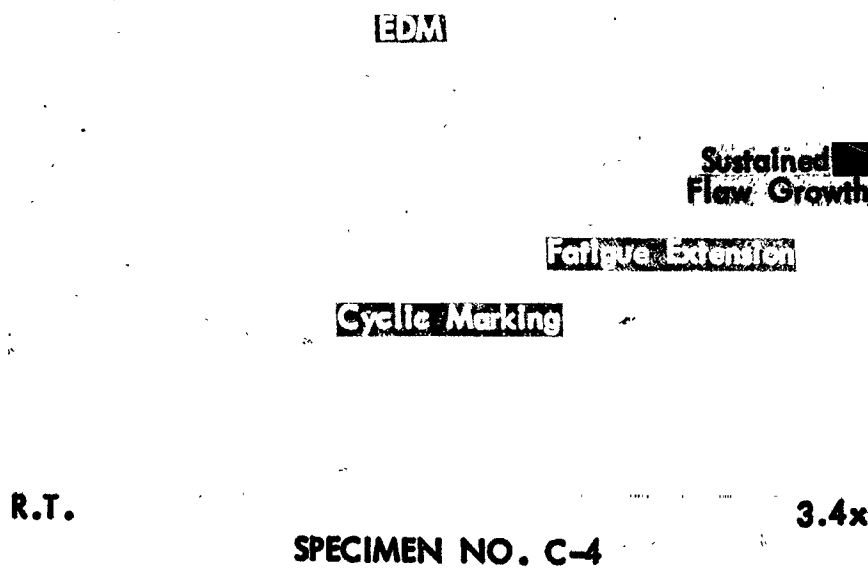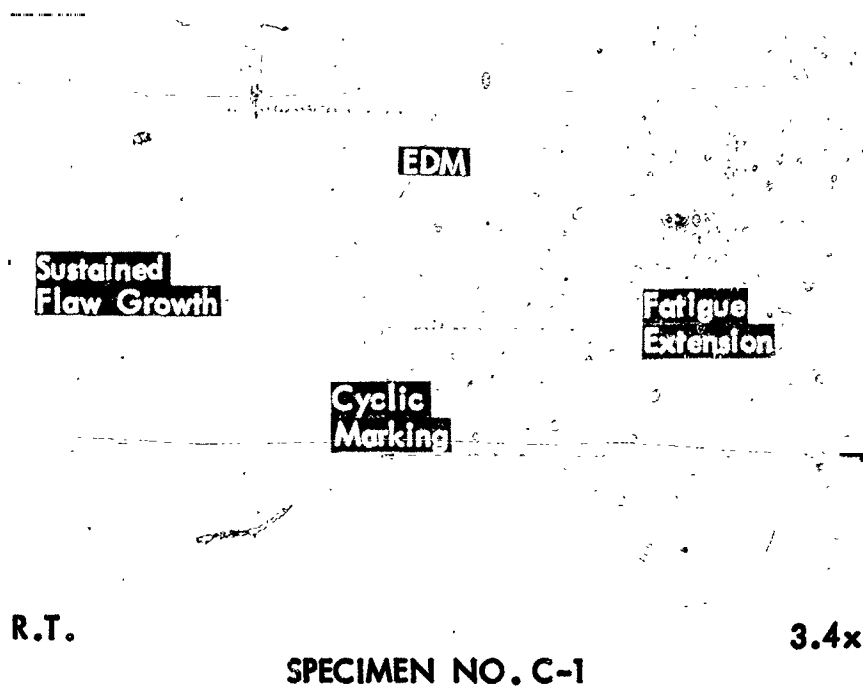
SPECIMEN NO. C-4

Figure 64:FRACTOGRAPHS OF 2219-T87 ALUMINUM SPECIMENS
TESTED AT ROOM TEMPERATURE (Specimens C-1 And C-4)
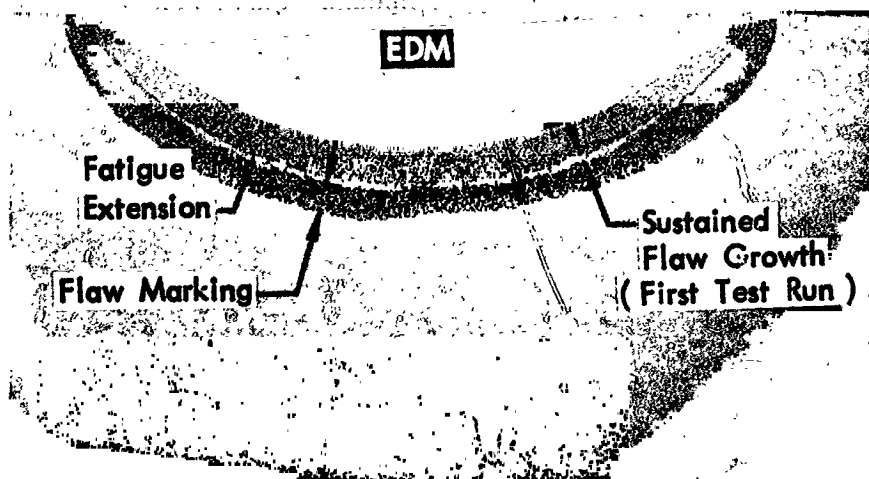
R.T.   4.1x

SPECIMEN NO. CA-34
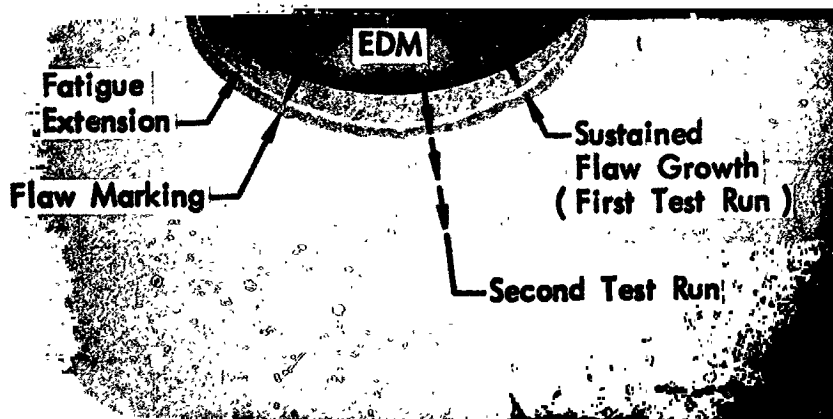
R.T.   3.1x

SPECIMEN NO. DA-33

Figure 65: FRACTOGRAPHS OF 2219-T87 ALUMINUM SPECIMENS
TESTED AT ROOM TEMPERATURE (Specimens CA-34
And DA-33)

-320 °F   2.5x

SPECIMEN NO. CA-40

-320 °F   3.2x
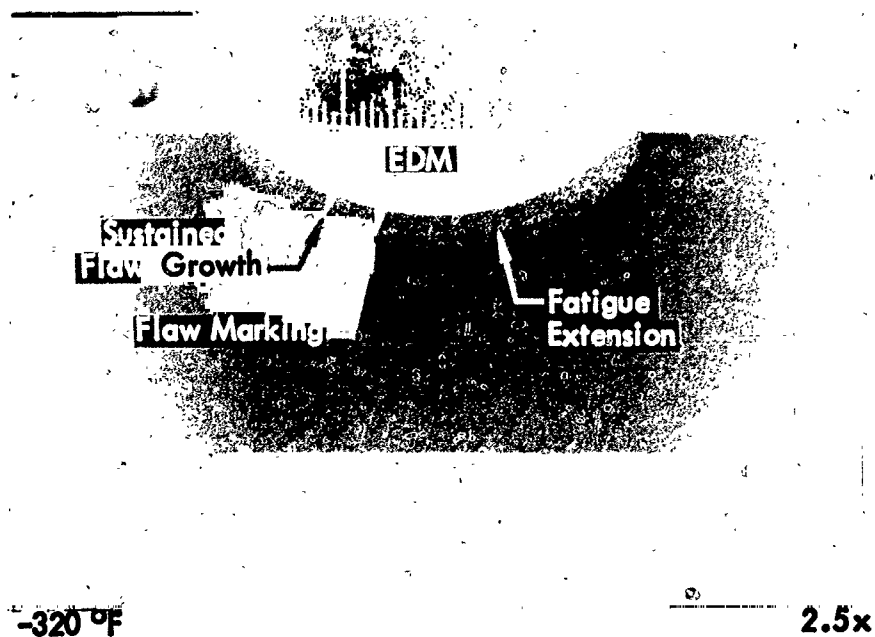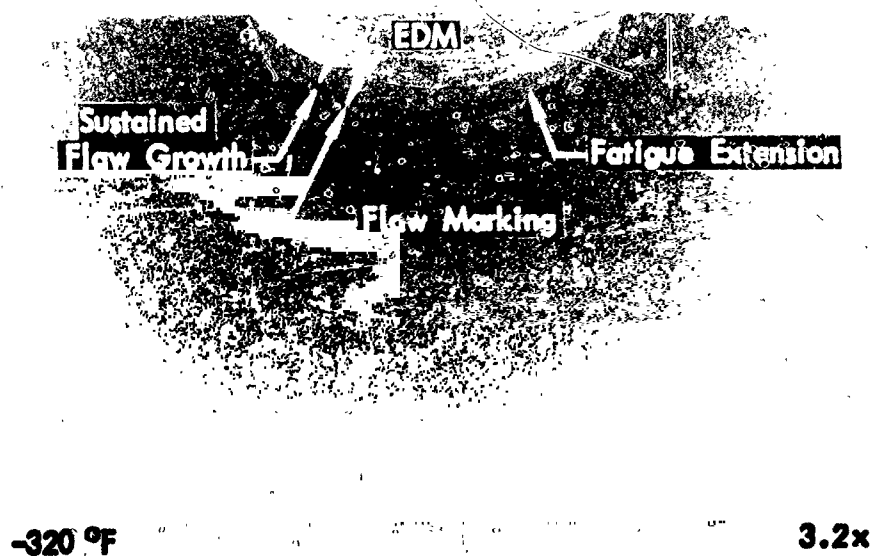
SPECIMEN NO. DA-31

Figure 66: FRACTOGRAPHS OF 2219-T87 ALUMINUM
SPECIMENS TESTED AT -320 °F
(Specimens CA-40 And DA-31)

Table 1: CHEMICAL COMPOSITION OF THE MATERIALS USED TO FABRICATE SPECIMENS AND TANKS

Material	Chemical Composition (% By Weight)											
	C	Mn	Si	Al	V	Zr	Sn	Cu	Mg	Zn	Ti	Fe
2219 Aluminum Plate 1.25 Inches Thick	--	.20-.40	.20 Max	Bal.	.05-.15	.10-.25	--	5.8-6.8	.02 Max	.10 Max	.10-.20	.30 Max
2319 Weld Wire, .062 Dia	--	.20-.40	.20 Max	Bal.	.05-.15	.10-.25	--	5.8-6.8	.02 Max	.10 Max	.10-.20	.30 Max
5 Al-2.5Sn (ELI) Titanium .200 In. Thick Plate Ht. No. G-28 H_2=.009 O_2=.08 E_2=.006	.025	.003	--	5.0	--		2.2	--	--	--	Bal.	.15
5 Al-2.5Sn (ELI) Titanium Weld Wire, .062 Dia Ht. No. 2936 H_2=.007 O_2=.063 H_2=.0028	--	--	--	5.16	--	--	2.59	--	--		Bal.	.09

135.

Table 2: WELD SETTINGS USED FOR FABRICATION OF ALUMINUM AND TITANIUM TANKS

Designation	Plate Thickness	Edge Configuration	Weld Position	Filler Wire Type	Dia (in.)	Feed (in./min.)	Inert Gas Torch	Trailing Cup	Back-Up	Voltage (volts)	Current (amps)	Travel Speed (in./min)
2219-287 Aluminum **Long. Shell Weld**												
1st Pass	1.25	90°B-V	V	--	--	--	He	--	--	12-13	470	2.4
2nd Pass	1.25	90°B-V	V	--	--	--	He	--	--	12-13	450	2.4
Filler Pass	1.25	V	V	2319	.062	50	He	--	--	15-16	225	4.0
Shell to Head Weld												
Fusion Pass	1.00	J	D	--	--	--	He	--	--	13	210	7.0
1st Pass	1.00	J	3 o'clock	--	--	--	He	--	--	12.5	280	3.75
2nd Pass	1.00	J	D	2319	.062	50-	He	--	--	14	240	10.0
Filler Pass	1.00	J	D	2319	.062	100	He	--	--	14	240	10.0
5Al-2.5Sn (ELI) Titanium **Long. Shell Weld**												
1st Pass	0.20	90°B	D	--	--	--	He	He	He	9-10	225	9.0
2nd Pass	0.20	90°B	D	5Al-2.5 Sn	.062	30	A₂	A₂	A₂	9-10	225	9.0
Shell to End Weld												
1st Pass	0.20	90°B	D	--	--	--	He	He	He	9-10	235	9.0
2nd Pass	0.20	90°B	D	5Al-2.5 Sn	.062	30	A₂	A₂	A₂	11	225	9.0

V = Vertical

D = Downhand

TABLE 3: MECHANICAL PROPERTIES OF 2219-T87 ALUMINUM PLATE

SPECIMEN NUMBER	TEST TEMPERATURE (°F)	GRAIN ORIENTATION	SPECIMEN DIA (INCHES)	ULTIMATE STRENGTH (KSI)	YIELD STRENGTH (KSI) 0.2 Percent Offset	YIELD STRENGTH (KSI) 0.02 Percent Offset	REDUCTION OF AREA (%)	ELONGATION IN TWO INCHES GAGE LENGTH (%)
A-1	RT	T	0.500	70.1	57.9	51.3	16.0	10.5
A-2	-320	T	0.500	79.4	66.1	59.6	18.0	9.5
A-3	-423	T	0.499	101.1	71.6	60.4	19.0	7.0
A-4	-423	T	0.499	103.9	75.5	69.4	25	9.5

TABLE 4: STATIC FRACTURE TOUGHNESS DATA OF 2219-T87 ALUMINUM PLATE

| SPECIMEN NUMBER | SPECIMEN SIZE (INCHES) | | TEST TEMPERATURE (°F) | FLAW SIZES (INCHES) | | | FRACTURE STRESS (KSI) | K_{Ic} (KSI $\sqrt{IN}$) |
	Thickness (t)	Width (W)		Flaw Depth (a)	Flaw Length (2c)	Flaw Size (a/Q)		
AA-2	0.648	6.00	RT	0.299	1.250	0.223	37.6	37.8
CA-8	0.657	6.00	RT	0.223	0.772	0.154	46.6	36.5
DA-14	0.656	6.00	RT	0.172	0.576	0.120	53.5	35.7
AA-3	0.655	6.00	-320	0.295	1.238	0.219	41.7	41.9
CA-7	0.666	6.00	-320	0.220	0.778	0.154	54.1	42.0
DA-13	0.655	6.00	-320	0.172	0.574	0.119	62.6	41.4
AA-4	0.650	6.00	-423	0.333	1.219	0.228	44.1	44.4
CA-9	0.657	6.00	-423	0.229	0.789	0.156	56.5	44.3
DA-16	0.669	6.00	-423	0.174	0.600	0.121	63.6	42.9

SPECIMEN NUMBER	SPECIMEN SIZE		CYCLIC EXTENSION OF EDM FLAW			FLAW SIZE BEFORE THE TEST RUN			SUSTAINED TEST RUN				Flaw Depth
	Thickness (Inches)	Width (Inches)	Temperature (°F)	Max Stress (Ksi)	Number Of Cycles (1,000)	Flaw Depth a (Inches)	Flaw Length 2c (Inches)	Flaw Size a/Q (Inches)	Test Temperature (°F)	Max Stress σ_{max} (Ksi)	Time @ σ_{max} (Hours)	K_{Ii} @ α (Ksi $\sqrt{In.}$)	
GROUP I													
AA-50	0.668	6.00	RT	15.0	4	0.335	1.317	1.238	RT	33.8	0.1*	36.5	[.
AA-51	0.661	6.00	RT	15.0	5	0.304	1.210	0.217	RT	32.0	15.3	30.3	0.
AA-1	0.660	6.00	RT	10.0	20	0.322	1.191	0.221	RT	33.8	38.6	32.2	0.
CA-37	0.665	6.00	RT	15.0	9	0.205	0.763	0.145	RT	41.9	24.0	29.0	0.
						0.212	0.815	0.154	RT	44.2	20.3	31.8	0.
						0.224	0.815	0.159	RT	46.5	0.7*	36.2	[.
CA-12	0.656	6.00	RT	15.0	25	0.263	0.831	0.168	RT	43.0	0.9*	34.8	[.
CA-39	0.661	6.00	RT	15.0	10	0.207	0.761	0.144	RT	39.5	19.0	27.5	0.
						0.225	0.785	0.153	RT	41.9	21.5	30.1	0.
						0.240	0.810	0.161	RT	44.2	1.6	32.8	0.
CA-42	0.680	6.00	RT	15.0	11	0.200	0.779	0.142	RT	34.9	17.2	24.6	0.
						0.226	0.851	0.153	RT	41.9	4.6	31.1	0.
CA-10	0.643	6.01	RT	15.0	12	0.217	0.766	0.149	RT	43.0	38.1	31.4	0.
DA-32	0.668	6.00	RT	15.0	14	0.161	0.560	0.112	RT	48.1	24.0	31.1	0.
DA-25	0.664	6.00	RT	15.0	14	0.165	0.597	0.112	RT	34.8	14.2	22.5	0.
GROUP II													
CA-43	0.658	6.00	RT	15.0	18	0.219	0.833	0.149	RT	40.0	123.7	29.0	0.
CA-41	0.656	6.00	RT	15.0	13	0.220	0.805	0.148	RT	32.5	115.6	24.9	0.

**   PULLED TO FAILURE

*   FAILED UNDER SUSTAINED LOADING

▷   NO DISTINGUISHABLE DEMARKATION LINES, K_{Ic} NOT DETERMINED

▶   AVERAGE STATIC K_{Ic} = 36.7 WAS USED IN RATIOS WHERE IT WAS NOT POSSIBLE TO OBT/
K_{Ic} FROM INDIVIDUAL SPECIMENS

139-1

	FLAW SIZE AFTER THE TEST RUN					CYCLIC FLAW MARKING			FLAW SIZE AFTER CYCLIC MARKING		
a (Inches)	Flaw Length 2c (Inches)	Flaw Size a/Q (Inches)	Direction Of Growth α (Deg.)	Flaw Increment Along α (In.)	K_{Ir} @ α (Ksi $\sqrt{IN}$)	Temperature (°F)	Max Stress (Ksi)	Number Of Cycles (1,000)	Flaw Depth a (Inches)	Flaw Length 2c (Inches)	Flaw Size a/Q (Inches)
V	-	-	-	-		-	-	-	-	-	-
.310	1.253	0.223	54	0.017	32.4	RT	22.6	1	0.324	1.272	0.22
.347	1.360	0.246	73	0.076	33.5	RT	22.6	1	0.349	1.362	0.24
.210	0.775	0.148	64	0.009	29.3	RT	27.9	1	0.212	0.812	0.14
.215	0.818	0.155	64	0.010	31.9	RT	27.9	1	0.224	0.818	0.15
VV	-	-	-	-		-	-	-	-	-	-
V	-	-	-	-		-	-	-	-	-	-
.216	0.771	0.148	61	0.015	28.0	RT	27.9	1	0.225	0.785	0.11
.229	0.811	0.157	61	0.010	30.6	RT	27.9	1	0.240	0.810	0.11
.243	0.829	0.164	61	0.012	33.2	RT	27.9	4	0.276	0.872	0.11
.202	0.779	0.143	56	0.008	24.7	RT	27.9	2	0.226	0.851	0.10
.228	0.851	0.161	56	0.007	31.9	RT	27.9	2	0.241	0.887	0.10
.228	0.778	0.153	50	0.021	31.9	RT	27.9	2	0.246	0.809	0.11
.176	0.603	0.121	0	0.014	32.4	RT	32.1	1	0.182	0.606	0.11
.176	0.603	0.115	0	0.008	22.8	RT	32.1	2	0.190	0.783	0.11
.225	0.838	0.151	0	0.006	29.2	RT	18.0	5	0.233	0.845	0.11
.220	0.805	0.150	0	0.006	25.0	RT	27.9	2	0.258	0.892	0.11

	TEST CONDITION AT FRACTURE			K_{Ic} @ $\alpha = 0$ (KSI $\sqrt{IN.}$)	K_{Ic} @ $\alpha \neq 0$ (KSI $\sqrt{IN.}$)	K_{Ii}/K_{Ic}	K_{If}/K_{Ic}	Ref. Symbol in Fig.
	Temperature (°F)	Flaw Size a/Q (Inches)	Fracture Stress σ (Ksi)					
	RT	0.238	33.8	-	-	0.995	1.0	●
28	RT	0.230	33.8		33.4**	0.906	0.97	○
16	RT	0.248	35.8	_	34.2**	0.942	0.98	△
15	-	-	:	-	-	0.79	0.797	▽
54	-	-	-	-	-	0.868	0.87	□
	RT		46.5	-	-	0.985	1.0	■
	RT		43.0	-	-	0.946	1.0	▲
47	-	-	:	-	33.4	0.824	0.839	✕
45	-	-	-	-	33.4	0.900	0.917	⊗
68	RT	0.176	42.8		33.4**	0.982	0.995	◪
54	-	-	-	-	35.2	0.700	0.703	◐
52	RT	0.172	45.4		35.2**	0.884	0.907	◑
54	RT	0.163	46.0		34.7**	0.905	0.92	◐
16	RT	0.124	50.8	35.0**	-	0.889	0.925	▣
38	RT	0.146	47.7	35.5**	-	0.635	0.642	▢
54	RT	0.166	47.2	36.1**	-	0.803	0.807	▼
67	RT	0.175	43.6	36.7**	-	0.679	0.683	▼

Table 5

SPECIMEN NUMBER	SPECIMEN SIZE		CYCLIC EXTENSION OF EDM FLAW			FLAW SIZE BEFORE THE TEST RUN			SUSTAINED TEST RUN				Flaw Depth
	Thickness (Inches)	Width (Inches)	Temperature (°F)	Max Stress (Ksi)	Number Of Cycles (1,000)	Flaw Depth a (Inches)	Flaw Length 2c (Inches)	Flaw Size a/Q (Inches)	Test Temperature (°F)	Max Stress σ_{max} (Ksi)	Time @ σ_{max} (Hours)	K_{Ii} @ α (Ksi $\sqrt{In.}$)	
GROUP III													
C-8	0.604	6.00	RT	15.0	15	0.215	0.813	0.153	RT	40.0	0.02	29.4	0
C-3	0.660	6.00	RT	15.0	20	0.262	0.848	0.168	RT	40.0	0.08	29.1	0
C-1	0.663	6.00	RT	15.0	15	0.241	0.843	0.163	RT	40.0	0.17	29.0	0
C-5	0.645	6.00	RT	15.0	15	0.245	0.860	0.166	RT	40.0	0.33	31.8	0
C-2	0.652	6.00	RT	15.0	15	0.247	0.853	0.166	RT	40.0	0.67	31.7	0
CA-44	0.663	6.00	RT	15.0	18	0.218	0.830	0.155	RT	40.0	1.00	29.6	0
C-4	0.671	6.00	RT	15.0	17	0.248	0.858	0.166	RT	40.0	1.33	29.6	0
C-6	0.656	6.00	RT	15.0	15	0.236	0.847	0.155	RT	23.7	1.00	18.7	0
C-7	0.652	6.00	RT	15.0	15	0.252	0.861	0.161	RT	23.7	4.70	18.9	0
C-9	0.653	6.00	RT	15.0	15	0.233	0.828	0.152	RT	23.7	30.00	18.6	0
GROUP IV													
C8-1	0.655	6.00	RT	20.0	6	0.148	0.561	0.107	RT	45.0	1.0	28.5	0
C6-1	0.653	6.00	RT	25.0	6	0.095	0.322	0.064	RT	45.0	1.0	21.5	0
C4-1	0.653	6.00	RT	30.0	6	0.051	0.178	0.035	RT	45.0	1.0	15.8	0
AC-7	0.650	6.00	RT	15.0	9	0.214	0.834	0.132	RT	33.0	1.0	23.9	0
						0.258	0.872	0.170	RT	39.1	1.0	31.8	0
AC-8	0.661	6.00	-320	15.0	7	0.175	0.828	0.133	RT	23.7	1.0	17.2	0
						0.260	0.887	0.169	RT	27.9	1.0	22.8	0

** PULLED TO FAILURE

▷1 SPECIMEN USED FOR - 320°F TEST
(SEE TABLE 9)

▶ AVERAGE STATIC K_{Ic} = 36.7 WAS USED IN RATIOS WHERE IT WAS NOT POSSIBLE TO OB
K_{Ic} FROM INDIVIDUAL SPECIMENS

140-1

a (Inches)	Flaw Length 2c (Inches)	Flaw Size a/Q (Inches)	Direction Of Growth α (Deg.)	Flaw Increment Along α (In.)	K_{If} @ α (Ksi $\sqrt{IN}$)	Temperature (°F)	Max Stress (Ksi)	Number Of Cycles (1,000)	Flaw Depth a (Inches)	Flaw Length 2c (Inches)	Flaw Size a/Q (Inches)
.223	0.813	0.155	58	0.019	29.6	RT	27.9	2	0.248	0.854	0.1
.265	0.851	0.169	71	0.024	29.2	RT	27.9	2	0.306	0.928	0.1
.248	0.846	0.165	68	0.009	29.2	RT	27.9	2	0.287	0.902	0.1
.250	0.860	0.167	46	0.012	31.9	RT	27.9	2	0.290	0.928	0.1
.256	0.853	0.168	67	0.016	31.9	RT	27.9	2	0.291	0.912	0.1
.223	0.831	0.157	0	0.005	29.8	RT	18.0	5	0.228	0.833	0.1
.256	0.861	0.168	65	0.009	29.8	RT	27.9	2	0.286	0.925	0.1
.247	0.858	0.159	0	0.004	19.0	RT	27.9	2	0.292	0.947	0.1
.259	0.867	0.163	0	0.006	19.0	RT	27.9	2	0.323	1.018	0.1
.238	0.834	0.154	0	0.005	18.7	RT	27.9	2	0.298	0.954	0.1
.150	0.561	0.108	0	0.002	28.6	-320	20.0	4	0.154	0.563	0.1
.095	0.322	0.064	0	0	21.5	-320	25.0	4	0.102	0.326	0.0
.051	0.178	0.035	0	0	15.8	-320	30.0	4	0.057	0.182	0.0
.218	0.834	0.135	71	0.003	24.2	-320	20.0	15	0.258	0.872	0.1
.272	0.876	0.171	71	0.023	31.9	-320	20.0	30	0.312	0.919	0.1
.175	0.828	0.133	0	0	17.2	-320	27.9	6	0.260	0.887	0.1
.260	0.887	0.169	0	0	22.8	-320	20.0	10	0.284	0.905	0.1

AIN

| | TEST CONDITION AT FRACTURE | | | K_{Ic} @ $\alpha = 0$ (KSI $\sqrt{IN.}$) | K_{Ic} @ $\alpha \neq 0$ (KSI $\sqrt{IN.}$) | K_{Il}/K_{Ic} | K_{If}/K_{Ic} | Ref. Symbol in Fig. |
	Temperature (°F)	Flaw Size a/Q (Inches)	Fracture Stress σ (Ksi)					
61	RT	0.169	44.5	–	33.2**	0.885	0.892	▽
81	RT	0.190	44.6	–	34.1**	0.854	0.856	◑
74	RT	0.184	46.0	–	35.0**	0.830	0.835	⊠
78	RT	0.187	44.5	–	36.2**	0.879	0.881	◁
76	RT	0.185	43.9	–	33.6**	0.944	0.950	▷
50	RT	0.163	47.7	36.2**	–	0.817	0.824	◇
77	RT	0.186	44.5	–	34.3**	0.863	0.870	◆
81	RT	0.190	42.3	36.0**	–	0.520	0.527	♂
97	RT	0.204	40.8	36.0**	–	0.525	0.527	ρ
84	RT	0.191	41.7	35.5**	–	0.524	0.526	⌑
02	RT	0.113	54.1	35.4**	–	0.805	0.808	◣
62	RT	0.070	57.1	–	–	0.586	0.586	◤
35	RT	0.040	60.8	–	–	0.431	0.431	◤
70	–	–	–	–	–	0.652	0.659	■
79	–	–	–	–	–	0.867	0.870	▲
69	–	–	–	–	–	0.469	0.469	◖
70	–	–	–	–	–	0.622	0.622	◗

Table 6

SPECIMEN NUMBER	SPECIMEN SIZE		CYCLIC EXTENSION OF EDM FLAW			FLAW SIZE BEFORE THE TEST RUN			SUSTAINED TEST RUN				Flaw Depth a (Inches)
	Thickness (Inches)	Width (Inches)	Temperature (°F)	Max Stress (Ksi)	Number Of Cycles (1,000)	Flaw Depth a (Inches)	Flaw Length 2c (Inches)	Flaw Size a/Q (Inches)	Test Temperature (°F)	Max Stress σ_{max} (Ksi)	Time @ σ_{max} (Hours)	K_{Ii} @ α (Ksi $\sqrt{In.}$)	
GROUP V													
CA-34	0.658	6.00	RT	15.0	13	0.212	0.767	0.142	RT	27.9	0.4		▷
									RT	32.5	1.1		▷
									RT	37.2	1.3		▷
									RT	41.8	18.7	31.1	0.22
									RT	37.7	0.5		▷
									RT	39.8	0.9		▷
									RT	40.8	0.25		▷
									RT	41.8	0.4		▷
									RT	43.1	0.2		▷
									RT	43.7	▷x		▷
DA-33	0.658	6.00	RT	15.0	20	0.173	0.603	0.121	RT	49.5	16.6	32.9	0.18
						0.195	0.649	0.132	RT	49.5	0.2	34.4	-
						▷-	-	-	RT	50.8	0.9*	35.2	-

▷x BROKE UPON LOADING

* FAILED UNDER SUSTAINED LOADING

▷ NO DISTINGUISHABLE DEMARKATION LINES

	FLAW SIZE AFTER THE TEST RUN					CYCLIC FLAW MARKING			FLAW SIZE AFTER CYCLIC MARKING		
	Flaw Length 2c (Inches)	Flaw Size a/Q (Inches)	Direction Of Growth α (Deg.)	Flaw Increment Along α (In.)	K_{If} @ α (Ksi $\sqrt{In}$)	Temperature (°F)	Max Stress (Ksi)	Number Of Cycles (1,000)	Flaw Depth a (Inches)	Flaw Length 2c (Inches)	Flaw Size a/Q (Inches)
	-	-	-	-		-	-	-	-	-	-
	-	-	-	-		-	-	-	-	-	-
	-	-	-	-		-	-	-	-	-	-
20	0.800	0.147	57	0.012	31.8	RT	27.9	4	0.253	0.875	0.16
	-	-	-	0		-	-	-	-	-	-
	-	-	-	0		-	-	-	-	-	-
	-	-	-	0		-	-	-	-	-	-
	-	-	-	0		-	-	-	-	-	-
	-	-	-	0		-	-	-	-	-	-
	-	-	-			-	-	-	-	-	-
31	0.616	0.124	23	0.014		RT	32.1	2	0.195	0.649	0.12
	-	-	-	-	-	-	-	-	-	-	-
	-	-	-	-	-	-	-	-	-	-	-

TEST CONDITION AT FRACTURE			K_{Ic} @ $\alpha = 0$ (KSI $\sqrt{\text{IN.}}$)	K_{Ic} @ $\alpha \neq 0$ (KSI $\sqrt{\text{IN.}}$)	K_{Ii}/K_{Ic}	K_{If}/K_{Ic}	Ref. Symbol in Fig.
Temperature (°F)	Flaw Size a/Q (Inches)	Fracture Stress σ (Ksi)					
-	-	-					
-	-	-					
-	-	-					
-	-	-		33.3	0.935	0.955	⊕
-	-	-					
-	-	-					
-	-	-					
RT	▷	43.7	-	33.3			
-	-	-					
-	-	-					
RT	▷	50.8		36.2	0.973	1.0	⊟

Table 7

SPECIMEN NUMBER	SPECIMEN SIZE		CYCLIC EXTENSION OF EDM FLAW			FLAW SIZE BEFORE THE TEST RUN			SUSTAINED TEST RUN				Flaw Depth
	Thickness (Inches)	Width (Inches)	Temperature (°F)	Max Stress (Ksi)	Number Of Cycles (1,000)	Flaw Depth a (Inches)	Flaw Length 2c (Inches)	Flaw Size a/Q (Inches)	Test Temperature (°F)	Max Stress σ_{max} (Ksi)	Time @ σ_{max} (Hours)	K_{Ii} @ α (Ksi $\sqrt{In.}$)	
GROUP I													
AA-58	0.660	6.00	RT	15.0	5	0.321	1.196	0.222	-320	39.6	0.03*	39.9	[
AA-49	0.666	6.00	RT	15.0	5	0.305	1.192	0.216	-320	37.5	19.7	32.7	0.
						0.332	1.358	0.242	-320	39.6	0.12*	37.8	[
AA-52	0.663	6.00	RT	15.0	5	0.313	1.192	0.218	-320	38.5	0.003	38.3	[
CA-11	0.658	6.00	RT	15.0	10	0.229	0.804	0.157	-320	48.6	17.1*	38.4	[
CA-38	0.664	6.00	RT	15.0	11	0.207	0.785	0.149	-320	48.7	18.8	35.3	0.
						0.228	0.814	0.159	-320	51.4	21.8	38.2	0.
						0.241	0.849	0.168	-320	54.1	0.21*	41.9	[
CA-47	0.649	6.00	RT	15.0	10	0.216	0.848	0.151	-320	50.1	24.6	36.0	0.
DA-17	0.641	6.00	RT	15.0	16	0.168	0.599	0.119	-320	56.4	48.0	37.6	0.
DA-35	0.658	6.00	RT	15.0	20	0.165	0.545	0.112	-320	59.5	0.05*	37.8	[
DA-31	0.665	6.00	RT	15.0	18	0.156	0.574	0.113	-320	56.4	18.9	36.0	0.
						0.191	0.619	0.128	-320	59.5	0.02*	40.8	[
GROUP II													
CA-40	0.673	6.00	RT	15.0	13	0.212	0.795	0.149	-320	43.3	120.0	33.0	0.
						0.238	0.864	0.167	-320	48.7	0.2*	39.5	[
CA-48	0.659	6.00	RT	15.0	10	0.213	0.750	0.142	-320	37.9	125.1	28.3	0.

*   FAILED UNDER SUSTAINED LOAD

**   PULLED TO FAILURE

▷ NO DISTINGUISHABLE DEMARKATION LINES

▶ AVERAGE STATIC K_{Ic} = 41.8 WAS USED IN DETERMINING K RATIOS WHERE IT WAS NOT PO[...]

K_{Ic} FROM SPECIMEN

SUSTAINED LOAD FLAW GROWTH DATA FOR 2219-T87
ALUMINUM AT - 320°F (Groups I and II)

	FLAW SIZE AFTER THE TEST RUN						CYCLIC FLAW MARKING			FLAW SIZE AFTER CYCLIC MARKING		
a (Inches)	Flaw Length 2c (Inches)	Flaw Size a/Q (Inches)	Direction Of Growth α (Deg.)	Flaw Increment Along α (In.)	K_{Ir} @ α (Ksi √In)	Temperature (°F)	Max Stress (Ksi)	Number Of Cycles (1,000)	Flaw Depth a (Inches)	Flaw Length 2c (Inches)	Flaw Size a/Q (Inches)
-	-	-	-	-	-	-	-	-	-	-	-
330	1.356	0.240	73	0.079	33.9	-320	25.0	1	0.332	1.358	0.2
-	-	-	-	-	-	-	-	-	-	-	-
-	-	-	-	-	-	-	-	-	-	-	-
-	-	-	-	-	-	-	-	-	-	-	-
212	0.800	0.152	54	0.014	35.6	-320	32.5	1	0.228	0.814	0.1
287	0.840	0.165	54	0.021	38.9	-320	32.5	1	0.241	0.849	0.1
-	-	-	-	-	-	-	-	-	-	-	-
242	0.819	0.162	62	0.041	37.2	-320	32.5	1	0.246	0.851	0.1
170	0.600	0.119	0	0.002	37.9	RT	15.0	16	-	-	-
-	-	-	-	-	-	-	-	-	-	-	-
184	0.600	0.123	12	0.030	37.6	-320	37.6	1	0.191	0.619	0.1
-	-	-	-	-	-	-	-	-	-	-	-
224	0.812	0.154	0	0.004	33.4	-320	32.5	1	0.238	0.864	0.1
-	-	-	-	-	-	-	-	-	-	-	-
216	0.750	0.144	0	0.005	28.5	-320	32.5	1	0.241	0.795	0.1

SSIBLE TO OBTAIN

142-2

	TEST CONDITION AT FRACTURE			K_{Ic} @ $\alpha = 0$ (KSI $\sqrt{IN.}$)	K_{Ic} @ $\alpha \neq 0$ (KSI $\sqrt{IN.}$)	K_{Ii}/K_{Ic}	K_{If}/K_{Ic}	Ref. Symbol in Fig.
	Temperature (°F)	Flaw Size a/Q (Inches)	Fracture Stress σ (Ksi)					
	-320		39.6	-	-	0.955	1.0	●
34	-	-	-	-	-	0.784	0.81	
	-320		39.6	-	-	0.905	1.0	◇
	-320		38.5	-	-	0.918	1.0	
	-320		48.6	-	-	0.920	1.0	○
51	-	-	-	-	42.5	0.831	0.838	◉
58	-	-	-	-	42.5	0.90	0.915	
	-	-	-	-	42.5	0.985	1.0	
59	-320	0.170	55.4	-	42.5**	0.847	0.875	□
	-	-	-	-	-	0.90	0.907	△
	-320	0.112	59.5	-	-	0.905	1.0	▼
21	-	-	-	-	-	0.862	0.90	
	-320	0.128	59.5	-	-	0.98	1.0	
59	-	-	-	-	-	0.79	0.80	
	-	-	-	-	-	0.945	-	
52	-320	0.159	49.5	39.0**	-	0.726	0.730	▷

Table 8

SPECIMEN NUMBER	SPECIMEN SIZE		CYCLIC EXTENSION OF EDM FLAW			FLAW SIZE BEFORE THE TEST RUN			SUSTAINED TEST RUN			
	Thickness (Inches)	Width (Inches)	Temperature (°F)	Max Stress (Ksi)	Number Of Cycles (1,000)	Flaw Depth a (Inches)	Flaw Length 2c (Inches)	Flaw Size a/Q (Inches)	Test Temperature (°F)	Max Stress σ_{max} (Ksi)	Time @ σ_{max} (Hours)	K_{Ii} @ α (Ksi $\sqrt{In.}$)
GROUP III												
AC-7+	0.650	6.00	-320	20.0	30	0.312	0.912	0.181	-320	32.0	1.0	26.9
AC-9	0.655	6.00	RT	15.0	11	0.227	0.784	0.146	-320	30.1	1.0	22.7
						0.321	1.053	0.202	-320	33.6	1.0	31.1
GROUP IV												
AA-59	0.657	6.00	RT	15.0	5	0.310	1.182	0.216	-320	37.5	0.3	37.0
									-320	38.6	16.0	-
									-320	39.6	0.4	-
									-320	40.6	0.01*	-
DA-36	0.655	6.00	RT	15.0	20	0.175	0.596	0.120	-320	56.3	0.3*	37.8

*   FAILED UNDER SUSTAINED LOAD

**   PULLED TO FAILURE

▷ -   NO DISTINGUISHABLE DEMARKATION LINES

\+   PRIOR LOAD HISTORY AT ROOM TEMPERATURE (SEE TABLE 6 GROUP IV)

▶   AVERAGE STATIC K_{Ic} = 41.8 USED IN DETERMINING K RATIOS WHERE IT WAS NOT POSSIBLE TO OBTAIN K_{Ic} FROM INDIVIDUAL SPECIMEN

	FLAW SIZE AFTER THE TEST RUN					CYCLIC FLAW MARKING			FLAW SIZE AFT CYCLIC MARKI	
Flaw Depth a (Inches)	Flaw Length 2c (Inches)	Flaw Size a/Q (Inches)	Direction Of Growth α (Deg.)	Flaw Increment Along α (In.)	K_{IF} @ α (Ksi $\sqrt{IN}$)	Temperature (°F)	Max Stress (Ksi)	Number Of Cycles (1,000)	Flaw Depth a (Inches)	Flaw Length 2c (Inches)
0.312	0.912	0.181	0	0	26.9	-320	25.0	1.5	0.313	0.912
0.227	0.784	0.146	0	0	22.7	-320	20.0	15.0	0.321	1.053
0.326	1.058	0.452	0	0.005	31.2	-320	20.0	16.2	0.640	2.470
▷	-	-	-	-	-	-	-	-	-	-
▷	-	-	-	-	-	-	-	-	-	-
▷	-	-	-	-	-	-	-	-	-	-
▷	-	-	-	-	-	-	-	-	-	-
▷	-	-	-	-	-	-	-	-	-	-

ER NG Flaw Size a/Q (Inches)	TEST CONDITION AT FRACTURE			K_{Ic} @ $\alpha = 0$ (KSI $\sqrt{IN.}$)	K_{Ic} @ $\alpha \neq 0$ (KSI $\sqrt{IN.}$)	K_{Ii}/K_{Ic}	K_{If}/K_{Ic}	Ref. Symbol in Fig.
	Temperature (°F)	Flaw Size a/Q (Inches)	Fracture Stress σ (Ksi)					
0.179	-320	0.184	43.0	36.7**	-	0.734	0.734	◀
0.445	-	-	-	-	-	0.544	0.544	●
0.435	-320	0.435	20.0	-	-	0.744	0.746	●
-	-	-	-	-	-	-	-	
-	-	-	-	-	-	-	-	
-	-	-	-	-	-	-	-	
-	-320	▷	40.6	-	-	-	-	
-	-320	0.120	56.3	-	-	0.905	1.0	X

Table 9

143 -3

SPECIMEN NUMBER	SPECIMEN SIZE		CYCLIC EXTENSION OF EDM FLAW			FLAW SIZE BEFORE THE TEST RUN			SUSTAINED TEST RUN			
	Thickness (Inches)	Width (Inches)	Temperature (°F)	Max Stress (Ksi)	Number Of Cycles (1,000)	Flaw Depth a (Inches)	Flaw Length 2c (Inches)	Flaw Size a/Q (Inches)	Test Temperature (°F)	Max Stress σ_{max} (Ksi)	Time @ σ_{max} (Hours)	K_{Ii} @ α (Ksi $\sqrt{In.}$)
GROUP I												
AA-21	0.656	6.00	RT	15.0	4	0.305	1.166	0.209	-423	30.9	12.4	30.0
AA-19	0.655	6.00	RT	15.0	4	0.308	1.210	0.220	-423	35.3	10.9	35.5
AA-61	0.661	6.00	RT	15.0	3	0.274	1.123	0.198	-423	39.7	10.3	37.5
CA-45	0.658	6.00	RT	15.0	11	0.211	0.761	0.146	-423	50.9	9.9	38.3
DA-22	0.662	6.00	RT	15.0	10	0.157	0.564	0.106	-423	44.6	10.8	27.9
DA-20	0.656	6.00	RT	15.0	12	0.267	0.758	0.156	-423	50.9	11.8	38.6
GROUP II												
DA-18	0.670	6.00	RT	15.0	16	0.189	0.598	0.121	-423	57.2	44.0	37.8

* SPECIMEN WAS DELAMINATED (SEE FIGURE 31)

** PULLED TO FAILURE @ ROOM TEMPERATURE

▷ AVERAGE STATIC K_{Ic} = 43.8 KSI   IN WAS USED IN DETERMINING ALL K RATIOS

144-1

10: SUSTAINED LOAD FLAW GROWTH DATA FOR 2219-T87 ALUMINUM AT - 423°F (Groups I and II)

FLAW SIZE AFTER THE TEST RUN						CYCLIC FLAW MARKING			FLAW SIZE AFT CYCLIC MARKI	
Flaw Depth a (Inches)	Flaw Length 2c (Inches)	Flaw Size a/Q (Inches)	Direction Of Growth α (Deg.)	Flaw Increment Along α (In.)	K_{If} @ α (Ksi $\sqrt{In}$)	Temperature (°F)	Max Stress (Ksi)	Number Of Cycles (1,000)	Flaw Depth a (Inches)	Flaw Length 2c (Inches)
0.305	1.166	0.209	0	0	30.0	RT	20.0	4	0.372	1.385
0.313	1.228	0.223	0	0.005	35.7	RT	20.0	2	0.368	1.382
0.286	1.123	0.202	0	0.012	37.9	RT	15.0	5	0.311	1.213
0.219	0.767	0.148	0	0.008	38.8	RT	27.9	3	0.261	0.945
0.157	0.564	0.106	0	0	27.9	RT	15.0	15	0.215	0.654
0.271	0.808	0.164	0	0.004	39.6	RT	20.0	12	0.387	1.139
0.199	0.601	0.123	0	0.010	38.2	RT	15.0	18	0.200	0.601

144-2

ER NG	TEST CONDITION AT FRACTURE			K_{Ic} @ $\alpha = 0$	K_{Ic} @ $\alpha \neq 0$			
Flaw Size a/Q (Inches)	Temperature (°F)	Flaw Size a/Q (Inches)	Fracture Stress σ (Ksi)	(KSI $\sqrt{IN.}$)	(KSI $\sqrt{IN.}$)	K_{Ii}/K_{Ic}	K_{If}/K_{Ic}	Ref. Symbol in Fig.
0.248	RT	0.254	30.6	34.0**	-	0.685	0.685	●
0.247	RT	0.254	32.3	36.8**	-	0.812	0.815	■
0.211	RT	0.221	34.5	35.1**	-	0.856	0.865	▲
0.174	RT	0.185	46.9	39.7*	-	0.875	0.886	▼
0.125	RT	0.136	48.5	35.1**	-	0.638	0.638	○
0.221	RT	0.227	34.1	33.5**	-	0.882	0.904	□
0.115	RT	0.126	50.5	34.1**	-	0.864	0.871	△

Table 10

SPECIMEN NUMBER	SPECIMEN SIZE		CYCLIC EXTENSION OF EDM FLAW			FLAW SIZE BEFORE THE TEST RUN			COMBINED CYCLIC-SUSTAINED			
	Thickness (Inches)	Width (Inches)	Temperature (°F)	Max Stress (Ksi)	Number Of Cycles (1,000)	Flaw Depth a (Inches)	Flaw Length 2c (Inches)	Flaw Size a/Q (Inches)	Test Temperature (°F)	Max Stress σ_{max} (Ksi)	Time @ σ_{max} (Minutes)	K_{Ti}
GROUP I												
AA-56	0.650	6.00	RT	15.0	5	0.322	1.226	0.220	-320	29.2	0.007	2
AA-55	0.658	6.00	RT	15.0	5	0.317	1.175	0.213	-320	29.2	0.250	2
AA-6	0.656	6.00	RT	12.0	11.5	0.377	1.319	0.245	-320	29.2	2.50	3
DA-29	0.650	6.00	RT	15.0	18	0.169	0.569	0.111	-320	43.8	0.007	2
DA-26	0.657	6.00	RT	15.0	18	0.165	0.544	0.107	-320	43.8	0.250	2
DA-30	0.663	6.00	RT	15.0	20	0.161	0.548	0.106	-320	43.8	2.50	2
GROUP II												
AA-54	0.674	6.00	RT	15.0	4	0.310	1.176	0.214	-320	35.4	0.007	3
AA-5	0.663	6.00	RT	10.0	15	0.313	1.203	0.218	-320	35.4	0.250	3
AA-53	0.660	6.00	RT	15.0	5	0.314	1.183	0.217	-320	35.4	2.50	3
AA-57	0.663	6.00	RT	15.0	6	0.317	1.181	0.217	-320	35.4	2.50	3
AA-60	0.654	6.00	RT	15.0	6	0.308	1.164	0.212	-320	35.4	30.0	3
DA-28	0.666	6.00	RT	15.0	18	0.174	0.594	0.119	-320	53.2	0.007	3
DA-46	0.652	6.00	RT	15.0	16	0.165	0.576	0.114	-320	53.2	0.250	3
DA-15	0.670	6.00	RT	15.0	15	0.162	0.597	0.116	-320	53.2	2.50	3
DA-27	0.652	6.00	RT	15.0	16	0.161	0.561	0.111	-320	53.2	30.0	3

* SEVERAL OVERLOADS, SPECIMEN PULLED TO FAILURE @ 42.2 KSI

GROWTH DATA

320°F

TEST		FLAW SIZE AFTER THE TEST RUN			TEST CONDITIONS AT FRACTURE			
K_{Ii} (Ksi $\sqrt{In.}$)	Cycles To Failure	Flaw Depth a (Inches)	Flaw Length 2c (Inches)	Flaw Size a/Q (Inches)	Temperature (°F)	Flaw Size a/Q (Inches)	Fracture Stress (Ksi)	K_{Ic} (KSI $\sqrt{In.}$)
9.4	1262	0.490	1.859	0.334	-320	0.334	29.2	43.9
8.7	1047	0.529	1.940	0.354	-320	0.354	29.2	44.0
1.6	291	0.480	1.775	0.323	-320	0.323	29.2	42.6
8.0	990	0.361	1.097	0.220	-320	0.220	43.8	42.0
7.3	1260	0.403	1.333	0.261	-320	0.261	43.8	48.8
7.4	1694	0.392	1.203	0.240	-320	0.240	43.8	44.3
4.8	144	0.456	1.514	0.290	-320	0.290	35.4	43.8
5.1	162	0.448	1.677	0.308	-320	0.308	35.4	46.7
5.0	48*	0.349	1.297	0.239	-320	0.239	42.2	44.7
5.0	18	0.383	1.415	0.260	-320	0.260	35.4	40.8
4.6	19	0.370	1.368	0.252	-320	0.252	35.4	39.9
5.3	20	0.237	0.701	0.145	-320	0.145	53.2	40.2
4.8	133	0.365	0.943	0.194	-320	0.194	53.2	45.6
5.1	35	0.273	0.779	0.163	-320	0.163	53.2	41.3
4.4	45	0.253	0.752	0.156	-320	0.156	53.2	40.3

Table 11

145 -2

SPECIMEN NUMBER	SPECIMEN SIZE		CYCLIC EXTENSION OF EDM FLAW			FLAW SIZE BEFORE THE TEST RUN			SUSTAINED TEST RUN			
	Thickness (Inches)	Width (Inches)	Temperature (°F)	Max Stress (Ksi)	Number Of Cycles (1,000)	Flaw Depth a (Inches)	Flaw Length 2c (Inches)	Flaw Size a/Q (Inches)	Test Temperature (°F)	Max Stress σ_{max} (Ksi)	Time @ σ_{max} (Hours)	K_{I1} @ α
0001	0.600	19.41	RT	18.3	6	0.223	0.844	0.155	RT	33.2	178	22
0002	0.623	19.41	RT	15.9	7	0.225	0.863	0.155	RT	27.0	132	19.

* DELAMINATED

146-1

Table 12: SUSTAINED LOAD FLAW GROWTH DATA FOR 2219-T87 ALUMINUM TANKS AT ROOM TEMPERATURE

FLAW SIZE AFTER THE TEST RUN						CYCLIC FLAW MARKING			FLAW SIZE AFTER CYCLIC MARKING		
Flaw Depth a (Inches)	Flaw Length 2c (Inches)	Flaw Size a/Q (Inches)	Direction Of Growth α (Deg.)	Flaw Increment Along α (In.)	K_{If} @ α (Ksi $\sqrt{IN}$)	Temperature (°F)	Max Stress (Ksi)	Number Of Cycles (1,000)	Flaw Depth a (Inches)	Flaw Length 2c (Inches)	
0.223	0.873	0.158	78	0.012	22.30	RT	18.3	0.5			
						RT	19.4	2.5	0.225	0.915	0.
0.225	0.881	0.157	71	0.010	19.88	RT	15.9	5	0.230	0.937	0.

146-2

Flaw Size a/Q (Inches)	TEST CONDITION AT FRACTURE			K_{Ic} @ $\alpha = 0$ (KSI $\sqrt{IN.}$)	K_{Ic} @ $\alpha \neq 0$ (KSI $\sqrt{IN.}$)	K_{Ii}/K_{Ic}	K_{If}/K_{Ic}	Ref. Symbol in Fig.
	Temperature (°F)	Flaw Size a/Q (Inches)	Fracture Stress σ (Ksi)					
168	RT	0.168*	42.7	-	30.0	0.742	0.743	✦
169	RT	0.169*	37.7	-	30.0	0.658	0.662	⊗

Table 12

TANK NUMBER	SPECIMEN SIZE		CYCLIC EXTENSION OF EDM FLAW			FLAW SIZE BEFORE THE TEST RUN			SUSTAINED TEST RUN				
	Shell Thickness (Inches)	Shell Dia (Nominal ID) (Inches)	Temperature (°F)	Max Stress (Ksi)	Number Of Cycles (1,000)	Flaw Depth a (Inches)	Flaw Length 2c (Inches)	Flaw Size a/Q (Inches)	Test Temperature (°F)	Max Stress σ_{max} (Ksi)	Time @ σ_{max} (Hours)	K_{Ii} (Ksi $\sqrt{In.}$)	Flaw Depth (Inch
0003 1st Flaw	0.618	19.41	[1]	[2]	5	0.188	0.818	0.144	-423	49.2	[x]	39.5	-
2nd Flaw	0.611	19.41	[1]	[2]	5	0.202	0.810	0.148	-423	49.8	[3]	38.5	0.208
004 1st Flaw	0.600	19.41	[1]	[2]	4	0.191	0.795	0.140	-423	42.4	[x]	32.2	-
2nd Flaw	0.596		[1]	[2]	4	0.186	0.830	0.141	-423	42.7	[x]	32.5	-

[1] LOCAL AREAS CONTAINING SURFACE FLAW WERE FLOODED WITH LIQUID NITROGEN TO REDUCE TEMPERATURE AND THUS PREVENT FORMATION OF DELAMINATION

[x] BURST UPON LOADING

[2] 14. BY

[3] FRA PRE

FLAW GROWTH DATA FOR 2219-T87

TANKS AT -423°F

FLAW SIZE AFTER THE TEST RUN				CYCLIC FLAW MARKING			FLAW SIZE AFTER CYCLIC MARKING			TEST CONDITION AT FRACTURE			K_{Ic} (KSI $\sqrt{IN.}$)
Flaw Length 2c (Inches)	Flaw Size a/Q (Inches)	Direction Of Growth α (Deg.)	Flaw Increment Along α (In.)	Temperature (°F)	Max Stress (Ksi)	Number Of Cycles (1,000)	Flaw Depth a (Inches)	Flaw Length 2c (Inches)	Flaw Size a/Q (Inches)	Temperature (°F)	Flaw Size a/Q (Inches)	Fracture Stress (Ksi)	
-	-	-	-	-	-	-	-	-	-	-423	0.144	49.2	39.5 [5]
0.835	0.390	0	0.006	-320	20.0	5	0.291	1.158	-	-320	-	[4]	-
-	-	-	-	-	-	-	-	-	-	-423	0.140	42.4	32.2
-	-	-	-	-	-	-	-	-	-	-423	0.141	42.7	32.5

KSI PLUS HOOP STRESS INDUCED
LOCALIZED COOLING

[4] FRACTURE STRESS NOT RECORDED

FAILURE OCCURRED IN THE FIRST FLAW DURING PRESSURIZATION TO TARGET HOOP STRESS OF 51.6 KSI

[5] CALCULATED USING INITIAL FLAW SIZE (FLAW GROWTH NOT INCLUDED)

Table 13

147-2

TABLE 14: MECHANICAL PROPERTIES OF 5AL-2.5 Sn(ELI) TITANIUM

SPECIMEN NUMBER	TEST TEMPERATURE (°F)	GRAIN ORIENTATION	SPECIMEN SIZE		ULTIMATE STRENGTH (KSI)	YIELD STRENGTH (KSI)		ELONGATION (% IN GAGE LENGTH SHOWN)	
			Gage Thickness (Inches)	Gage Width (Inches)		0.2 Percent Offset	0.02 Percent Offset	One Inch Gage Length	Two Inches Gage Length
TT-1	RT	L	0.196	0.498	119.2	110.0	106.8	23	15
TT-2	-320	L	0.198	0.498	192.6	180.2	172.3	14	12
TT-4	-423	L	0.198	0.498	225.3	210.2	200.1	8	6
TT-3	-423	L	0.198	0.498	228.7	-	-	8	6

TABLE 15: STATIC FRACTURE TOUGHNESS DATA OF 5AL-2.5 Sn (ELI) TITANIUM

SPECIMEN NUMBER	SPECIMEN SIZE (INCHES)		TEST TEMPERATURE (°F)	FLAW SIZE (INCHES)			FRACTURE STRESS (KSI)	K_{Ic} (KSI $\sqrt{IN}$)
	Thickness (t)	Width (W)		Flaw Depth (a)	Flaw Length (2c)	Flaw Size (a/Q)		
9T-9	0.193	2.00	-320	0.112	0.380	0.073	111.5	64.35
6T-5	0.195	2.00	-320	0.059	0.259	0.049	172.9	77.2
5T-11	0.192	2.00	-320	0.056	0.195	0.040	177.4	69.1
5T-38	0.202	2.00	-320	0.052	0.179	0.037	177.1	66.0
6T-37	0.202	2.00	-423	0.064	0.225	0.043	133.0	53.7
5T-25	0.200	2.00	-423	0.054	0.204	0.038	145.0	55.2
9T-40	0.202	2.00	-423	0.090	0.332	0.060	92.7	47.4

SPECIMEN NUMBER	SPECIMEN SIZE		CYCLIC EXTENSION OF EDM FLAW			FLAW SIZE BEFORE THE TEST RUN			SUSTAINE	
	Thickness (Inches)	Width (Inches)	Temperature (°F)	Max Stress (Ksi)	Number Of Cycles (1,000)	Flaw Depth a (Inches)	Flaw Length 2c (Inches)	Flaw Size a/Q (Inches)	Test Temperature (°F)	Max Stress $\sigma_{. r}$ (Ksi)
GROUP I										
5T-20	0.194	2.00	RT	40.0	25	0.054	0.198	0.039	-320	165.2
5T-46	0.200	2.00	RT	40.0	28	0.052	0.196	0.035	-320	165.2
						-	-		-320	173.5
6T-6	0.194	2.00	RT	40.0	30	0.076	0.255	0.052	-320	157.5
6T-34	0.198	2.00	RT	40.0	15	0.070	0.255	0.050	-320	151.:
6T-17	0.193	2.00	RT	40.0	18	0.065	0.248	0.049	-320	154.4
						-	-		-320	162.1
6T-36	0.193	2.00	RT	40.0	17	0.066	0.245	0.048	-320	159.3
9T-30	0.194	2.00	RT	40.0	5	0.093	0.349	0.065	-320	115.C
9T-23	0.193	2.00	RT	40.0	5	0.097	0.349	0.066	-320	113.C
						-	-		-320	118.6
						-	-		-320	124.5
						-	-		-320	130.7
						-	-		-320	134.2
9T-22	0.194	2.00	RT	40.0	5	0.089	0.347	0.064	-320	118.6
						-	-		-320	124.5
						-	-		-320	129.8
9T-32	0.201	2.00	RT	40.0	4	0.087	0.345	0.063	-320	122.4
9T-72	0.203	2.00	RT	40.0	4	0.088	0.362	0.065	-320	114.3

▷ BROKE UPON LOADING

* FAILED UNDER SUSTAINED LOADING

▶ AVERAGE STATIC & SUSTAINED K_{Ic} = 68.4 KSI IN USED IN DETERMI
RATIOS FOR SPECIMENS WHERE INDIVIDUAL K_{Ic} WAS NOT OBTAINED.

FLAW GROWTH DATA

itanium @ -320°F

imens)

TEST RUN		FLAW SIZE AFTER THE TEST RUN					K_{Ic} (KSI $\sqrt{IN.}$)	K_{Ti}/K_{Ic}
Time @ σ_{max} (Hours)	K_{Ti} (Ksi $\sqrt{In.}$)	Flaw Depth a (Inches)	Flaw Length 2c (Inches)	Flaw Size a/Q (Inches)	Direction Of Growth, α (Deg.)	Flaw Increment Along α (In.)		
3.1*	63.6						-	0.93
16.8	60.3						-	0.882
0.17*	63.3						-	0.927
x	71.5						71.5	1.0
x	68.1						68.1	1.0
4.0	68.2						71.6	0.95
0.02*	71.6	FLAW GROWTH DETECTION TECHNIQUES					71.6	1.0
x	69.5						69.5	1.0
x	63.4	(i.e. INSTRUMENTATION AND CYCLIC					63.4	1.0
9.9	61.6	FLAW MARKING) NOT USED.					72.9	0.846
4.0	64.7						72.9	0.888
4.0	67.8						72.9	0.930
16.0	71.2						72.9	0.978
x	72.9						72.9	1.0
4.2	63.7						70.0	0.91
4.0	66.9						70.0	0.955
x	70.0						70.0	1.0
x	65.0						65.0	1.0
x	63.0						63.0	1.0

IN3 K

Table 16

SPECIMEN NUMBER	SPECIMEN SIZE		CYCLIC EXTENSION OF EDM FLAW			FLAW SIZE BEFORE THE TEST RUN			SUSTAINED	
	Thickness (Inches)	Width (Inches)	Temperature (°F)	Max Stress (Ksi)	Number Of Cycles (1,000)	Flaw Depth a (Inches)	Flaw Length 2c (Inches)	Flaw Size a/Q (Inches)	Test Temperature (°F)	Max Stress σ_{max} (Ksi)
GROUP II										
5T-12	0.191	2.00	RT	40.0	35	0.058	0.186	0.038	-320	138.9
						-	-	-	RT	0
						-	-	-	-320	138.9
						0.062	0.209	0.041	-320	138.9
						0.069	0.232	0.045	-320	138.9
8T-3	0.195	2.00	RT	40.0	20	0.089	0.298	0.058	-320	117.3
						0.093	0.303	0.060	-320	117.3
						0.097	0.308	0.061	-320	117.3
						0.101	0.313	0.062	-320	117.3

*   NO DISTINGUISHABLE DEMARKATION LINES, FLAW SIZES PRORATED.

**   PULLED TO FAILURE

▷1   TEST INTERRUPTED, SPECIMEN UNLOADED AND LEFT AT RT FOR 16.7 HOU

▷2   FLOW OF NITROGEN INTERRUPTED, SPECIMEN WARMED UP AND FAILED WHI

Table 17 : SUSTAINED LOAD FLAW GROWTH DATA FOR
5 AL-2 1/2 Sn (ELI) Titanium @ -320°F
(Group II Specimens)

Time σ max (Hours)	K_{LI} (Ksi √In.)	Flaw Depth a (Inches)	Flaw Length 2c (Inches)	Flaw Size a/Q (Inches)	Direction Of Growth, α (Deg.)	Flaw Increment Along α (In.)	Temperature (°F)	Max Stress (Ksi)	Number Of Cycles (1,000)	Flaw Depth a (Inches)	Flaw Length
76.9	51.9	-	-	-	-	-	-	-	-	-	-
.6.7	1▷	-	-	-	-	-	-	-	-	-	-
2.6	51.9	0.058	0.186	0.038	0	0	RT	40.0	7	0.062*	0.1
?2.3	53.8	0.062	0.209	0.041	0	0	RT	40.0	10	0.069*	0.2
?4.1	56.4	0.069	0.232	0.045	0	0	RT	40.0	10	0.076	0.2
?9.7	59.1	0.089	0.298	0.058	0	0	RT	40.0	10	0.093*	0.3
?9.4	60.1	0.093	0.303	0.060	0	0	RT	40.0	10	0.097*	0.3
?4.5	60.6	0.097	0.308	0.061	0	0	RT	40.0	10	0.101*	0.3
?6.7	61.1	0.101	0.313	0.062	0	0	RT	40.0	10	0.105	0.3

▶ AVERAGE STATIC & SUSTAINED K_{Ic} = 68.4 KSI

K RATIOS FOR SPECIMENS WHERE INDIVIDUAL K_{Ic}

S.

E UNDER THE LOAD.

151-2

AFTER MARKING		TEST CONDITION AT FRACTURE				
c (Inches)	Flaw Size a/Q (Inches)	Temperature (°F)	Flaw Size a/Q (Inches)	Fracture Stress (Ksi)	K_{Ic} (KSI $\sqrt{IN}$)	K_{Ii}/K_{Ic}
	-	-	-	-	-	0.803
	-	-	-	-	-	-
39	0.038	-	-	-	64.5	0.803
32	0.042	-	-	-	64.5	0.835
56	0.047	-320	0.050	143.6	64.5	0.875
03	0.057	-	-	-	-	0.865
08	0.058	-	-	-	-	0.88
13	0.059	-	-	-	-	0.887
18	0.061	2	0.064	117.3	-	0.895

IN WAS USED IN DETERMINING

WAS NOT DETERMINED.

Table 17

Table 18 : SUSTAINED LOAD FI

5 AL-2 1/2 Sn (ELI) Tit

(Group III Spec

SPECIMEN NUMBER	SPECIMEN SIZE		CYCLIC EXTENSION OF EDM FLAW			FLAW SIZE BEFORE THE TEST RUN			SUSTA	
	Thickness (Inches)	Width (Inches)	Temperature (°F)	Max Stress (Ksi)	Number Of Cycles (1,000)	Flaw Depth a (Inches)	Flaw Length 2c (Inches)	Flaw Size a/Q (Inches)	Test Temperature (°F)	Max Stress
GROUP III										
4T-15	0.194	2.00	RT	40.0	45	0.048	0.159	0.033	-320	15
5T-18	0.193	2.00	RT	40.0	23	0.052	0.191	0.039	-320	16
5T-48	0.194	2.00	RT	40.0	38	0.055	0.183	0.035	-320	(
						-	-	-	RT	
						-	-	0.036	-320	13
						-	-	-	-320	14
						-	-	0.037	-320	14
						-	-	-	-320	15
						-	-	-	RT	
						0.055	0.183	0.038	-320	15
						-	-	-	-320	16
6T-21	0.194	2.00	RT	40.0	15	0.063	0.224	0.045	-320	15
						-	-	-	-320	16
6T-33	0.202	2.01	RT	40.0	18	0.061	0.253	0.047	-320	14
						-	-	-	-320	15
						-	-	-	-320	16

*   FAILED UNDER SUSTAINED LOAD

▷   OBSERVED FROM FRACTURE FACE (STAINED REGION)

152-1

σ_{max} (Ksi)	Time @ σ_{max} (Hours)	K_{Ii} (Ksi $\sqrt{In.}$)	FLAW SIZE AFTER THE TEST RUN					K_{Ic} (Ksi $\sqrt{In.}$)	K_{Ii}/K_{Ic}
			Flaw Depth a (Inches)	Flaw Length 2c (Inches)	Flaw Size a/Q (Inches)	Direction Of Growth, α (Deg.)	Flaw Increment Along α (In.)		
8.3	21.1*	55.2	0.100	0.232	0.051	0	▷ 0.052	66.6	0.83
5.0	34.0*	63.8	-	-	-	-	▶	-	0.935
2.3	0.01	29.2	-	-	-	-	0	-	0.427
0	240.0	0	-	-	-	-	0	-	-
6.1	0.1	49.4	-	-	-	-	0	-	0.723
4.5	0.1	52.9	-	-	-	-	0	-	0.774
9.7	0.2	54.8	-	-	-	-	0	-	0.80
3.1	0.2	55.4	-	-	-	-	0	-	0.81
0	312.0	0	-	-	-	-	0	-	-
8.3	2.7	58.6	-	-	-	-	▷	-	0.857
6.2	1.5	61.5	-	-	-	-	▷	-	0.902
6.8	22.7	65.2	-	-	-	-	▷	72.0	~0.92
4.6	0.4	69.5	0.075	0.241	0.050	0	0.012 ▷	72.0	~0.965
9.7	21.5	65.9	-	-	-	-	0	72.5	0.91
7.5	27.3	69.3	-	-	-	-	▷	72.5	0.955
5.5	3*sec	72.5	-	-	-	-	-	72.5	1.0

▷ FLAW GROWTH DETECTED FROM CRACK OPENING DISPLACEMENT MEASUREMENTS, EXACT AMOUNT OF GROWTH IS UNKNOWN

▶ AVERAGE STATIC AND SUSTAINED K_{Ic} = 68.42 KSI IN WAS USED IN DE MINING K RATIOS FOR SPECIMENS WHERE INDIVIDUAL K_{Ic} WAS NOT OBTAINED

Table 18

SPECIMEN NUMBER	SPECIMEN SIZE		CYCLIC EXTENSION OF EDM FLAW			FLAW SIZE BEFORE THE TEST RUN			S
	Thickness (Inches)	Width (Inches)	Temperature (°F)	Max Stress (Ksi)	Number Of Cycles (1,000)	Flaw Depth a (Inches)	Flaw Length 2c (Inches)	Flaw Size a/Q (Inches)	Test Temperature (°F)
GROUP III (Continued)									
9T-29	0.197	2.00	RT	40.0	5	0.083	0.325	0.058	-32C
						-	-	-	-32C
						-	-	-	-32C
						~	-	-	-32C
						-	-	-	-32C
						-	-	-	-32C
						-	-	-	-32C
						-	-	-	-32C
						-	-	-	-32C
9T-83	0.194	2.01	RT	40.0	3	0.084	0.336	0.061	-32C
						-	-	-	-32C
						-	-	-	-32C
						-	-	-	-32C
						-	-	-	-32C
						-	-	-	-320
						-	-	-	-320

▷1▷ TEST INTERRUPTED, SPECIMEN UNLOADED AND LEFT AT RT

▷2▷ BROKE UPON LOADING

* FAILED UNDER SUSTAINED LOADING

** ESTIMATED FROM RESULTS OF SPEC. 9T-29

▶ FLAW GROWTH DETECTED FROM CRACK OPENING DISPLACEMENT MEASUREMENTS, EXACT AMOUNT OF GROWTH IS UNKNOWN

153-1

~ ... FLAW GROWTH ... FOR
(...) Titanium 6 ... F
(... Specimens)

TAINED TEST RUN			FLAW SIZE AFTER THE TEST RUN					K_{Ic} (KSI √IN.)	K_{Ii}/K_{Ic}
Max Stress σ_{max} (Ksi)	Time @ σ_{max} (Hours)	K_{Ii} (Ksi √In.)	Flaw Depth a (Inches)	Flaw Length 2c (Inches)	Flaw Size a/Q (Inches)	Direction of Growth, α (Deg.)	Flaw Increment Along α (In.)		
121.6	5.4	61.8	-	-	-	-	0	70.9	0.875
0	▷1▷	-	-	-	-	-	0	-	-
126.7	0.4	64.4	-	-	-	-	0	70.0	0.909
128.8	0.7	65.5	-	-	-	-	0	70.9	0.925
130.0	0.3	66.1	-	-	-	-	0	70.9	0.935
131.7	0.3	66.9	-	-	-	-	c	70.9	0.943
133.3	0.5	67.7	-	-	-	-	0	70.9	0.955
135.0	1.6	68.6	-	-	-	-	0	70.9	0.970
139.6	▷x▷	70.9	-	-	-	-	0	70.9	1.0
117.3	1.6	61.5	-	-	-	-	0	70.9**	0.868
122.4	0.5	64.2	-	-	-	-	0	70.9**	0.906
125.3	0.4	65.7	-	-	-	-	0	70.9**	0.927
122.4	21.1	64.2	-	-	-	-	0	70.9**	0.906
127.4	2.6	66.8	-	-	-	-	0	70.9**	0.942
130.5	24.2	68.4	-	-	-	-	0	70.9**	0.965
133.6	0.01*	70.0	-	-	-	-	▷	70.9**	0.989

Table 19

SPECIMEN NUMBER	SPECIMEN SIZE		CYCLIC EXTENSION OF EDM FLAW			FLAW SIZE BEFORE THE TEST RUN			SUSTAINED	
	Thickness (Inches)	Width (Inches)	Temperature (°F)	Max Stress (Ksi)	Number Of Cycles (1,000)	Flaw Depth a (Inches)	Flaw Length 2c (Inches)	Flaw Size a/Q (Inches)	Test Temperature (°F)	Max Stress σ_{max} (Ksi)
GROUP I										
3T-58	0.207	2.00	RT	40.0	70	0.047	0.148	0.030	-423	160.0
3T-63	0.205	2.00	RT	40.0	60	0.043	0.133	0.028	-423	179.0
3T-64	0.205	2.00	RT	40.0	71	0.049	0.143	0.030	-423	162.8
3T-78	0.201	2.00	RT	40.0	73	0.052	0.146	0.030	-423	154.6
5T-24	0.195	2.00	RT	40.0	25	0.049	0.210	0.037	-423	136.8
5T-79	0.199	2.00	RT	40.0	20	0.050	0.186	0.035	-423	137.1
						-	-	-	RT	0
						-	-	-	-423	137.1
5T-76	0.208	2.00	RT	40.0	20	0.048	0.181	0.034	-423	137.0
5T-74	0.207	2.01	RT	40.0	20	0.054	0.203	0.038	-423	140.4
5T-75	0.207	2.01	RT	40.0	21	0.049	0.193	0.037	423 ◁4	140.4
						-	-	-		0
						-	-	-	-423	140.4
						-	-	-	-	-
6T-70	0.207	2.00	RT	40.0	14	0.072	0.238	0.046	-423	116.5
6T-69	0.207	2.00	RT	40.0	15	0.073	0.235	0.046	-423	119.2
6T-54	0.202	2.01	RT	40.0	15	0.074	0.248	0.047	-423	110.5
9T-60	0.199	2.00	RT	40.0	3	0.089	0.368	0.063	-423	83.6

FAILED UNDER SUSTAINED LOAD
NO DISTINGUISHABLE DEMARKATION LINES
BROKE UPON LOADING
PULLED TO FAILURE TO CHECK STATIC K_{Ic}
SPECIMEN UNLOADED AND WARMED UP TO ROOM TEMPERATURE OVERNIGHT
ACCIDENTAL OVERLOAD
AVERAGE K_{Ic} = 58.34 KSI IN WAS USED IN DETERMINING K RATIOS FOR
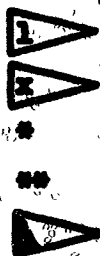SPECIMENS WHERE INDIVIDUAL K_{Ic} WAS NOT OBTAINED

Table 20: SUSTAINED LOAD FLAW GROWTH DATA FOR
5 Al-2 1/2 Sn (ELI) Titanium @ -423 F

TEST RUN		FLAW SIZE AFTER THE TEST RUN					CYCLIC FLAW MARKING			FLAW SI. CYCLIC	
Time @ σ max (Hours)	K_{Ii} (Ksi √in.)	Flaw Depth a (Inches)	Flaw Length 2c (Inches)	Flaw Size a/Q (Inches)	Direction Of Growth, α (Deg.)	Flaw Increment Along α (In.)	Temperature (°F)	Max Stress (Ksi)	Number Of Cycles (1,000)	Flaw Depth a (Inches)	Flaw Length
12.3	52.0	0.047	0.148	0.030	0	0	RT	46.0	60	0.072	0.
	56.2	-	-	-	-	-	-	-	-	-	-
x	53.5	-	-	-	-	-	-	-	-	-	.
x	50.9	-	-	-	-	-	-	-	-	-	.
1.8	50.8	-	-	-	-	-	-	-	-	-	.
8.9	49.6	-	-	-	-	-	-	-	-	-	.
	-										
10.7	49.6	0.050	0.186	0.035	0	0	RT	50.0	20	0.064	0.
3.5*	48.8	-	-	-	-	-	-	-	-	-	.
0.9	53.5	-	-	-	-	-	-	-	-	-	.
1.0	52.2	-	-	-	-	-	-	-	-	-	.
8.2	-	-	-	-	-	-	-	-	-	-	.
7.1	52.2	0.049	0.193	0.034	0	0	RT	25.0	60	-	.
.	-		-	-	-	-	RT	60.0	5	0.070	0.
x	48.9	-	-	-	-	-	-	-	-	-	.
x	50.1	-	-	-	-	-	-	-	-	-	.
6.7	47.3	0.074	0.248	0.047	0	0	RT	60.0	3	0.115	0.
4.0	45.8	0.089	0.368	0.063	0	0	RT	50.0	2	0.107	0.

1 ▷ SPECIMEN UNLOADED OVERNIGHT AND WAS KEPT
** PULLED TO FAILURE
3 ▷ AFTER CYCLIC MARKING SPECIMEN WAS BROKE

154-2

AFTER MARKING		TEST CONDITION AT FRACTURE			K_{Ic} (KSI $\sqrt{\text{IN.}}$)	K_{Ii}/K_{Ic} [5]
(inches)	Flaw Size a/Q (Inches)	Temperature (°F)	Flaw Size a/Q (Inches)	Fracture Stress (Ksi)		
3	0.040	-	-	-	[3]	0 992
	-	-423	0.028	179.0	56.2**	1.0
	-	-423	0.030	162.8	53.5	1.0
	-	-423	0.030	154.6	50.8	1.0
	-	-423	0.037	149.6	55.5+	0.916
	-	-	-	-	-	0.95
	-	-	-	-	-	-
6	0.035	-	-	-	[3]	0.95
	-	-423	[-]	137.0	-	0.935
	-	-	-	-	-	~1.0
	-	-	-	-	-	0.972
	-	-	-	-	-	-
	-	-	-	-	-	-
0	0.040	-	-	-	[3]	0.972
	-	-423	0.046	116.5	48.9	1.0
	-	-423	0.046	119.2	50.1	1.0
9	0.060	-	-	-	[3]	0.905
5	0.072	-	-	-	[3]	0.875

BELOW 0°F.

Table 20

154 - 3

SPECIMEN NUMBER	SPECIMEN SIZE		CYCLIC EXTENSION OF EDM FLAW			FLAW SIZE BEFORE THE TEST RUN			C	
	Thickness (Inches)	Width (Inches)	Temperature (°F)	Max Stress (Ksi)	Number Of Cycles (1,000)	Flaw Depth a (Inches)	Flaw Length 2c (Inches)	Flaw Size a/Q (Inches)	Test Temperature (°F)	Max Stress
GROUP I										
3T-7	0.196	2.00	RT	40.0	71	0.040	0.141	0.029	-320	1
3T-10	0.194	2.00	RT	40.0	70	0.049	0.147	0.031	-320	1
3T-8	0.195	2.00	RT	40.0	80	0.044	0.136	0.029	-320	1
3T-50	0.207	2.01	RT	40.0	55	0.048	0.135	0.029	-320	1
5T-28	0.199	2.00	RT	40.0	35	0.062	0.184	0.038	-320	1
5T-35	0.197	2.00	RT	40.0	28	0.060	0.203	0.040	-320	1
5T-27	0.202	2.00	RT	40.0	30	0.054	0.200	0.039	-320	1
5T-13	0.194	2.00	RT	40.0	49	0.052	0.196	0.038	-320	1
5T-19	0.194	2.00	RT	40.0	30	0.063	0.194	0.039	-320	1
5T-26	0.201	2.00	RT	40.0	25	0.047	0.182	0.033	-320	1

COMBINED CYCLIC-SUSTAINED TEST				FLAW SIZE AFTER THE TEST RUN			TEST CONDITIONS AT FRACTURE				
σ_{max} (Ksi)	Time @ σ_{max} (Minutes)	K_{Ii} (Ksi √In.)	Cycles To Failure	Flaw Depth a (Inches)	Flaw Length 2c (Inches)	Flaw Size a/Q (Inches)	Temperature (°F)	Flaw Size a/Q (Inches)	Fracture Stress (Ksi)	K_{Ic} (KSI √IN.)	K_{Ii}/K_{Ic}
2.2	0.007	53.0	250	0.084	0.198	0.043	-320	0.043	162.2	64.8	0.82
2.2	0.05	54.2	338	0.097	0.215	0.047	-320	0.047	162.2	66.8	0.811
2.2	0.25	52.4	231	0.092	0.212	0.046	-320	0.046	162.2	66.2	0.791
2.2	2.50	51.9	166	0.087	0.219	0.048	-320	0.048	162.2	67.2	0.772
3.9	0.007	52.3	131	0.095	0.242	0.051	-320	0.051	138.9	60.6	0.862
3.9	0.007	54.0	301	0.121	0.292	0.062	-320	0.062	138.9	67.2	0.802
.9	0.05	53.7	309	0.106	0.265	0.056	-320	0.056	138.9	64.3	0.850
3.9	0.13	52.7	229	0.111	0.263	0.056	-320	0.056	138.9	64.1	0.823
3.9	0.25	53.0	271	0.117	0.255	0.054	-320	0.054	138.9	62.1	0.853
.9	30.00	48.8	409	0.120	0.270	0.058	-320	0.058	138.9	64.7	0.754

Table 21

155-2

155-2

SPECIMEN NUMBER	SPECIMEN SIZE		CYCLIC EXTENSION OF EDM FLAW			FLAW SIZE BEFORE THE TEST RUN				CYCLIC
	Thickness (Inches)	Width (Inches)	Temperature (°F)	Max Stress (Ksl)	Number Of Cycles (1,000)	Flaw Depth a (Inches)	Flaw Length 2c (Inches)	Flaw Size a/Q (Inches)	Test Temperature (°F)	Max Stress σ_{max} (Ksl)
GROUP II										
3T-43	0.202	2.00	RT	40.0	90	0.050	0.151	0.033	-320	175.0
3T-2	0.196	2.00	RT	40.0	70	0.045	0.123	0.027	-320	171.0
3T-45	0.204	2.00	RT	40.0	90	0.046	0.138	0.029	-320	171.0
3T-4	0.195	2.00	RT	40.0	71	0.046	0.133	0.029	-320	171.0
3T-47	0.200	2.00	RT	40.0	70	0.037	0.132	0.027	-320	171.0
8T-42	0.194	2.00	RT	40.0	15	0.079	0.282	0.055	-320	133.0
8T-31	0.197	2.00	RT	40.0	12	0.064	0.271	0.049	-320	133.0
8T-52	0.205	2.00	RT	40.0	12	0.087	0.284	0.057	-320	132.7
8T-57	0.206	2.01	RT	40.0	10	0.090	0.301	0.059	-320	123.3
8T-73	0.201	2.00	RT	40.0	10	0.070	0.267	0.051	-320	133.0
8T-49	0.202	2.01	RT	40.0	10	0.086	0.327	0.060	-320	110.7
8T-16	0.194	2.00	RT	40.0	13	0.079	0.296	0.057	-320	133.0
8T-55	0.202	2.01	RT	40.0	8	0.079	0.269	0.053	-320	132.0
8T-56	0.206	2.00	RT	40.0	5	0.067	0.270	0.050	-320	133.0
8T-62	0.206	2.01	RT	40.0	7	0.070	0.302	0.054	-320	133.0

1   SPECIMEN FAILED AT 9 CYCLES. THE LAST FOUR CYCLES

2   BROKE AS SOON AS IT REACHED THE LOAD

x   BROKE UPON LOADING

3   LN₂ FLOW WAS INTERRUPTED. SPECIMEN WARMED UP AND FAILED

BASED UPON AVERAGE K_Ic FROM CYCLIC SPECIMENS (SEE DISCUSSION)

CYCLIC LOAD FLAW GROWTH DATA

Titanium @ -320°F

(specimens)

BINED STAINED TEST			FLAW SIZE AFTER THE TEST RUN			TEST CONDITIONS AT FRACTURE				
(Minutes)	K_{I1} (Ksi √In.)	Cycles To Failure	Flaw Depth a (Inches)	Flaw Length 2c (Inches)	Flaw Size a/Q (Inches)	Temperature (°F)	Flaw Size a/Q (Inches)	Fracture Stress (Ksi)	K_{Ic} (KSI √IN.)	
.008	60.5	47	0.066	0.167	0.037	-320	0.037	175.0	63.8	0.949
.05	53.1	95	0.077	0.177	0.039	-320	0.039	171.0	63.8	0.833
.25	55.2	76	0.078	0.183	0.041	-320	0.041	171.0	65.6	0.841
.50	54.6	47	0.006	0.166	0.036	-320	0.036	171.0	60.2	0.908
.00	53.5	3 1/3	0.058	0.157	0.034	-320	0.034	171.0	60.4	0.886
.05	63.4	21	0.096	0.306	0.062	-320	0.062	133.0	67.6	0.937
.25	59.9	67	0.115	0.253	0.054	-320	0.054	133.0	-	0.931*
.50	63.7	x	-	-	-	-320	0.057	132.7	63.7	1.00
.50	60.8	x	-	-	-	-320	0.059	123.3	60.8	1.00
.50	60.4	95	0.099	0.315	0.063	-320	0.063	133.0	67.1	0.90
.0	56.1	x	-	-	-	-320	0.060	110.7	56.1	1.00
.0	65.1	2	-	-	-	-320	0.057	133.0	65.1	1.00
.0	60.4	x	-	-	-	-320	0.053	132.0	60.4	1.00
.0	59.9	2	-	-	-	3	-	-	-	-
.0	64.5	47	0.085	0.319	0.061	-320	0.061	133.0	68.5	0.942

Table 22

TANK NUMBER	TANK SIZE		CYCLIC EXTENSION OF EDM FLAW			FLAW SIZE BEFOR THE TEST RUN		
	Shell Thickness (Inches)	Shell I. D. (Inches)	Temperature (°F)	Max Stress (Ksi)	Number of cycles (1,000)	Flaw Depth a (Inches)	Flaw Length 2c (Inches)	Flaw Size
0013	0.172	15.2	RT	▷2	14	0.024*	0.170*	0.
0014	0.165	15.2	RT	▷2	16	0.024	0.170	0.

▷1 NOTCHED AND BROKEN TO EXPOSE FRACTURE SURFACE

▷2 EXTENSION OF EDM FLAW WAS DONE BY CYCLIC FLEXING SECTION CONTAINING FLAW

* FLAWS IN EACH TANK WAS MACHINED TO THE SAME SIZE AS FOR 0014 TANK.

Table 23: SUSTAINED LOAD FLAW GROWTH DATA

For 5 Al-2 1/2 Sn (ELI) TITANIUM TANK AT -423°F

	SUSTAINED TEST RUN				FLAW SIZE AFTER THE TEST RUN					CYCLIC FLAW MARKING		
	Test Temperature (°F)	Max Stress σ_{max} (Ksi)	Time @ σ_{max} (Hours)	K_{Ii} (Ksi$\sqrt{In.}$)	Flaw Depth a (Inches)	Flaw Length 2c (Inches)	Flaw Size a/Q (Inches)	Direction of Growth, ℓ (Deg.)	Flaw Increment Along ℓ (In.)	Temperature (°F)	Max Stress (Ksi)	Number of Cycles
3	-423	131.5	1.1	38.8	0.024*	0.170*	0.023	-	-	RT		
3	-423	165.1	2.8	48.9	0.024	0.170	0.023	0	0	RT		

| (1,000) | FLAW SIZE AFTER CYCLIC MARKING | | | TEST CONDITION AT FRACTURE | | | K_{Ic} (KSI $\sqrt{IN.}$) | K_{Ii}/K_{Ic} |
	Flaw Depth a (Inches)	Flaw Length 2c (Inches)	Flaw Size a/Q (Inches)	Temperature (°F)	Flaw Size a/Q (Inches)	Fracture Stress (Ksi)		
	0.027	0.172	0.026	-423	0.026	176.7	55.5	-
	0.037	0.175	0.032	-320	0.032	△1	-	0.90

Table 23

DISTRIBUTION LIST FOR FINAL REPORT NASA CR-72252
CONTRACT NAS3-6290

"Extended Loading of Cryogenic Tanks"

The Boeing Company
Seattle, Washington

Copies

National Aeronautics and Space Administration
Lewis Research Center
21000 Brookpark Road
Cleveland, Ohio 44135

Attention:	Contracting Officer, MS 500-210	1
	Liquid Rocket Technology Branch, MS 500-209	8
	Technical Report Control Office, MS 5-5	1
	Technology Utilization Office, MS 3-16	1
	AFSC Liaison Office, MS 4-1	2
	Library	2
	Office of Reliability & Quality Assurance, MS 500-203	1
	Richard Kemp, MS 49-1	2
	W. F. Brown, MS 105-1	1
	J. L. Shannon, MS 105-1	1
	J. E. Srawley, MS 105-1	1
	D. L. Nored, MS 500-209	1
	W. E. Roberts, MS 3-17	1

National Aeronautics & Space Administration
Washington, D.C. 20546

Attention: Code RV-2   2